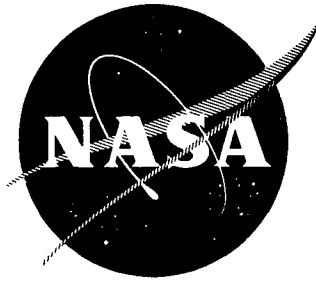


UNCLASSIFIED

AD NUMBER
ADB211395
NEW LIMITATION CHANGE
TO Approved for public release, distribution unlimited
FROM Distribution authorized to U.S. Gov't. agencies and their contractors; Administrative/Operational Use; JAN 1971. Other requests shall be referred to National Aeronautics and Space Administration, Washington, DC.
AUTHORITY
NASA TR Server Website

THIS PAGE IS UNCLASSIFIED



NASA CR-72753
Arde 41001

FINAL REPORT
DEVELOPMENT OF A FILAMENT-OVERWRAPPED
CRYOFORMED METAL PRESSURE VESSEL

by

D. Gleich

prepared for

NATIONAL AERONAUTICS AND SPACE ADMINISTRATION

January 1971
Contract NAS3-11194

Technical Management
NASA Lewis Research Center
Cleveland, Ohio

Liquid Rocket Technology Branch
J. R. Faddoul

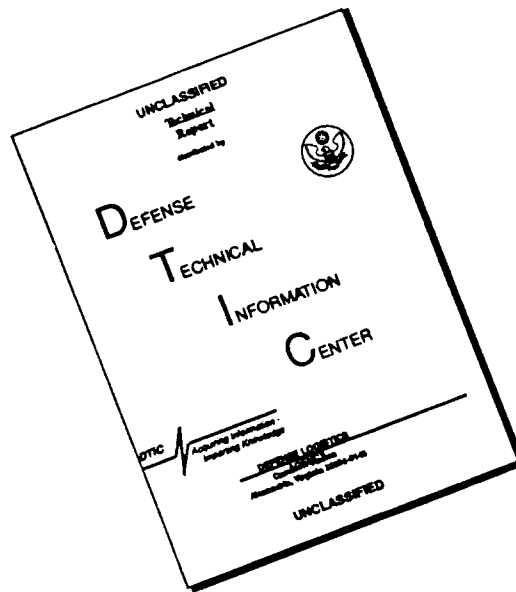
"DTIC USERS ONLY"

ARDE, INC.
Mahwah, New Jersey

19960610 085

PLAS 15403

DISCLAIMER NOTICE



THIS DOCUMENT IS BEST QUALITY AVAILABLE. THE COPY FURNISHED TO DTIC CONTAINED A SIGNIFICANT NUMBER OF PAGES WHICH DO NOT REPRODUCE LEGIBLY.

NOTICE

This report was prepared as an account of Government - sponsored work. Neither the United States, nor the National Aeronautics and Space Administration (NASA), nor any person acting on behalf of NASA:

- (A) Makes any warranty or representation, expressed or implied, with respect to the accuracy, completeness, or usefulness of the information contained in this report, or that the use of any information, apparatus, method, or process disclosed in this report may not infringe privately-owned rights; or
- (B) Assumes any liabilities with respect to the use of, or for damages resulting from the use of any information, apparatus, method or process disclosed in this report.

As used above, "person acting on behalf of NASA" includes any employee or contractor of NASA, or employee of such contractor, to the extent that such employee or contractor of NASA, or employee of such contractor prepares, disseminates, or provides access to, any information pursuant to his employment or contract with NASA, or his employment with such contractor.

Requests for copies of this report should be referred to:

NASA Scientific and Technical Information Facility
P.O. Box 33
College Park, Maryland, 20740

FINAL REPORT
DEVELOPMENT OF A FILAMENT-OVERWRAPPED
CRYOFORMED METAL PRESSURE VESSEL

by

D. Gleich

THIS QUALITY INSPECTED

prepared for

NATIONAL AERONAUTICS AND SPACE ADMINISTRATION

January 1971
Contract NAS3-11194

Technical Management
NASA Lewis Research Center
Cleveland, Ohio

Liquid Rocket Technology Branch
J. R. Faddoul

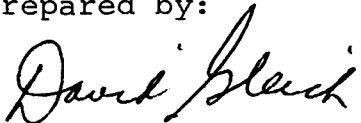
ARDE, INC.
Mahwah, New Jersey

FOREWORD

This report is submitted by Arde, Inc. in fulfillment of contract NAS 3-11194 and covers the period from July, 1967 to August, 1970. Principal investigators were David Gleich and Martin Scheinberg.

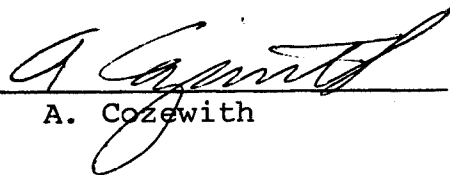
Guidance and many helpful suggestions were provided throughout the program by the NASA Project Manager, J. R. Faddoul of the Liquid Rocket Technology Branch, Lewis Research Center.

Prepared by:



David Gleich

Approved by:



A. Cozewith

DEVELOPMENT OF A FILAMENT-OVERWRAPPED
CRYOFORMED METAL PRESSURE VESSEL

by

D. Gleich

ABSTRACT

High performance ARDEFORM cryoformed 301 stainless steel glass fiber reinforced (GFR) vessels were demonstrated by room temperature tests of 13 1/2" diameter spheres. Ten (10) GFR spheres were delivered for NASA cryogenic testing and evaluation.

Considerable weight saving can be realized. Tests verified that the performance of ARDEFORM spherical GFR vessels not only exceeded that of all metal construction, but also bettered previous GFR experimental results by 50%. Further improved ARDEFORM GFR configurations have been identified. Achievement of full strength of fiber-glass in a spherical wrap pattern was again verified by tests. A low GFR vessel fabrication scrap factor of 13% was demonstrated in this development program.

CONTENTS

	Page
SUMMARY	xi
1. INTRODUCTION.	1
2. DESCRIPTION OF GFR VESSELS	3
3. TECHNICAL DISCUSSION.	4
3.1 Material Procurement and Certification	4
3.2 Materials Properties	4
3.3 Vessel Design	7
3.4 Vessel Fabrication	21
3.5 Vessel Testing	33
4. GFR VESSEL PERFORMANCE EVALUATION	54
4.1 Current Vessels.	54
4.2 Improved Vessels	57
5. CONCLUSIONS AND RECOMMENDATIONS	61
6. REFERENCES	65
7. APPENDICES	A-1
7.1 Appendix 1 - Material Certification Data	A-1
7.2 Appendix 2 - Bi-axial Coupon Data	A-1
7.3 Appendix 3 - Tension-Compression Coupon Data	A-16
7.4 Appendix 4 - Coefficient of Thermal Contraction Data	A-16
7.5 Appendix 5 - Design.	A-38
7.6 Appendix 6 - Vessel Testing.	A-54
7.7 Appendix 7 - Increased Ductility Liner High Performance Spherical GFR Vessel	A-62
7.8 Appendix 8 - Low Stress Liner GFR Vessel Configuration	A-64
7.9 Appendix 9 - Distribution List	A-66

LIST OF FIGURES

<u>Figure</u>		<u>Page</u>
1	Elastic Buckling Stresses for Filament Over- wrapped ARDEFORM 301 Stainless Steel Shells.	7
2	Elastic Buckling Stress Divided by Density for Filament Overwrapped ARDEFORM 301 Stainless Steel Shells	8
2a	Stress-Strain Diaphragm (Parametric Vessel Design)	.12
2b	Stress-Strain Diaphragm (Initial GFR Spherical Vessel Configuration15
2c	Stress-Strain Diaphragm.16
3	GFR Pressure Vessel Weldment Assembly - Preform. . .	.22
4	GFR Pressure Vessel Weldment Assembly - Postform Prior to Winding23
5	Filament Winding Pattern24
6	GFR Pressure Vessel Filament Wound Postform.25
7	GFR Pressure Vessel Weldment Assembly - Preform. . .	.26
8	GFR Pressure Vessel Weldment Assembly - Postform . .	.27
9	Filament Winding Pattern for Type A GFR Vessel28
10	GFR Pressure Vessel Filament Wound Postform (Type A)29
11	Schematic Cryogenic Stretch Forming Facility31
12	GFR Vessel Liner32
13	Sphere Winding Set-Up.34
14	Spherical Winding Machine.35
15	Fiber Overwrapped Spherical Liner36
16	Completed GFR Vessels P/N D3731 and D3770.37
17	Elastomer Lined Filament Wound Sphere After Burst Test39
18	Hydrostatic Test of S/N 9 Liner.42
19	Schematic Hydrotest Set-Up44
20	Test Set-Up Hydrostatic Proof and Burst Test45
21	Failure Region of S/N 15 GFR Vessel.48
22	S/N 15 GFR Vessel After Burst Test49
23	S/N 15 GFR Vessel Hydrostatic Test (Hoop Strain at Equator).50

LIST OF FIGURES

Figure		Page
24	S/N 15 GFR Vessel Hydrostatic Test (Hoop Strain at Poles)	51
25	S/N 16 GFR Vessel Hydrostatic Test (Hoop Strain at Equator)	52
26	S/N 16 GFR Vessel Hydrostatic Test (Hoop Strain at Poles)	53
27	Summary Comparison, GFR-Metal and Homogeneous-Metal Pressure Vessel Performance Levels.	56
28	Heat 76235, Sphere Design Chart	59
A-1	True Stress Vs. True Strain at -320°F (Heat 50793).	A-6
A-2	Nominal Stress Vs. Nominal Strain at -320°F (Heat 50793).	A-7
A-3	Room Temperature Response (Heat 50793).	A-8
A-4	Responst at -320°F (Heat 50793)	A-9
A-5	Heat 50793 Biaxial (1:1) Stress-Strain Data	A-10
A-6	Heat 50793 Sphere Design Chart (Based on Tensile Tests & Plasticity Theory).	A-11
A-7	Heat 50793 Sphere Design Chart (Based on Vessel Data)	A-12
A-8	Double Cryogenic Stretch with Intermediate Room Temperature Age (S/N 125)	A-14
A-9	Double Cryogenic Stretch with Intermediate Cure Cycle Age (S/N 139)	A-15
A-10	Biaxial Tensile Specimen Dimensions	A-18
A-11	Test Specimen and Special Grips	A-19
A-12	Biaxial Coupon Test Data, Double Cryogenic Stretch Thermal Aging (True Cryogenic Prestress = 260 ksi).	A-24
A-13	Biaxial Coupon Test Data, Double Cryogenic Stretch R.T. Age (True Cryogenic Prestress - 264 ksi)	A-25

LIST OF FIGURES

Figure		Page
A-14	Biaxial Coupon Test Data, Single Cryogenic Stretch (True Cryogenic Pre-Stress = 305 ksi). .	A-26
A-15	Biaxial Coupon Test Data (Annealed Specimens) .	A-27
A-16	True Stress Vs. True Strain, Double Cryogenic Stretch-Thermal Age-Test Temperature -423°F . .	A-28
A-17	True Stress Vs. True Strain, Double Cryogenic Stretch - R.T. Age, Test Temperature = -423°F	A-29
A-18	True Stress Vs. True Strain, Single Cryogenic Stretch, Test Temperature = -423°F	A-30
A-19	Initial Tensile Loading Cycle and First Tension Tension-Compression Cycle.	A-32
A-20	Typical Loading Cycle	A-33
A-21	Tensile - Compression Test S/N 101	A-34
A-22	Tensile - Compression Test S/N 106	A-35
A-23	Tensile - Compression Test S/N 108	A-36
A-24	Tensile - Compression Test S/N 120	A-37
A-25	Stress-Strain Diagram (Parametric Vessel Design)	A-46
A-26	Stress-Strain Diagram (Initial GFR Spherical Vessel Configuration).	A-53
A-27	Stress-Strain Diagram	A-55
A-28	Stress-Strain Diagram (Low Stress Liner)	A-65

LIST OF TABLES

Table		Page
3-1	Operating and Proof Pressure Ratios for a GFR Sphere Design.	10
3-2	Material Properties for Parametric Vessel Design .	11
3-3	Design Parameters for Initial GFR Spherical Vessel Configurations.	14
3-4	Line Failure Mode Test Results Summary	17
3-5	Summary Tensile Coupon Tests	18
3-6	List of Vessels (Contract NAS 3-11194)	19
3-7	GFR Spherical Vessel Data.	41
4-1	GFR Vessels - Room Temperature Structural Performance Factors.	55
A-1	ARDEFORM Material Inspection Record.	A-2
A-2	ARDEFORM Material Inspection Record.	A-4
A-3	Plasticity Relations Applied to Tensile Coupons and Internally Pressurized Spheres and Cylinders.	A-13
A-4	Bi-Axial Coupon Spheres.	A-17
A-5	Summary of Biaxial Coupon Data, Double Cryogenic Stretch - Room Temperature Aging (True Cryogenic Pre-Stress = 260 ksi).	A-20
A-6	Summary of Biaxial Coupon Test Data, Double Cryogenic Stretch - Thermal Aging between Stretches (True Cryogenic Pre-stress = 260 ksi). .	A-21
A-7	Summary of Biaxial Coupon Tests, Single Cryogenic Stretch. (True Cryogenic Pre-Stress = 305 ksi). .	A-22
A-8	Summary of Biaxial Coupon Tests (Annealed Specimens)	A-23
A-9	Tension-Compression Test Data Summary.	A-31
A-10	Selected Liner Materials Properties.	A-43
A-11	Materials Properties for Parametric Vessel Design	A-45
A-12	Design Parameters for Initial GFR Spherical Vessel Configurations.	A-51
A-13	Liner Failure Mode Test Summary.	A-57
A-14	Summary of Tensile Coupon Tests.	A-58
A-15	GFR Spherical Vessel Data.	A-60

DEVELOPMENT OF A FILAMENT-OVERWRAPPED CRYOFORMED METAL PRESSURE VESSEL

by

D. Gleich

SUMMARY

An analytic and experimental program was performed to define and demonstrate the advantages of using a spherical vessel consisting of a load-bearing cryogenically stretched ARDEFORM 301 stainless steel liner overwrapped with fiberglass for high pressure fluid storage in the 75 to -423°F temperature range. Design, analysis, uniaxial testing at room and cryogenic temperature, vessel fabrication, vessel processing and room temperature vessel testing efforts were conducted. The experimental results demonstrated that ARDEFORM 301 stainless steel spherical glass fiber reinforced (GFR) vessels can be designed to utilize the maximum load-carrying capacities of both the metal liner and the fiberglass in lightweight tankage.

Room temperature hydrostatic tests of three (3) 13 1/2" nominal diameter spherical GFR vessels with nominal 20 mil thick ARDEFORM 301 stainless steel load-bearing liners resulted in (PoV/W) performance parameters (operating pressure times volume divided by weight) 30% higher than those reported for homogeneous 5 Al-2.5 Sn titanium spheres and 40 to 50% higher than previous test results given for inconel X-750 oblate spheroid GFR vessels. The PoV/W value for GFR ARDEFORM 301 stainless steel was in the range of $.44 \times 10^6$ to $.46 \times 10^6$ in.

ARDEFORM GFR sphere test performance equalled theoretical projections previously made for 5 Al-2.5 Sn titanium GFR oblate spheroids. Attainment of the (PV/W) values projected for the titanium GFR vessels is uncertain because of biaxial elongation capability limitations of titanium weldments. This adds significance to the test results obtained in this program.

Parametric studies of ARDEFORM 301 spherical GFR vessels, utilizing cryogenic materials properties obtained in uniaxial testing, project operating pressures at -320°F and -423°F of 26% and 32% higher respectively, than the 3000 psi room temperature value. Ten (10) spherical GFR vessels, with a configuration similar to those tested at room temperature, were delivered for NASA cryogenic testing and evaluation to verify these predicted cryogenic performance increases.

Hydrostatic burst tests of GFR spherical vessels and a fiberglass spherical shell wrapped over an elastimer liner as well as NOL ring specimen tests, have verified again that the full ultimate strength of the fiberglass is developed using the ARDE spherical wrap pattern. Attainment of the 200 ksi minimum design ultimate tensile strength of the unaged ARDEFORM 301 stainless steel spherical liner was also demonstrated by the GFR vessel burst tests.

Stretching techniques at room temperature and at -320°F were successfully used with the thin (20 mil) spherical liners. After the GFR fabrication processing and vessel configuration had been defined by vessel and uniaxial tests, a low GFR vessel development fabrication scrap factor of 13% was demonstrated.

Improved structural performance ARDEFORM 301 stainless steel GFR vessel configurations for temperatures down to -320°F have been identified. By use of other available grades of 301 stainless steel, increased values of burst pressure per unit weight may be obtained. Additional options exist for utilizing the GFR vessel at low liner stress (small tension or compression) at operating pressure thereby providing "fail safe" design in terms of fracture mechanics considerations while still maintaining good operating pressure (PoV/W) values with a high burst to operating pressure safety factor. Investigations are warranted to evaluate the projected performance advantages of these configurations.

1. INTRODUCTION

1.1 Background

Glass filament wound construction has high structural efficiency and good properties in the room to cryogenic temperature range. In order to utilize this material in pressure vessels for cryogenic fluid storage, a metal liner is needed to provide a seal for the permeable fiberglass.

Flexible metal liners (including configurations bonded to the fiberglass shell) have been investigated extensively, references 5 - 10, with little success. In addition to fabrication problems, liners have buckled as well as failed in fatigue under the high biaxial strain cycling required to follow the large deflections that occur during operation of the high strength and relatively low modulus fiberglass shell.

Another metal liner approach is to use a load-bearing non-buckling metal shell that does not have to be bonded to the fiberglass shell. This glass fiber reinforced (GFR) vessel construction can provide considerable weight savings compared to all metal pressure vessels. However, in order for the metal liner and fiberglass shell to operate at their maximum structural efficiencies, a proper prestress (compression in the liner and tension in the fiberglass) must be achieved when the vessel is unpressurized.

The design requirements and advantages of combining a load-bearing metal shell with an overwrapped glass filament shell for high pressure fluid storage in the 75 to -423°F temperature range were investigated analytically and experimentally under a previous NASA contract, NAS 3-6292, references 1 and 2. The results of this study projected significant theoretical weight advantages for 5 Al-2.5 Sn titanium and 2219-T62 aluminum GFR oblate spheroid pressure vessels.

Because of anticipated biaxial elongation problems with welded material, the theoretically advantageous titanium and aluminum GFR configurations were not selected for manufacture. Instead, inconel X-750 oblate spheroid GFR vessels were fabricated and tested to check feasibility. The experimental results with the inconel X-750 GFR oblate spheroid showed feasibility of concept and demonstrated that

PV/W, or achieved weight values could be calculated reliably.

ARDE's processing techniques were selected as the most promising method of overcoming the existing problem areas in that (1) cryoforming techniques permitted stretching welds and parent material without degradation, (2) spherical fiberglass wrap patterns had been demonstrated to be as efficient as oblate spheroids and (3) metal characteristics after forming showed high toughness down to -423°F .

The present program was undertaken, therefore, to verify the high performance potential of ARDEFORM 301 stainless steel GFR spherical vessels and to evaluate the application of this technology to high pressure fluid storage in the 75 to -423°F temperature range. An ARDEFORM 301 GFR spherical vessel design point of 1200 in³ internal volume, 3000 psi operating pressure and 100 cycles of operation between the unpressurized and operating pressure states was selected by NASA for the evaluation. This report presents a detailed summary and discussion of all work performed during the program.

1.2 Program Description

The objective of this analytic and experimental work was to define the design and fabrication parameters and to demonstrate the advantages of an ARDEFORM 301 cryoformed stainless steel GFR spherical vessel configuration for high pressure fluid storage in the 75 to -423°F temperature range.

The program consisted of a six-task effort which included material procurement and evaluation, determination of material properties at 75°F , -320°F and -423°F , parametric studies and vessel design, vessel fabrication, vessel testing and evaluation of results. After design, as well as vessel and uniaxial testing effort, had defined the fabrication processing and configuration of the ARDEFORM 301 stainless steel cryoformed GFR vessel, thirteen (13) of the finalized configuration 13 1/2" nominal diameter GFR spheres were fabricated. Three (3) vessels were tested at room temperature and ten (10) vessels were delivered for NASA cryogenic testing and evaluation.

2. DESCRIPTION OF GFR VESSELS

The glass filament reinforced (GFR) vessel considered herein is composed of a cryogenically stretch formed, high strength ARDEFORM 301 stainless steel spherical liner overwrapped with fiberglass. Both the metal liner and the fiberglass resist part of the pressure load. The metal liner achieves its strengthening and final size by means of the straining done during the cryogenic stretch forming operations at LN₂ temperature. Since the ultimate strain of the fiberglass is about 3%, and the ultimate biaxial strain of the spherical metal liner composed of initially annealed material is approximately 8%, a two-stage cryogenic stretch forming operation must be done. The liner, by itself, is cryogenically stretch formed typically 4% plastically in the first operation and then fiber wrapped. The fiber wrapped liner is then subjected to a second cryogenic plastic stretch of approximately 1-2%. After the cryogenic stretch pressure is removed and the vessel has sprung back elastically to its room temperature state, the fiberglass is in initial tension and the metal liner is in initial compression. The GFR vessel operates then, between its initial prestressed state at zero internal pressure and its operating pressure condition. One hundred (100) such cycles at room temperature between zero and 3000 psi operating pressure at high structural efficiency (large PV/W values) are required for the 1200 cubic inch internal volume GFR spherical vessel configuration.

The problems were: (1) to design the vessel, selecting the appropriate design and fabrication parameters needed to achieve the required vessel performance (high PV/W with specified cycle life) without the liner buckling or yielding in compression and without fiberglass creep or premature fatigue of the liner and/or the fiberglass and (2) to successfully fabricate these high performance GFR vessel configurations.

The efforts and accomplishments made to define and resolve these problems are discussed in the next section.

3. TECHNICAL DISCUSSION

This section describes the technical effort and accomplishments, presents analytic and test data, details problem areas encountered during the program and discusses approaches taken to resolve these problems. The program effort included materials properties and fabrication processing determination, development of appropriate design data as well as parametric design studies in support of the GFR vessel design and fabrication work. Testing was performed to define and verify the design, fabrication and performance of the GFR vessels. These various aspects of the program are discussed in detail herein.

3.1 Material

A low silicon heat (HT 50793) was procured, inspected and certified. ARDE inspection data, together with tensile test results and bi-axial correlation information are given in Appendix 1, Section 7.1.

3.2 Material Test Results

3.2.1 Material Properties

A modified ELI grade of 301 (HT 50793) characterized by low carbon, low silicon, low gas content and tight chemistry control was procured for use as GFR liners. Uniaxial and biaxial testing and correlation was accomplished. In addition, tensile specimens cut from three (3) spheres approximately 22 inches in diameter were utilized to determine yield point, ultimate tensile strength, Young's modulus and Poisson's ratio at room temperature, -320°F and -423°F . Samples of cryostrained specimens were also sent to the National Bureau of Standards for determination of thermal contraction coefficients and density values. The material certification, detail test procedures and results are shown in the Appendix, Sections 7.1 to 7.4.

A summary of average or design values obtained are shown in the following table. Note that the biaxial coupons were double stretched and thermally treated to simulate the two step cryostraining and the resin curing process. Comparison of data reported in the Appendix for a single stretch, no thermal treatment indicated similar results.

ARDE, INC.

AVERAGE RESULTS FOR HT. 50793 AFTER 260,000 PSI
TRUE PRE-STRESS AT -320°F

UNIAXIAL COUPONS

BIAXIAL COUPONS

SPHERES

(Double cryostretch immediate thermal age)

Nominal .2% Yield Strength, PSI

194,000 @ R. T.	171,000 @ R. T.	200,000 @ R.T.
285,000 @ -320°F	226,000 @ -320°F	
----- @ -423°F	274,000 @ -423°F	

Nominal Ultimate Strength, PSI

212,000 @ R. T.	213,000 @ R. T.
299,000 @ -320°F	292,000 @ -320°F
----- @ -423°F	310,000 @ -423°F

Modulus of Elasticity PSI x 10⁻⁶

21.5 @ R. T.
22.7 @ -320°F
27.7 @ -423°F

Poisson's Ratio

.29 @ R. T.
.29 @ -320°F
.32 @ -423°F

Elongation 2" Gage Length

7.7% @ R. T.	7.7% @ R. T.
12.2% @ -320°F	12.2% @ -320°F
1.7% @ -423°F	1.7% @ -423°F

Thermal Contraction Coefficient

<u>R.T. to -320°F</u>
4.59 x 10 ⁻⁶ in/in°F
<u>R. T. to -423°F</u>
3.78 x 10 ⁻⁶ in/in°F

Density

.27 #/in³

CERTIFIED CHEMISTRY, % Unless Noted

C - .03, Mn - .01, Si - .07, CR - 18.16, Ni - 7.57, Mo - 2.7, N - .04, P&S - .015, H - 20 PPM,
O - 37 PPM

3.2.2 Tension - Compression Coupon Data

Uniaxial tensile - compression specimens were fabricated, prestrained at -320°F and thermally treated, as applicable. The specimens were then tension - compression cycled at room temperature. The prescribed initial loading consisted of plastic tension to determine the initial .2% tensile yield point. This was followed by the first tension - compression cycle between $\pm 90\%$ of initial .2% tensile yield. It was found that compression yield point was less than 90% of tensile yield point. The material was, therefore, initially yielded both in tension and compression. Tension - compression cycles at $\pm 90\%$ of initial .2% tensile yield point were then continued for a total of 100 cycles or failure, whichever occurred first. These aforementioned tension - compression loading cycles are sketched on Figures A-19 and A-20 of Appendix 3, Section 7.3, together with a summary of the test data as well as typical variations of tensile and compressive .2% yield point and total strain with number of cycles.

The tension - compression test data indicated the following:

1. Neglecting such factors as buckling at the grips, necking and fracture outside of the gage section, most specimens achieved the required 100 cycles at the prescribed high cyclic tension - compression stress level.
2. A considerable Bauschinger effect was produced by tension - compression cycling. There was significant reduction in .2% tensile and compressive yield points as well as an increase in total strain with increased number of cycles. These results are not surprising considering the high cyclic stress level ($\pm 90\%$ of initial .2% tensile yield stress) following an initial tensile and compressive plastic loading.

In terms of GFR vessel design, it is apparent that:

- A) The liner should not be yielded in tension at operating or proof pressure or yielded in compression at the zero pressure condition. The liner should be elastically cycled between zero pressure compression and operating pressure tension so that fatigue (or elastic buckling) and

not Bauschinger effect (followed by plastic buckling) will govern the liner design. This elastic behavior is feasible with the ARDEFORM GFR configuration since the plastic deformation, which transforms the material and raises its tensile and compressive yield points as well as provides the prestress in the liner and fiberglass upon release of load, is performed as part of the fabrication process. The liner will subsequently behave elastically up to its new yield points. There is no need to ever again plastically deform the liner, except to determine burst pressure.

B) If the ARDEFORM 301 stainless steel liner is yielded initially in tension and compression, the cyclic stress level applied for 100 cycle operation should be less than $\pm 90\%$ of initial tensile yield stress. A preliminary value of $\pm 65\%$ of initial tensile yield stress is estimated based on analysis of the test data as summarized in Table A-9 of Appendix 3.

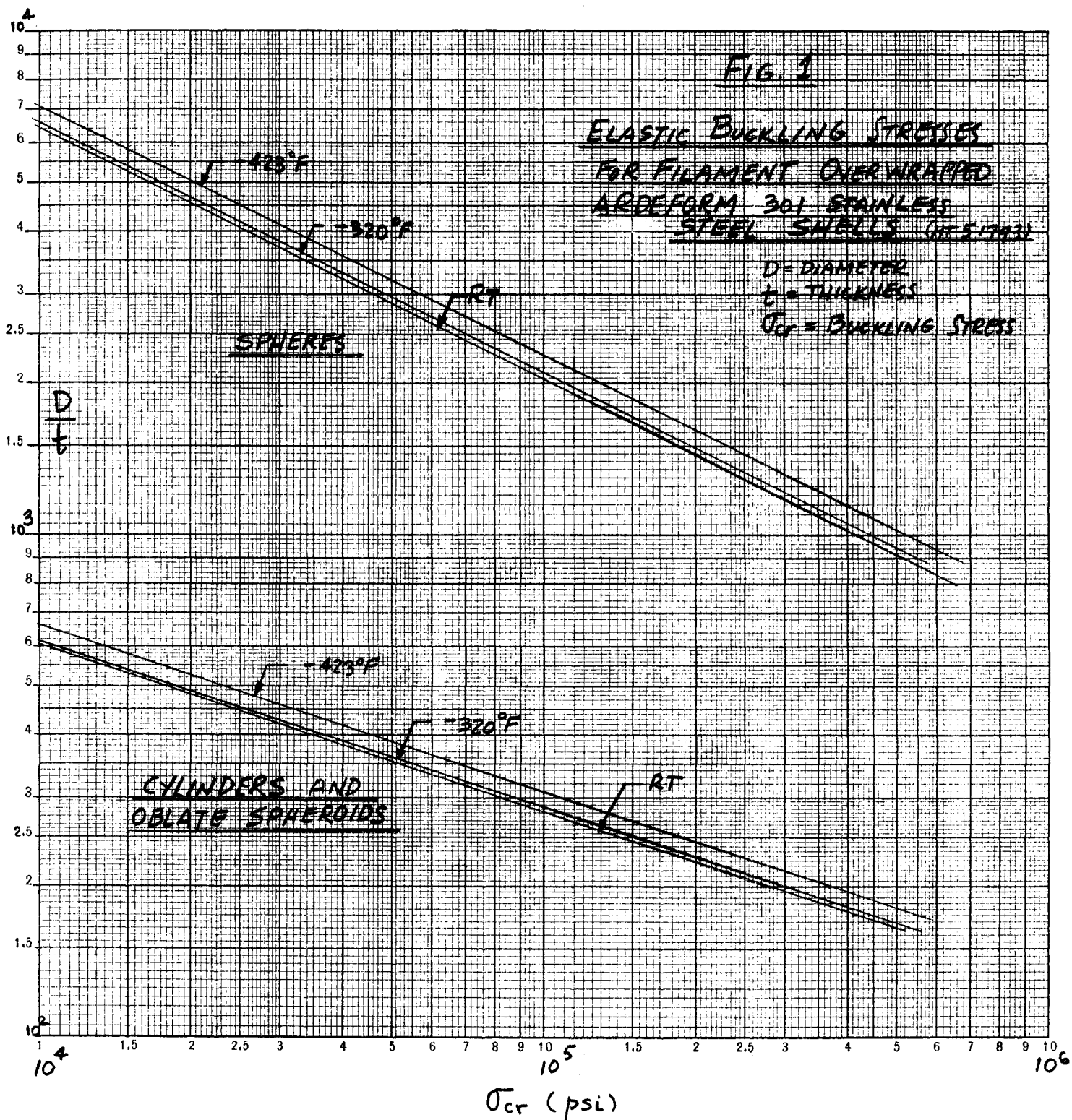
C) Although a severe (and interesting) condition, plastically yielding the liner initially in both tension and compression followed by cycling is not realistic for ARDEFORM liners for the reasons given in A) above. Test data for initial elastic tensile and compressive loading ($< .2\%$ offset strain) followed by elastic cycling are obviously needed before one can define the permissible magnitude of cyclic stress for ARDEFORM 301 stainless steel liners.

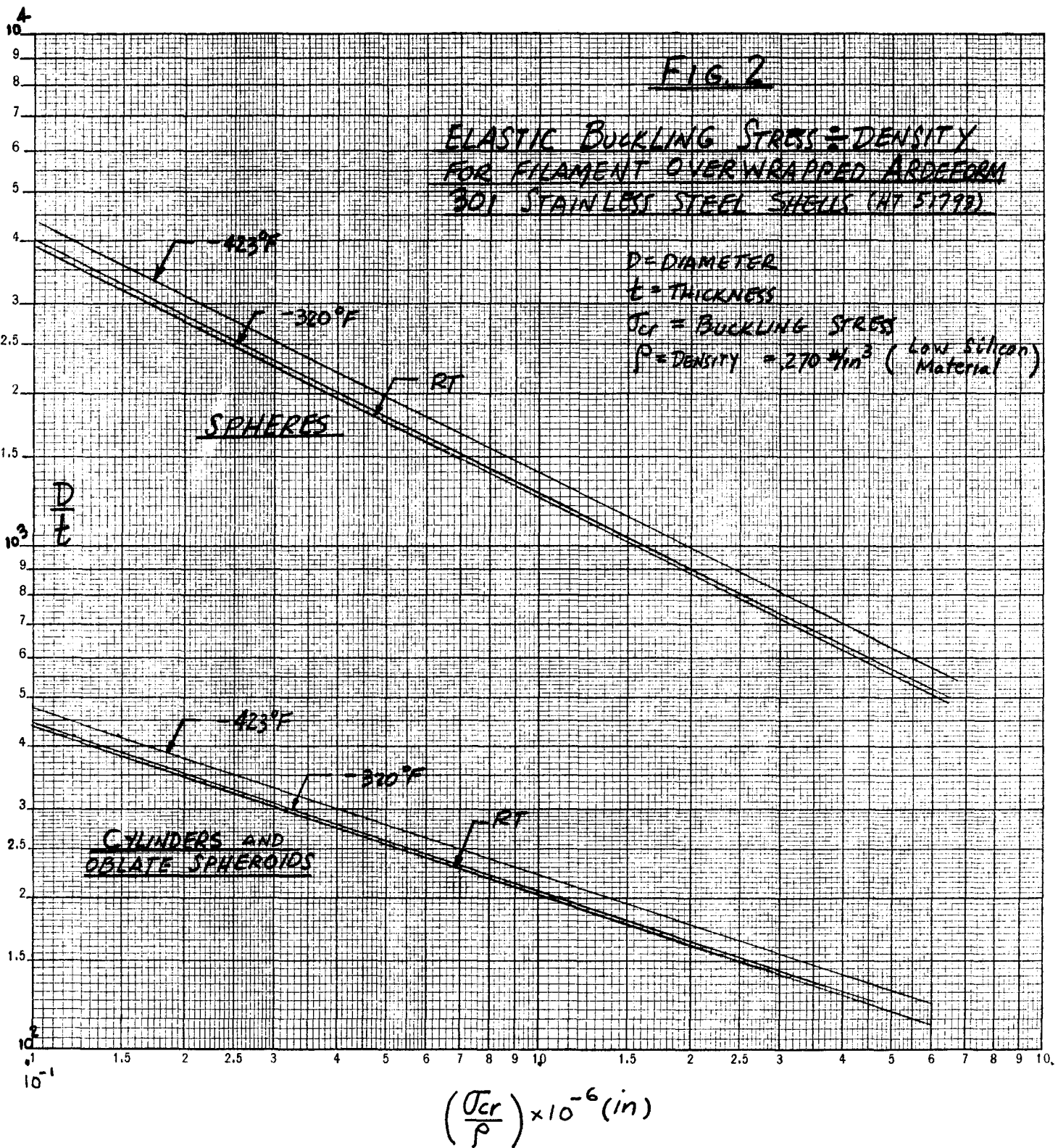
3.3 Vessel Design

3.3.1 Parametric Design Curves

Figures 1 and 2 herein, give elastic buckling stresses and elastic buckling stress divided by density versus diameter to thickness ratio for spheres, cylinders and oblate spheroids at room temperature, -320°F and -423°F .

These buckling design curves are based on the materials property data described in section 3.2. Empirical buckling equations given in NASA CR-54855 (reference 1) were used as a basis for establishing elastic compressive allowable stresses. The detailed equations





are discussed in the Appendix 5, Section 7.5.1.

3.3.2 Vessel Parametric Design

A GFR spherical vessel parametric design was made based on a prescribed 10% margin between proof and operating pressure at room temperature. The objective of this parametric design was to determine the ratios of proof and operating pressures at cryogenic temperatures to the corresponding room temperature values. Materials properties used were based on the ARDEFORM 301 stainless steel test results discussed in Section 3.2 and typical S994 fiberglass properties.

The results of this spherical GFR vessel parametric design study are given in Table 3-1 below:

TABLE 3-1 Operating and Proof Pressure Ratios
For a GFR Sphere Design

Temperature	RT	-320°F	-423°F
<u>Proof Pressure at Temp.</u> Operating Pressure at RT	1.10	1.34	1.42
<u>Operating Pressure at Temp.</u> Operating Pressure at RT	1.00	1.26	1.32
<u>Operating Pressure at Temp.</u> Proof Pressure at RT	0.91	1.15	1.20

The calculations are detailed in Appendix 5, Section 7.5.2. The materials properties utilized and the resultant stress-strain diagrams are shown in Table 3-2 and Figure 2a.

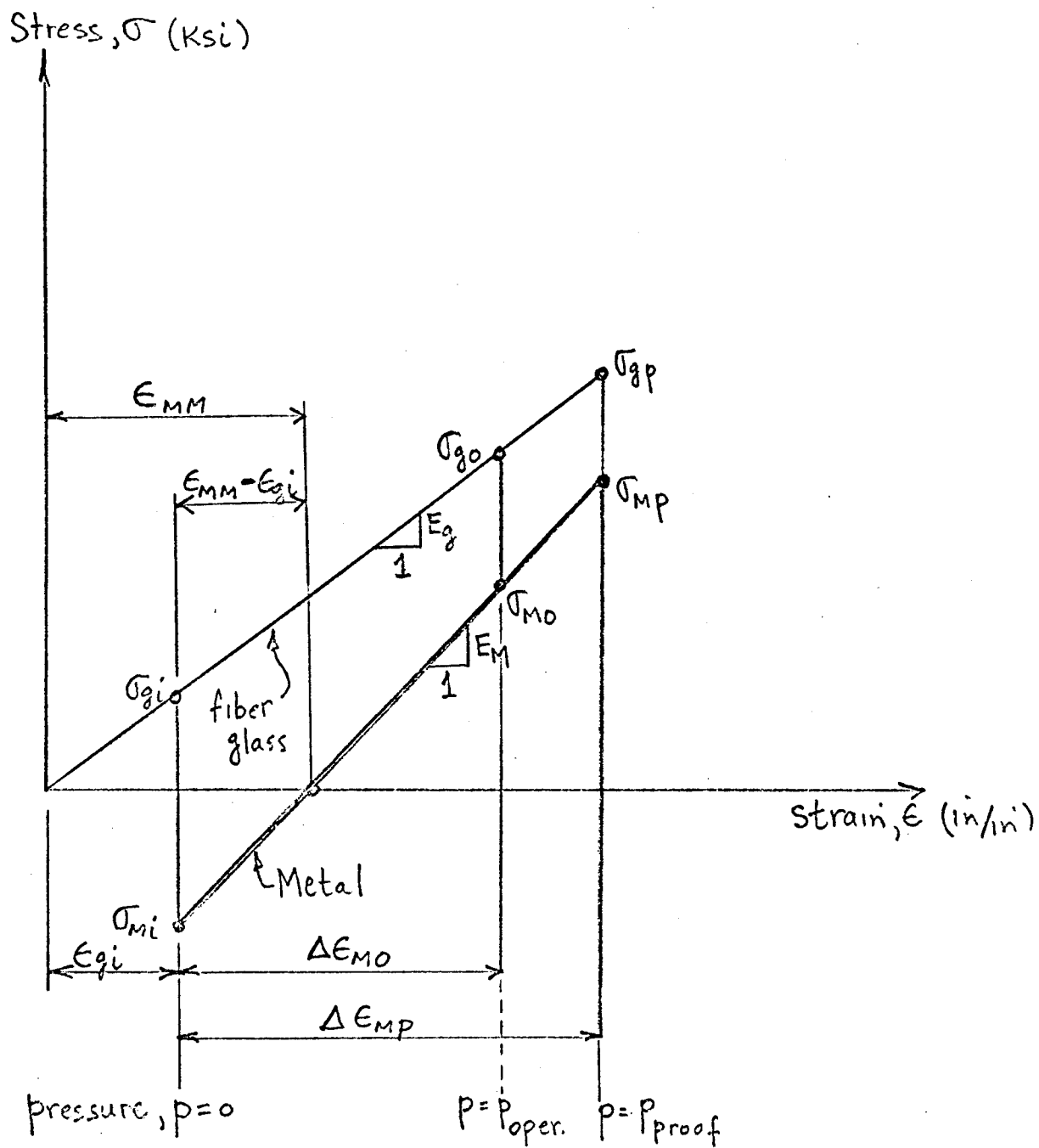
3.3.3 Initial Spherical GFR Design(s)

Based on the parametric studies and the test data discussed in sections 3.3.1 and 3.3.2, a series of initial spherical GFR vessel designs were made and the vessels constructed and/or tested. The GFR spherical vessels were designed to operate at 3000 psi pressure at 75°F and to have internal volume of 1200 cubic inches. S-994 glass with a resin system consisting of Epon 828/DSA/Empol

TABLE 3-2

MATERIAL PROPERTIES FOR PARAMETRIC VESSEL DESIGN

Metal Liner	RT	-320°F	-423°F
Allowable Operating Tensile Stress (ksi), σ_{Mo}	$\left(\begin{matrix} 180 = .9x \\ \sigma_{yrt} \end{matrix} \right)$	$1.41 \times 180 = 254$	$1.65 \times 180 = 297$
Allowable Max. Operating Compressive Stress (ksi), σ_{Mi}	$-.65 (180) = -117$	$-1.41 \times 117 = -165$	$-1.65 \times 117 = -193$
Young's Modulus, $E_M \times 10^{-3}$ (ksi)	21.5	22.7	27.7
Poisson's Ratio, ν	.29	.29	.32
Coefficient of Contraction	---	4.59	3.78
$\alpha \left(\begin{matrix} \text{between} \\ \text{R.T. and T} \end{matrix} \right) \text{ (in/in}^\circ\text{F)} \times 10^6$			
<u>S-994 Glass</u>			
Allow Operating Tensile Stress (ksi), σ_{go}	200	297	297
$E_g \times 10^{-3}$ (ksi)	12.4	13.6	13.6
$\alpha \left(\begin{matrix} \text{between} \\ \text{R.T. and T} \end{matrix} \right) \text{ (in/in}^\circ\text{F)} \times 10^6$	---	2.01	2.01



STRESS-STRAIN DIAGRAM
(Parametric Vessel Design)

FIGURE 2a

1040/BDMA with the distribution in parts by weight of 100/115.9/20/1 was prescribed as the fiber wrap. The design parameters initially utilized are shown Table 3-3 and Figures 2b and 2c. These vessels either failed during the second cryogenic stretch forming operation at -320°F or failed prematurely during room temperature hydrotesting for vessel serial number (S/N) 1, 2 (heat 73413) and S/N 1, 3, 8, 10, 11 and 13 for heat 50793. Table 3-6, following, lists all vessels manufactured. Typical design calculations are given in Appendix 5, Section 7.5.3. The GFR vessel designs are illustrated on ARDE drawings D 3728 and D 3731 (Figures 3 and 6) which give the vessel preform and postform (final assembly) configurations.

Revised designs, incorporating the results of the aforementioned initial design configuration experience and additional tensile test and liner test data, were then made. These final GFR vessel design configurations are discussed in detail in the next section.

3.3.4 Final Spherical GFR Vessel Designs (Revised Design)

The results of the fabrication and/or test failures of the initial GFR vessel configurations were analyzed. In addition, liner "failure mode" tests were made to determine the probable failure causes. Summary of these tests are shown in Tables 3-4 and 3-5. Detailed discussion is given in Appendix 6, Section 7.6.2.

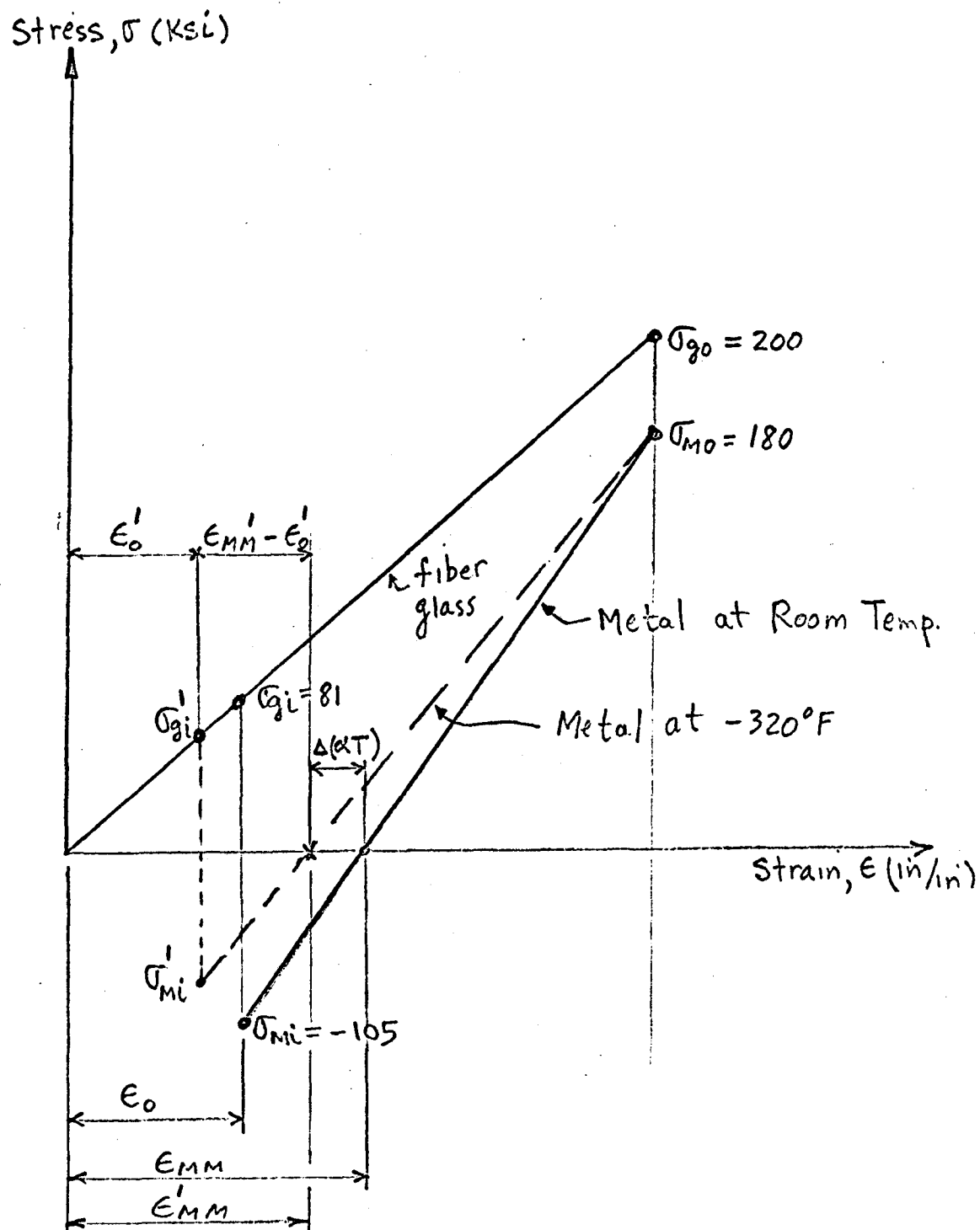
All failures were in the metal liner boss region on the spherical membrane shell side of the boss to head weld. The problem was not weld induced (failures were in parent material) and no metallurgical causes could be found. Further, the failure regions were not necessarily the thinnest liner areas; local head areas about 1 to 2 inches from the girth weld were thinner in many cases. The problem was caused by weld distortion effects produced by the boss weld in the thin (approximately 20 mil) liner head which resulted in sharp local curvatures. This region of very sharp local curvature, verified by inspection of liners, was strained considerably more than other regions of the vessel during stretching and/or pressurization and this high local strain exceeded the available elongation capacity of the liner materials which

TABLE 3-3

DESIGN PARAMETERS FOR INITIAL GFR SPHERICAL VESSEL CONFIGURATIONS

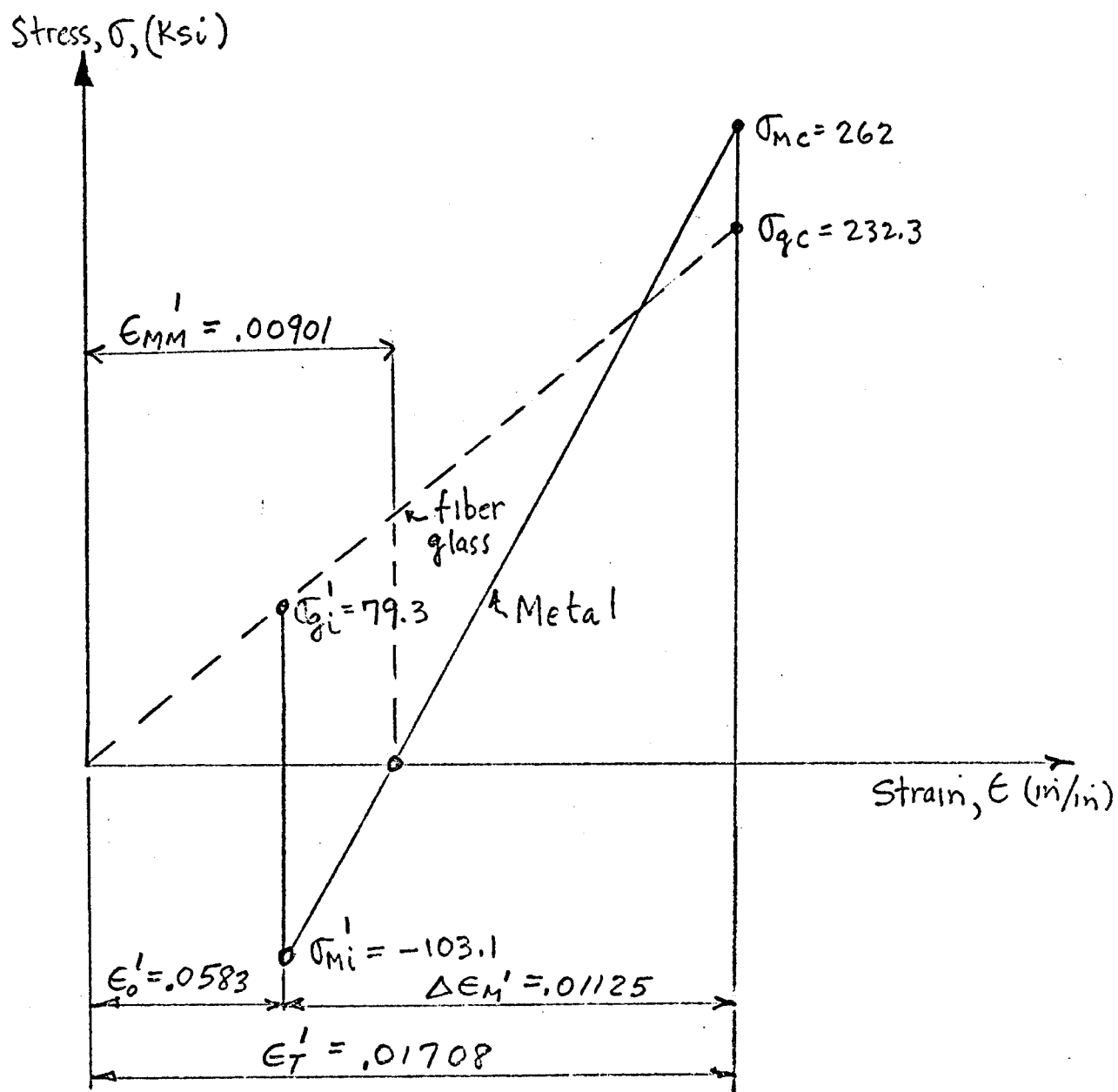
Vessel Internal Volume, $V = 1,200 \text{ in}^3$
 Operating Pressure, $P_o = 3,000 \text{ psi}$

<u>Operating Stress Level (ksi)</u>	<u>RT</u>	<u>-320°F</u>
Metal, $\sigma_{mo} = (.9 \times \text{yield point})$	= 180	---
Fiber Glass, $\sigma_{go} = (.6 \times \text{ultimate})$	= 200	297
<u>Young's Modulus (ksi $\times 10^{-3}$)</u>		
Metal, E_m	= 21	23
Fiber Glass, E_g	= 12.4	13.6
<u>Poisson's Ratio</u>		
Metal ν_m	= .29	.29
<u>Coefficient of Thermal Contraction</u> (between R.T. and -320°F) in/in °F $\times 10^6$		
Metal, α_m	=	4.59
Fiber Glass, α_g	=	2.01
<u>Density (#/in³)</u>		
Metal, $\rho_m = (.270)$		
Composite Fiberglass, $\rho_{gc} = (.074)$		
<u>Volume Fraction Fiberglass</u> (.65, corresponding to 20% resin content)		



STRESS-STRAIN DIAGRAM
(Initial GFR Spherical Vessel Configuration)

FIGURE 2b



STRESS-STRAIN DIAGRAM AT -320°F

FIGURE 2c

TABLE 3-4 - LINER FAILURE MODE TEST RESULTS SUMMARY

<u>S/N</u>	<u>Remarks</u>
9	No failure; cryostrains exceeded total liner strain required for GFR vessel. Proved material satisfactory if no thermal cure cycle effects present.
10	Demonstrated lack of elongation due to weld distortion effects, high first cryostretch and thermal aging effects.
11	Plastic strain at burst much more than required in GFR vessel. Proved that reduction in first cryostrains would result in sufficient elongation to failure.
13	Failure mode same as for tests with water. Proved hydrogen embrittlement not the problem.
33	This thicker vessel with much less weld distortion subsequently hydrostretched to 1.5% plastic strain without failure. Demonstrated material and construction satisfactory if weld distortion effects minimized.

TABLE 3-5

SUMMARY OF TENSILE COUPON TESTS

	S/N 500	S/N 503	S/N 504
A_0 (Initial Area) - in^2	.0617	.0626	.0627
P_1 (Initial Stretch Load) - #	6170	7500	8480
σ_{N1} (Nominal Stress - 1st Stretch) - $\#/\text{in}^2$	100,000	120,000	135,000
A_1 (Area After 1st Stretch) - in^2	.0589	.0590	.0585
ϵ_{p1} (Plastic Strain) - in/in	.047	.060	.072
σ_{T1} (True Stress - 1st Stretch) - $\#/\text{in}^2$	105,000	127,000	145,000
Thermal Aging 2 hrs. @ 150°F & 4 hrs. @ 300°F			
P_2 (2nd Stretch Load) - #	9600	11,900	13,000
σ_{N2} (Nominal Stress) - $\#/\text{in}^2$	163,000	202,000	222,000
A_2 (Area After 2nd Stretch) - in^2	.058	.058	.0576
ϵ_{p2} (Plastic Strain) - in/in	.017	.018	.017
σ_{T2} (True Stress) - $\#/\text{in}^2$	165,000	205,000	226,000
Room Temperature Nominal Yield Strength - $\#/\text{in}^2$	134,000	143,000	163,000
Room Temperature Nominal Ultimate Strength - $\#/\text{in}^2$	192,000	202,000	199,000

TABLE 3-6
LIST OF VESSELS
(Contract NAS 3-11194)

<u>Vessel S/N</u>	<u>Heat No.</u>	<u>Description</u>	<u>Remarks</u>
1	73413	Buckling test GFR Vessel	Failed prematurely during second cryostretch.
2	73413	Buckling test GFR Vessel	Failed prematurely during second cryostretch.
1	50793	GFR Vessel	Failed prematurely during RT hydro test
2	50793	GFR Vessel liner--hydrostretch plus first cryostretch	Scrapped--too much thin out in annealed weld regions; defective boss weld.
3	50793	GFR Vessel--hydrostretch plus first cryostretch	Failed prematurely during second cryostretch.
4	50793	GFR Vessel liner--hydrostretch plus first cryostretch	Scrapped--too much thin out in annealed weld regions.
5	50793	GFR Vessel liner--hydrostretch plus first cryostretch	Scrapped--too much thin out in annealed weld regions.
6	50793	GFR Vessel liner--hydrostretch plus first cryostretch	Scrapped--too much thin out in annealed weld regions.
7	50793	GFR Vessel liner--hydrostretch plus first cryostretch	Scrapped--too much thin out in annealed weld regions.
8	50793	GFR Vessel	Failed prematurely on second cryostretch.
9	50793	GFR Vessel liner--modified design pilot unit	Hydrotested at RT after complete processing.
10	50793	GFR Vessel	Failed during second cryostretch.
11	50793	GFR Vessel	Failed during second cryostretch.
12	50793	GFR Vessel liner-hydrostretched and annealed	Scrapped--very thin zones found in equator region.
13	50793	GFR Vessel	Failed during second cryostretch.
14	50793	GFR Vessel P/N D3731	Completely processed and successfully tested.
15	50793	GFR Vessel P/N D3731	Completely processed and successfully tested.
16	50793	GFR Vessel P/N D3731	Completely processed and successfully tested.
33	50793	Heat Evaluation Sphere (7.34" Diameter--X.055 Well)	No failure after cryostretching.
17, 19, 21 to 26	50793	GFR Vessels P/N D3731	NASA Delivery Units
1 to 3	50793	GFR Vessels (Lightweight Boss P/N D3771)	NASA Delivery Units

resulted in liner failure. Three distinct and related steps were taken to resolve the liner problem:

1. Round the vessel (reduce weld distortion curvature effects) by relatively small plastic room temperature hydrostatic and cryogenic straining followed by annealing prior to vessel cryogenic straining for strengthening and final sizing.
2. Reduce the magnitude of the first cryogenic straining for strengthening in order to provide more available elongation capacity for the final cryogenic stretching after fiber wrap.
3. Reduce the yield point of the liner material which results in increased elongation capability and which requires smaller final cryogenic straining. For high structural efficiency configurations, Item 3 generally results from Item 2.

Tensile tests (specimens S/N 500, 503 and 504) were made to provide a basis for the selection of cryogenic stress and room temperature yield point levels. Table 3-5 gives the results of these tests. Specimen S/N 504 test values were selected as the basis for the revised liner design point. These results were verified by processing a vessel liner (S/N 9) to the selected design point(s) followed by successful hydrostatic testing as detailed in Section 3.5.3.

The revised GFR vessel design (and processing sequence) is outlined below:

A. Round Vessel

Room temperature hydrostatic stretch $\approx 1\%$ strain, anneal. Cryogenic stretch ($S_2 = 100$ ksi nominal stress corresponding to $\approx 2 \frac{1}{2}\%$ strain, anneal.

B. First Cryogenic Stretch for Strengthening

Stretch at LN_2 temperature to $S_2 = 135$ ksi nominal stress and then fiber wrap.

C. Final Cryogenic Stretch

Stretch at LN_2 temperature to a nominal stress of $S_2 = 220$ ksi which will give a room temperature yield point of $S_1 \approx 163$ ksi.

Design strength values selected for the metal liner and fiberglass respectively, at operating pressure were,

$$\begin{aligned}\sigma_{MO} &= .9 (\sigma_{yield}) = .9 (163) = 147 \text{ ksi} \\ \sigma_{go} &= 200 \text{ ksi}\end{aligned}$$

These remedial steps, which successfully resolved the liner problem, resulted in only a small penalty in vessel structural performance. The projected PV/W value at 3000 psi operating pressure for the revised design was reduced only about 4% compared to the estimated value for the original GFR vessel design ($.50 \times 10^6$ versus $.52 \times 10^6$ in.)

Three (3) GFR vessels, S/N 14, 15 and 16 were designed to the aforementioned revised design configuration and successfully built and tested as detailed in section 3.5.4, thus verifying vessel design and fabrication. All subsequent GFR vessels were built to the revised design configuration. Design calculations for the revised GFR vessel design are similar to those previously discussed in Section 3.3.3 and detailed in the appendix, Section 7.5.3, except for the use of the different operating and cryogenic liner stress values.

3.4 Vessel Fabrication

ARDE drawings D3728 to D3731 and D3770 to D3773 (Figures 3 to 10) detail the GFR spherical vessel configurations built. The vessel bosses were designed primarily to interface with the fiberglass wrap vendor's winding machine and hence were not designed specifically for light weight. GFR configuration P/N D3731 (Figure 6) had particularly heavy bosses. A "first cut" lighter weight boss configuration, P/N D3770 is shown on Figure 10. Table 2 gives a complete list of all the GFR vessels built during the program. The finalized GFR vessel fabrication processing used is briefly described below.

3.4.1 Vessel Liner Preform Fabrication

(P/N D3728 or D3771, Figure 3 or 7)

A. Weld Components

Bosses machined from bar stock are welded to hemispherical heads hydroformed from sheet. Two (2) hemispherical head sub-assemblies are welded together at the girth to complete the liner preform assembly; x-ray and die check weld.

B. Round Vessel Liner

Room temperature hydrostretch liner to approximately 1% strain and/or cryogenic stretch at LN_2 temperature to

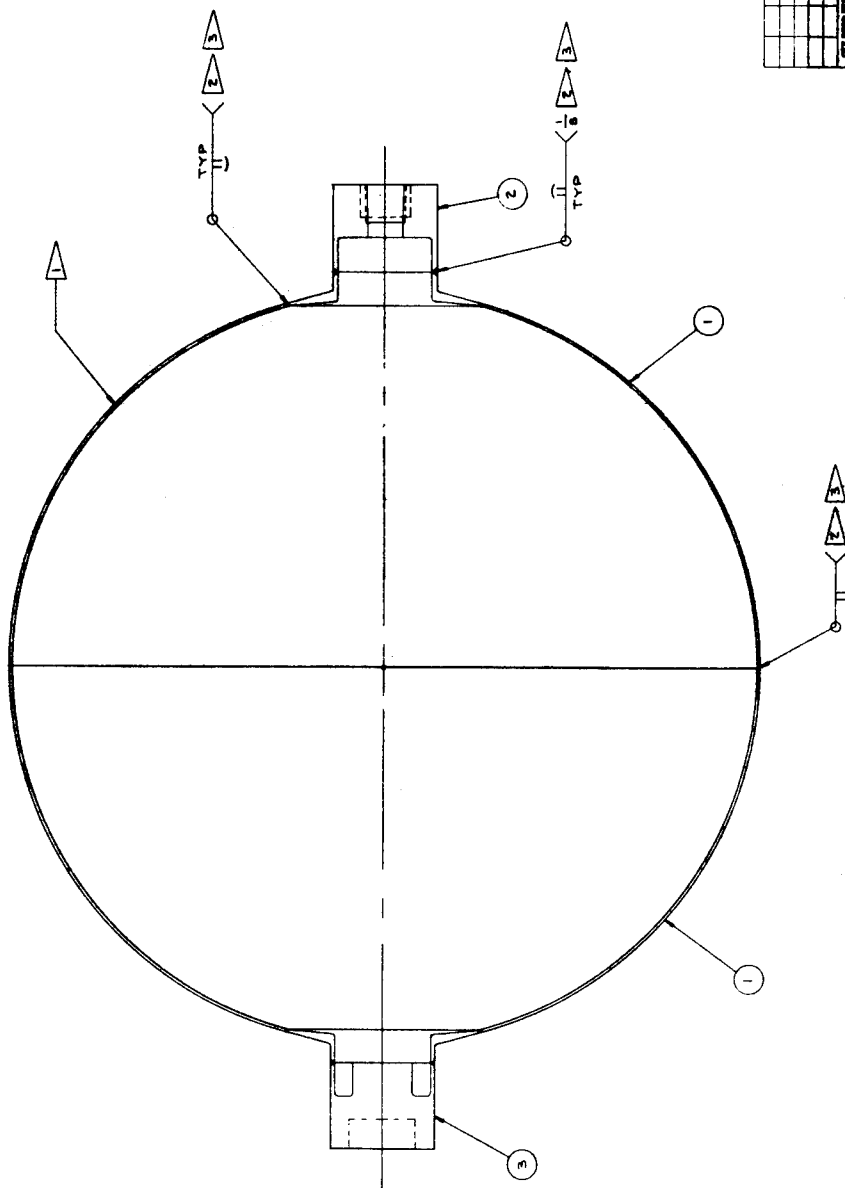
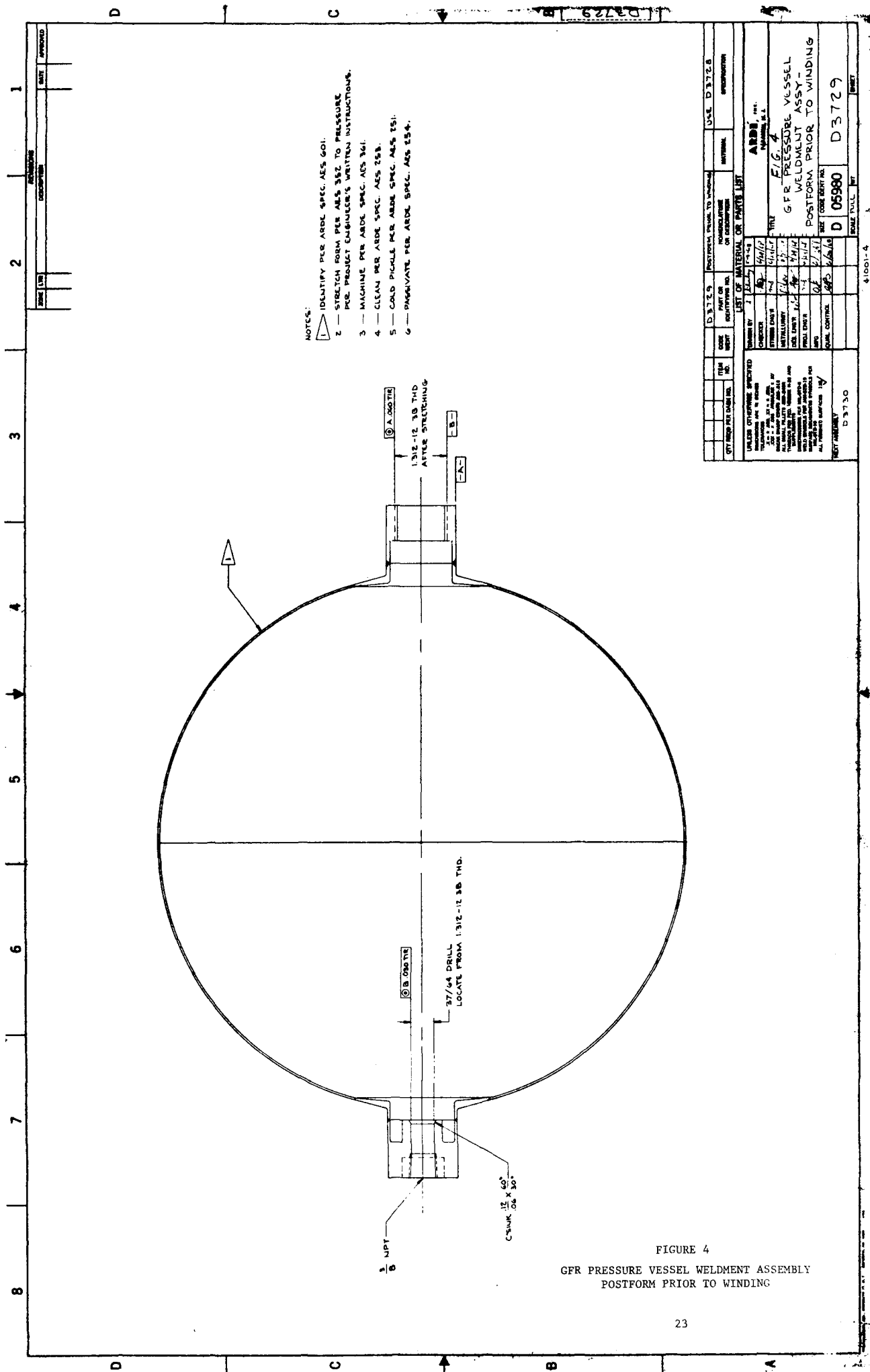


FIGURE 3
GFR PRESSURE VESSEL WELDMENT ASSEMBLY PREFORM

- NOTES:
- 1 IDENTIFY PER ARDE SPEC. AES 601
 - 2 WELD PER ARDE SPEC. AES 801
 - 3 INSPECT WELD PER ARDE SPEC. AES 550
 - 4 HYDRO-STRETCH PER INSTRUCTIONS OF PROJECT ENGINEER.
 - 5 PROCESS PER ARDE SPEC. AES 555 TABLE III, SCHEMATIC 1 THRU 3

DESIGNATION		DATE		APPROVED	
1		2		3	
4		5		6	
7		8		9	
10		11		12	
13		14		15	
16		17		18	
19		20		21	
22		23		24	
25		26		27	
28		29		30	
31		32		33	
34		35		36	
37		38		39	
40		41		42	
43		44		45	
46		47		48	
49		50		51	
52		53		54	
55		56		57	
58		59		60	
61		62		63	
64		65		66	
67		68		69	
70		71		72	
73		74		75	
76		77		78	
79		80		81	
82		83		84	
85		86		87	
88		89		90	
91		92		93	
94		95		96	
97		98		99	
100		101		102	
103		104		105	
106		107		108	
109		110		111	
112		113		114	
115		116		117	
118		119		120	
121		122		123	
124		125		126	
127		128		129	
130		131		132	
133		134		135	
136		137		138	
139		140		141	
142		143		144	
145		146		147	
148		149		150	
151		152		153	
154		155		156	
157		158		159	
160		161		162	
163		164		165	
166		167		168	
169		170		171	
172		173		174	
175		176		177	
178		179		180	
181		182		183	
184		185		186	
187		188		189	
190		191		192	
193		194		195	
196		197		198	
199		200		201	
202		203		204	
205		206		207	
208		209		210	
211		212		213	
214		215		216	
217		218		219	
220		221		222	
223		224		225	
226		227		228	
229		230		231	
232		233		234	
235		236		237	
238		239		240	
241		242		243	
244		245		246	
247		248		249	
250		251		252	
253		254		255	
256		257		258	
259		260		261	
262		263		264	
265		266		267	
268		269		270	
271		272		273	
274		275		276	
277		278		279	
280		281		282	
283		284		285	
286		287		288	
289		290		291	
292		293		294	
295		296		297	
298		299		300	
301		302		303	
304		305		306	
307		308		309	
310		311		312	
313		314		315	
316		317		318	
319		320		321	
322		323		324	
325		326		327	
328		329		330	
331		332		333	
334		335		336	
337		338		339	
340		341		342	
343		344		345	
346		347		348	
349		350		351	
352		353		354	
355		356		357	
358		359		360	
361		362		363	
364		365		366	
367		368		369	
370		371		372	
373		374		375	
376		377		378	
379		380		381	
382		383		384	
385		386		387	
388		389		390	
391		392		393	
394		395		396	
397		398		399	
400		401		402	
403		404		405	
406		407		408	
409		410		411	
412		413		414	
415		416		417	
418		419		420	
421		422		423	
424		425		426	
427		428		429	
430		431		432	
433		434		435	
436		437		438	
439		440		441	
442		443		444	
445		446		447	
448		449		450	
451		452		453	
454		455		456	
457		458		459	
460		461		462	
463		464		465	
466		467		468	
469		470		471	
472		473		474	
475		476		477	
478		479		480	
481		482		483	
484		485		486	
487		488		489	
490		491		492	
493		494		495	
496		497		498	
499		500		501	
502		503		504	
505		506		507	
508		509		510	
511		512		513	
514		515		516	
517		518		519	
520		521		522	
523		524		525	
526		527		528	
529		530		531	
532		533		534	
535		536		537	
538		539		540	
541		542		543	
544		545		546	
547		548		549	
550		551		552	
553		554		555	
556		557		558	
559		560		561	
562		563		564	
565		566		567	
568		569		570	
571		572		573	
574		575		576	
577		578		579	
580		581		582	
583		584		585	
586		587		588	
589		590		591	
592		593		594	
595		596		597	
598		599		600	
601		602		603	
604		605		606	
607		608		609	
610		611		612	
613		614		615	
616		617		618	
619		620		621	
622		623		624	
625		626		627	
628		629		630	
631		632		633	
634		635		636	
637		638		639	
640		641		642	
643		644		645	
646		647		648	
649		650		651	
652		653		654	
655		656		657	
658		659		660	
661		662		663	
664		665		666	
667		668		669	
670		671		672	
673		674		675	
676		677		678	
679		680		681	
682		683		684	
685		686		687	
688		689		690	
691		692		693	
694		695		696	
697		698		699	
700		701		702	
703		704		705	
706		707		708	
709		710		711	
712		713		714	
715		716		717	
718		719		720	
721		722		723	
724		725		726	
727		728		729	
730		731		732	
733		734		735	
736		737		738	
739		740		741	
742		743		744	
745		746		747	
748		749		750	
751		752		753	
754		755		756	
757		758		759	
760		761		762	
763		764		765	
766		767		768	
769		770		771	
772		773		774	
775		776		777	
778		779		780	
781		782		783	
784		785		786	
787		788		789	
790		791		792	
793		794		795	
796		797		798	
799		800		801	
802		803		804	
805		806		807	
808		809		810	
811		812		813	
814		815		816	
817		818		819	
820		821		822	
823		824		825	
826		827		828	
829		830		831	
832		833		834	
835		836		837	
838		839		840	
84					



- NOTES:
- 1 — IDENTIFY PER ARDE SPEC. AES 601.
 - 2 — STRETCH FORM PER AES 352 TO PRESSURE PER PROJECT ENGINEER'S WRITTEN INSTRUCTIONS.
 - 3 — MACHINE PER ARDE SPEC. AES 361.
 - 4 — CLEAN PER ARDE SPEC. AES 353.
 - 5 — COLD PICKLE PER ARDE SPEC. AES 351.
 - 6 — PASSIVATE PER ARDE SPEC. AES 354.

ITEM NO.	ITEM DESCRIPTION	QTY	UNIT	DATE	BY	CHKD	APP'D
1	1/2 NPT	1	PC	10/1/74	WJ		
2	3/8 NPT	1	PC	10/1/74	WJ		
3	1/2 NPT	1	PC	10/1/74	WJ		
4	3/8 NPT	1	PC	10/1/74	WJ		
5	1/2 NPT	1	PC	10/1/74	WJ		
6	3/8 NPT	1	PC	10/1/74	WJ		
7	1/2 NPT	1	PC	10/1/74	WJ		
8	3/8 NPT	1	PC	10/1/74	WJ		
9	1/2 NPT	1	PC	10/1/74	WJ		
10	3/8 NPT	1	PC	10/1/74	WJ		
11	1/2 NPT	1	PC	10/1/74	WJ		
12	3/8 NPT	1	PC	10/1/74	WJ		
13	1/2 NPT	1	PC	10/1/74	WJ		
14	3/8 NPT	1	PC	10/1/74	WJ		
15	1/2 NPT	1	PC	10/1/74	WJ		
16	3/8 NPT	1	PC	10/1/74	WJ		
17	1/2 NPT	1	PC	10/1/74	WJ		
18	3/8 NPT	1	PC	10/1/74	WJ		
19	1/2 NPT	1	PC	10/1/74	WJ		
20	3/8 NPT	1	PC	10/1/74	WJ		
21	1/2 NPT	1	PC	10/1/74	WJ		
22	3/8 NPT	1	PC	10/1/74	WJ		
23	1/2 NPT	1	PC	10/1/74	WJ		
24	3/8 NPT	1	PC	10/1/74	WJ		
25	1/2 NPT	1	PC	10/1/74	WJ		
26	3/8 NPT	1	PC	10/1/74	WJ		
27	1/2 NPT	1	PC	10/1/74	WJ		
28	3/8 NPT	1	PC	10/1/74	WJ		
29	1/2 NPT	1	PC	10/1/74	WJ		
30	3/8 NPT	1	PC	10/1/74	WJ		
31	1/2 NPT	1	PC	10/1/74	WJ		
32	3/8 NPT	1	PC	10/1/74	WJ		
33	1/2 NPT	1	PC	10/1/74	WJ		
34	3/8 NPT	1	PC	10/1/74	WJ		
35	1/2 NPT	1	PC	10/1/74	WJ		
36	3/8 NPT	1	PC	10/1/74	WJ		
37	1/2 NPT	1	PC	10/1/74	WJ		
38	3/8 NPT	1	PC	10/1/74	WJ		
39	1/2 NPT	1	PC	10/1/74	WJ		
40	3/8 NPT	1	PC	10/1/74	WJ		
41	1/2 NPT	1	PC	10/1/74	WJ		
42	3/8 NPT	1	PC	10/1/74	WJ		
43	1/2 NPT	1	PC	10/1/74	WJ		
44	3/8 NPT	1	PC	10/1/74	WJ		
45	1/2 NPT	1	PC	10/1/74	WJ		
46	3/8 NPT	1	PC	10/1/74	WJ		
47	1/2 NPT	1	PC	10/1/74	WJ		
48	3/8 NPT	1	PC	10/1/74	WJ		
49	1/2 NPT	1	PC	10/1/74	WJ		
50	3/8 NPT	1	PC	10/1/74	WJ		
51	1/2 NPT	1	PC	10/1/74	WJ		
52	3/8 NPT	1	PC	10/1/74	WJ		
53	1/2 NPT	1	PC	10/1/74	WJ		
54	3/8 NPT	1	PC	10/1/74	WJ		
55	1/2 NPT	1	PC	10/1/74	WJ		
56	3/8 NPT	1	PC	10/1/74	WJ		
57	1/2 NPT	1	PC	10/1/74	WJ		
58	3/8 NPT	1	PC	10/1/74	WJ		
59	1/2 NPT	1	PC	10/1/74	WJ		
60	3/8 NPT	1	PC	10/1/74	WJ		
61	1/2 NPT	1	PC	10/1/74	WJ		
62	3/8 NPT	1	PC	10/1/74	WJ		
63	1/2 NPT	1	PC	10/1/74	WJ		
64	3/8 NPT	1	PC	10/1/74	WJ		
65	1/2 NPT	1	PC	10/1/74	WJ		
66	3/8 NPT	1	PC	10/1/74	WJ		
67	1/2 NPT	1	PC	10/1/74	WJ		
68	3/8 NPT	1	PC	10/1/74	WJ		
69	1/2 NPT	1	PC	10/1/74	WJ		
70	3/8 NPT	1	PC	10/1/74	WJ		
71	1/2 NPT	1	PC	10/1/74	WJ		
72	3/8 NPT	1	PC	10/1/74	WJ		
73	1/2 NPT	1	PC	10/1/74	WJ		
74	3/8 NPT	1	PC	10/1/74	WJ		
75	1/2 NPT	1	PC	10/1/74	WJ		
76	3/8 NPT	1	PC	10/1/74	WJ		
77	1/2 NPT	1	PC	10/1/74	WJ		
78	3/8 NPT	1	PC	10/1/74	WJ		
79	1/2 NPT	1	PC	10/1/74	WJ		
80	3/8 NPT	1	PC	10/1/74	WJ		
81	1/2 NPT	1	PC	10/1/74	WJ		
82	3/8 NPT	1	PC	10/1/74	WJ		
83	1/2 NPT	1	PC	10/1/74	WJ		
84	3/8 NPT	1	PC	10/1/74	WJ		
85	1/2 NPT	1	PC	10/1/74	WJ		
86	3/8 NPT	1	PC	10/1/74	WJ		
87	1/2 NPT	1	PC	10/1/74	WJ		
88	3/8 NPT	1	PC	10/1/74	WJ		
89	1/2 NPT	1	PC	10/1/74	WJ		
90	3/8 NPT	1	PC	10/1/74	WJ		
91	1/2 NPT	1	PC	10/1/74	WJ		
92	3/8 NPT	1	PC	10/1/74	WJ		
93	1/2 NPT	1	PC	10/1/74	WJ		
94	3/8 NPT	1	PC	10/1/74	WJ		
95	1/2 NPT	1	PC	10/1/74	WJ		
96	3/8 NPT	1	PC	10/1/74	WJ		
97	1/2 NPT	1	PC	10/1/74	WJ		
98	3/8 NPT	1	PC	10/1/74	WJ		
99	1/2 NPT	1	PC	10/1/74	WJ		
100	3/8 NPT	1	PC	10/1/74	WJ		

FIGURE 4
GFR PRESSURE VESSEL WELDMENT ASSEMBLY
POSTFORM PRIOR TO WINDING

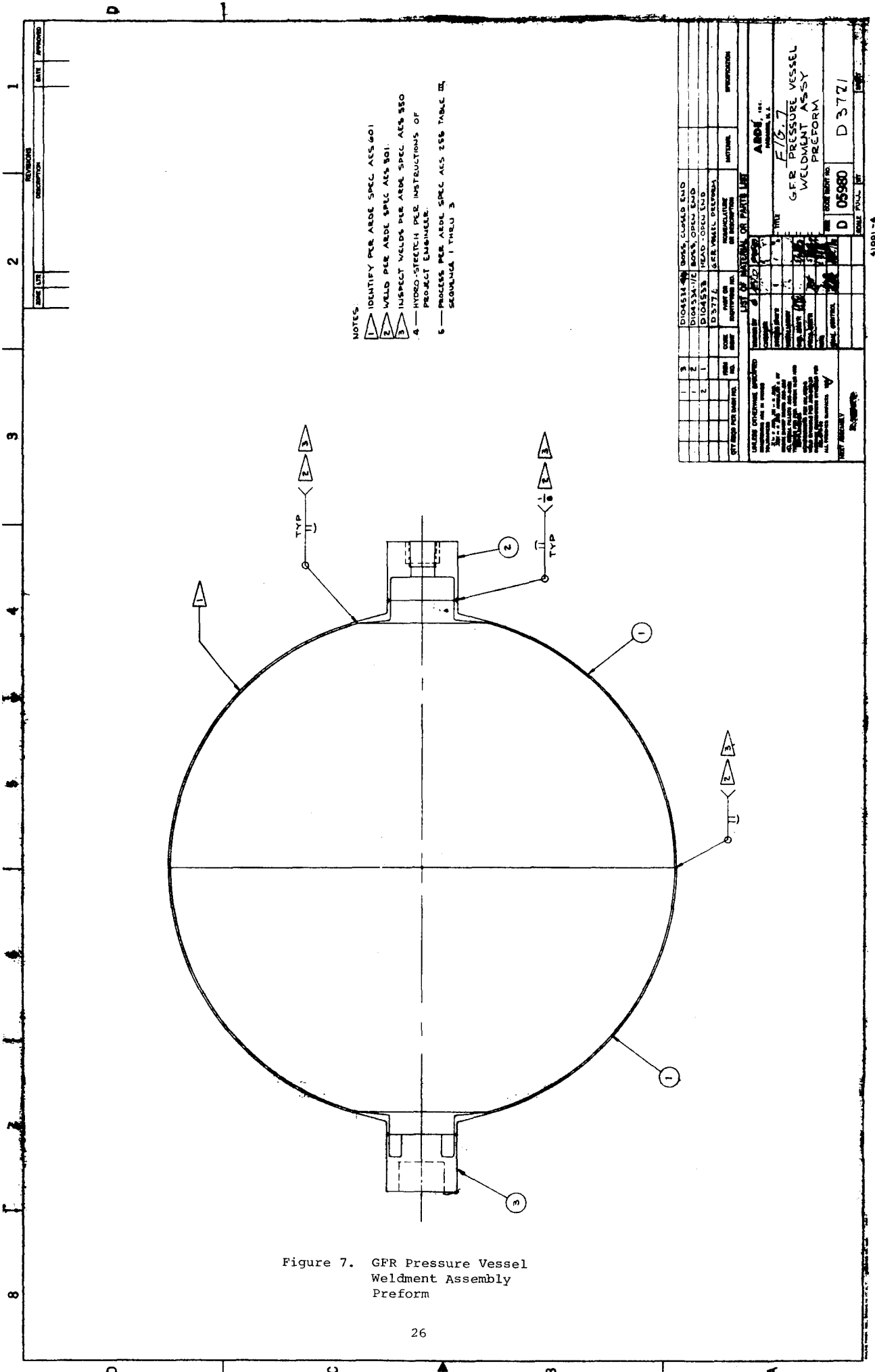
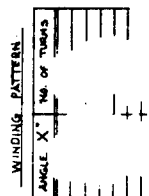


Figure 7. GFR Pressure Vessel Weldment Assembly Preform



NOTES.

ABOVE ATTACHED BAGS ON 1/28
OF 30 BAGS, 100 POUNDS EACH
END 0.0055 - CRAWFORD DR. FARMER, NY
5 GLASS WITH BEING
SYSTEM CONTAINING 20 BAGS 100 POUNDS EACH
1850/1900A. WITH ATTACHMENT OF BAGS IN
WEIGHT OF 100/18750/1.

[illegible]

Figure 9. Filament Winding
Pattern For Type A
GFR Vessel

nominal stress, $S_2 = 100$ ksi. An intermediate and final anneal is used for a two-stage rounding and only a final anneal is utilized for a one-stage rounding process.

C. First Cryogenic Stretch for Strengthening

(P/N D3729 or D3772, Figure 4 or 8) In this operation, the liner preform is immersed in and pressurized with LN_2 to a prescribed stretch pressure value utilizing ARDE's cryogenic stretch forming facility. This facility, schematically shown on Figure 11 for a cylindrical preform, consists, in general, of a stretch pit, LN_2 supply, LN_2 pumps, cryostat, associated instrumentation and controls and a stretch die (if required). No stretch die was used in this program.

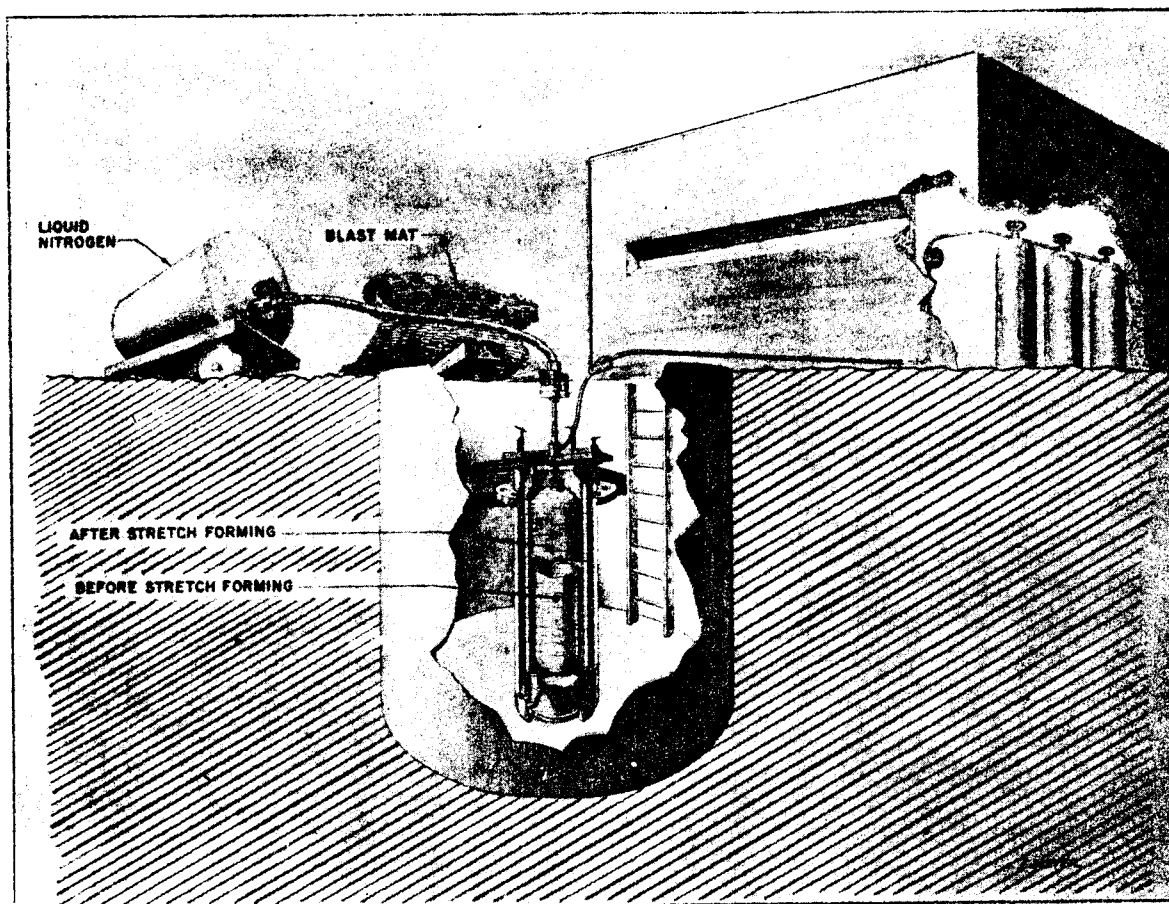
During the first cryogenic stretch for strengthening the vessel liner preform is stretched at LN_2 temperature to a nominal stress of $S_2 = 135$ ksi. It is then cleaned and packaged for shipment to the fiberglass wrap vendor. A photograph of a fabricated spherical liner is shown on Figure 12.

3.4.2 Fiberglass Overwrap of Vessel Liner

(P/N D3730 or D3773, Figure 5 or 9) The partially cryogenically stretch formed liner is next overwrapped with fiberglass. Wet winding using S994 glass and a NASA prescribed resin system composed of Epon 828/DSA/Empol 1040/BDMA with the distribution in parts by weight of 100/115.9/20/1 was utilized. The elevated temperature cure cycle employed was two hours at $150^\circ F$ followed by four hours at $300^\circ F$.

The ARDE high structural efficiency fiberglass wrap pattern used was a great circle winding type. Essentially uniaxial fiberglass properties were obtained in the biaxial sphere wrap. This was evidenced by comparison of NOL ring test results with burst test results of a spherical fiberglass vessel as detailed in Section 3.5.2.

The fiber wrapping, designed and specified by ARDE, was performed by Walter Kidde and Company under a subcontract. An existing spherical winding machine, modified by a special cam to give the prescribed ARDE wrap



SCHEMATIC-CRYOGENIC
STRETCH FACILITY

FIGURE 11

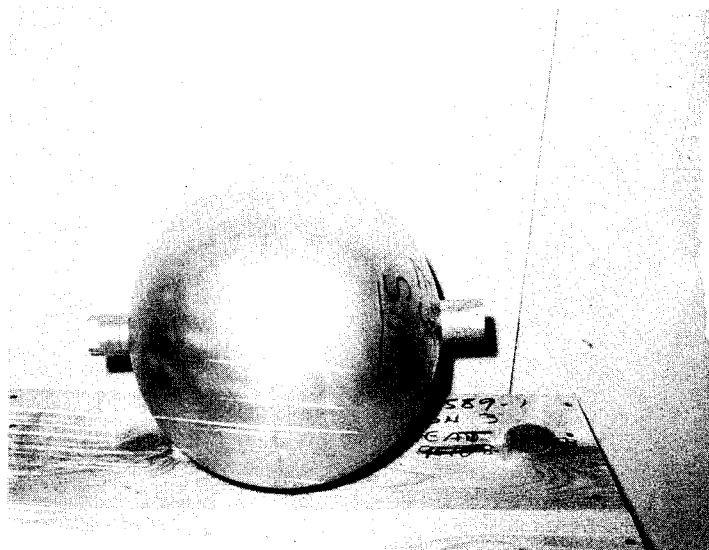


FIGURE 12

GFR VESSEL LINER

pattern, was utilized for this effort. A schematic and a photograph of the spherical winding machine are given on Figures 13 and 14. A completed fiber wrapped liner is shown on Figure 15.

3.4.3 Final Cryogenic Stretch Forming Operation

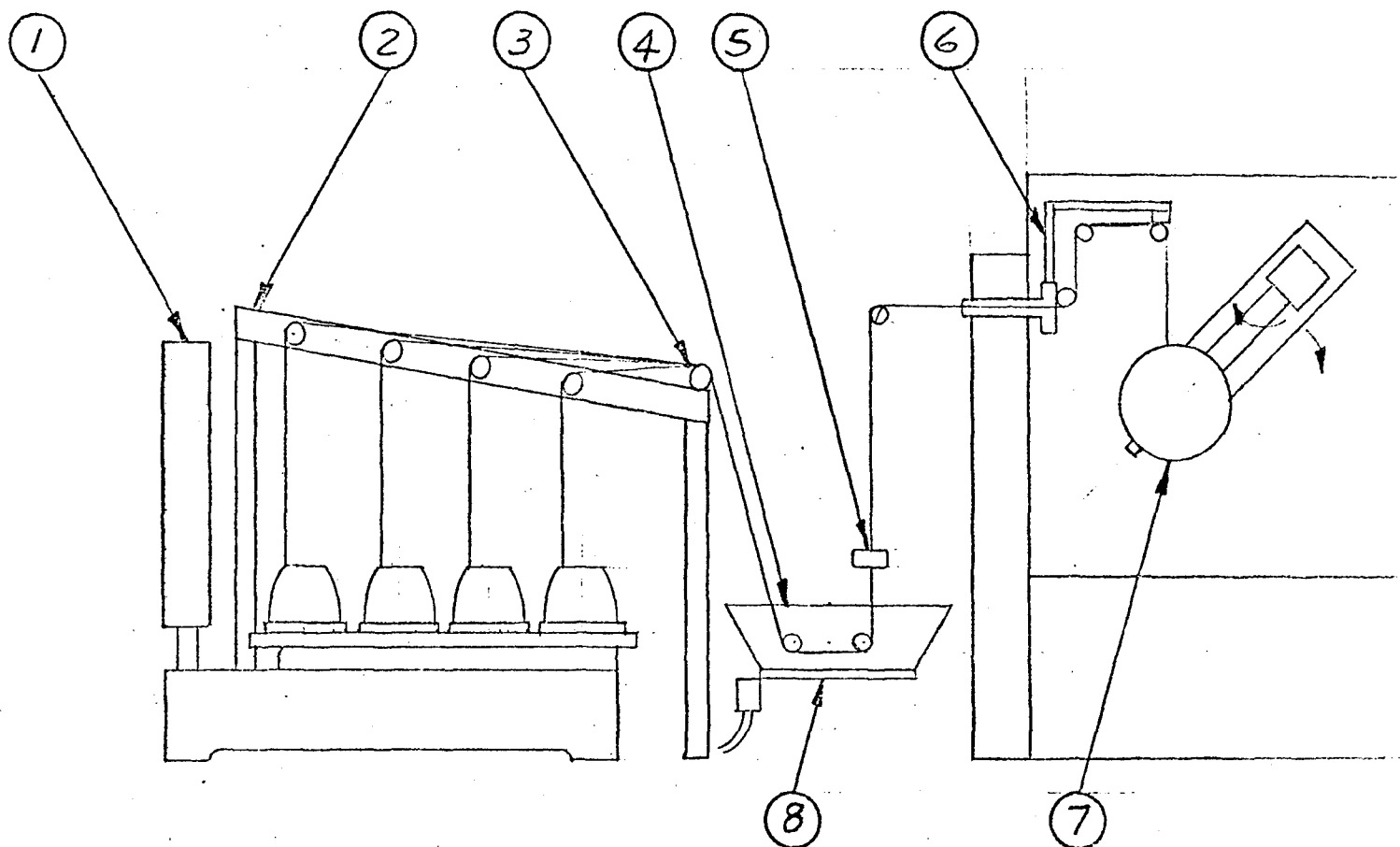
(P/N D3731 or D3770, Figure 6 or 10) The fiber wrapped liner D3730 or D3773 (Figure 5 or 9) is cryogenically stretched to a nominal stress of $S_2 = 220$ ksi at LN_2 temperature for final strengthening and sizing to complete the vessel construction. Internal vessel volume is measured before and after final cryogenic stretching. This gives data on the prestress level at zero pressure and room temperature since the prestrain, ϵ_{gi} , is given by $1/3$ the volume change. Fiberglass and metal liner prestresses are then computed from this prestrain using appropriate values of Young's Modulus and thickness as detailed in the Appendix, Section 7.5.2. These "measured" prestress values agreed closely with design estimates. Data relating to fabrication of GFR vessels are given on Table A-15 of the Appendix, Section 7.6.3. A photograph of completed GFR vessels, P/N D3731 and D3770 is shown on Figure 16.

3.5 Vessel Testing

Vessel testing was performed in support of the design and fabrication effort and to evaluate GFR vessel structural performance. The types of tests performed included buckling tests, fiber wrap and resin burn-out tests and liner and GFR vessel hydrostatic tests. These tests are discussed in detail in this section.

3.5.1 Buckling Tests

Two (2) buckling test vessels (S/N 1 and 2 of Table 2) were designed and fabricated from heat 73413 to determine the threshold value(s) for buckling of the metal liner of the fiberglass overwrapped spherical vessel due to initial fiber prestress loads on the liner. Both these vessels failed prematurely during the final cryogenic stretch operation, thus precluding buckling testing. A "lower bound" buckling design value may be obtained from the liner prestress values derived from measured initial strains of unbuckled vessels subsequent to cryogenic stretching of GFR vessels listed in Table A-15. A lower bound compressive buckling stress design value of about 72%



1. SCALE
2. CREEL
3. FIBERGLASS YARN
4. RESIN TANK
5. WIPER
6. FLYER
7. SPHERE
8. HEATER

SPHERE WINDING SETUP

SIZE	CODE IDENT NO.	
A	33525	FIGURE 13
SCALE		SHEET

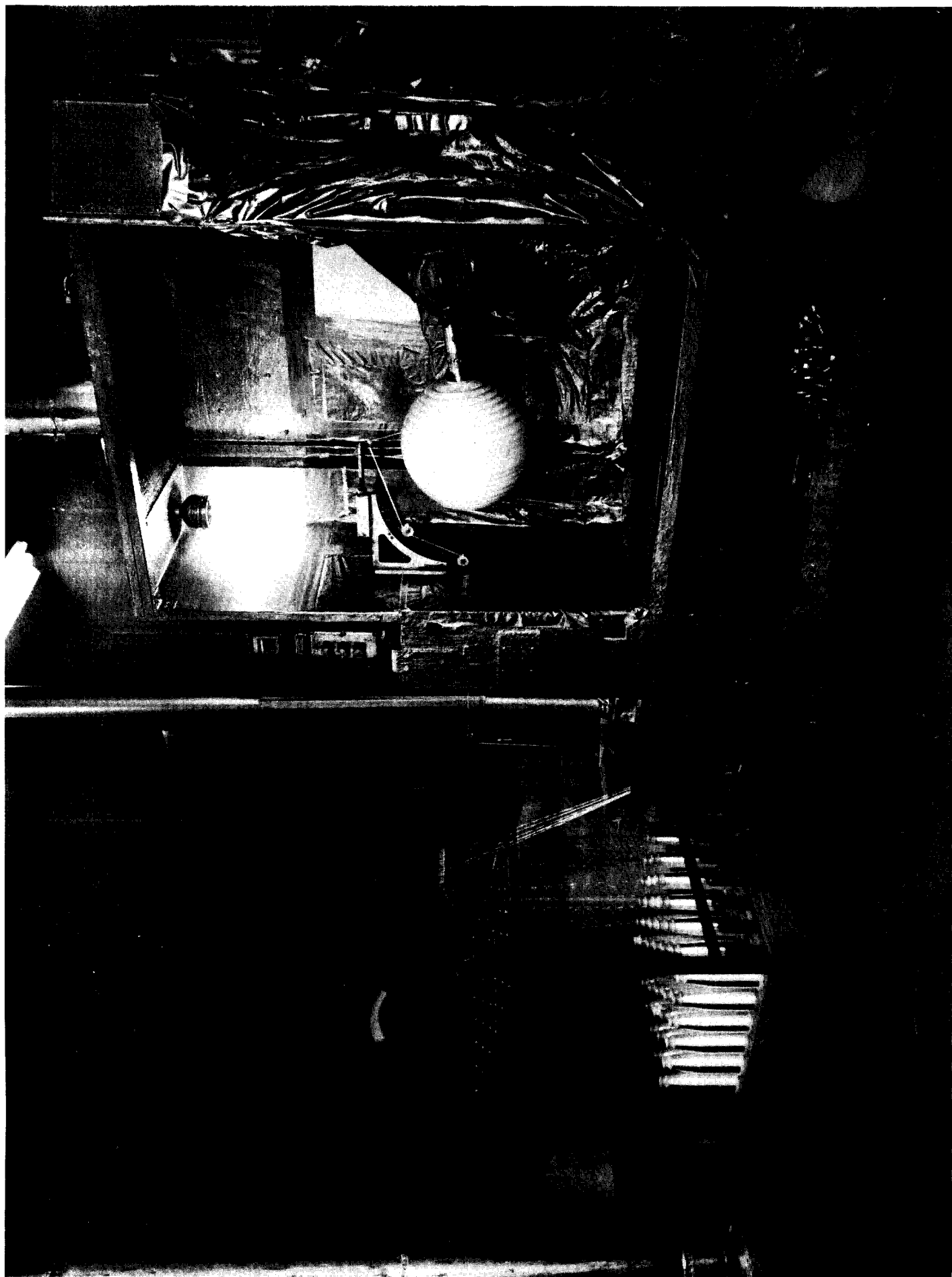


FIGURE 14
SPHERICAL WINDING MACHINE

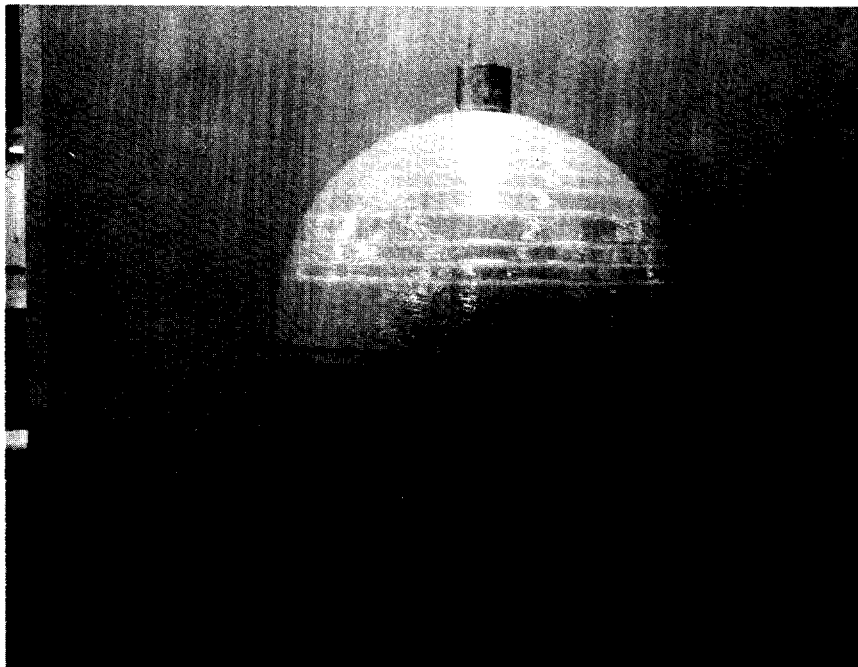


FIGURE 15

FIBER OVERWRAPPED SPHERICAL LINER

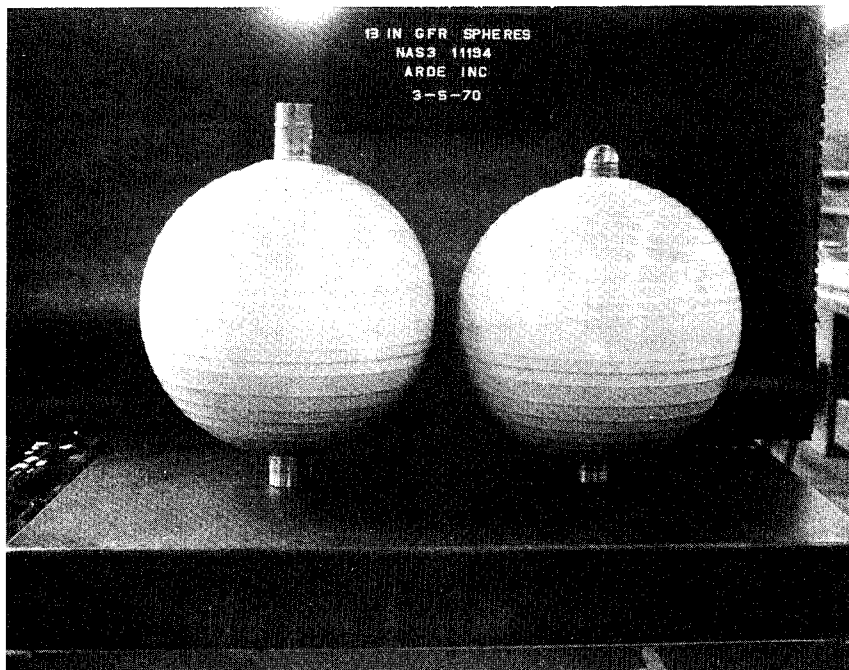


FIGURE 16

COMPLETED GFR VESSEL P/N D3731 AND D3770

of liner tensile yield point (or ≈ 118 ksi) is indicated from this data for a diameter to thickness ratio (D/t) of 650. Additional test data for various (D/t) ratios at compressive stresses high enough to produce vessel buckling is obviously needed.

3.5.2 Fiber Wrap Pattern Tests

3.5.2.1 NOL Rings and Spherical Vessel

Three (3) NOL fiberglass rings and a fiberglass sphere were built and tested at room temperature to check the structural efficiency of the ARDE spherical wrap pattern and to verify fiber wrap fabrication and processing. The glass-resin system and cure cycle were identical to those previously detailed in Section 3.4.2.

The NOL rings were fabricated in accordance with ASTM D-2291-64T and tested per ASTM D2290-64T. The NOL ring room temperature tensile strengths ranged from 268 to 295 ksi.

A fiberglass sphere was wrapped using the ARDE fiber winding pattern projected for use with the GFR spherical vessels. The sphere was wrapped on an elastomer liner with molded-in boss fittings. The elastomer liner was supported on a die cast mandrel of low temperature melting alloy. After the sphere was fiberglass wrapped and cured, the mandrel was melted out with super-heated steam.

The fiberglass sphere was hydrostatically tested to failure at room temperature. A burst pressure of 3940 psi was achieved. A photograph of the fiberglass vessel after burst testing is shown on Figure 17. The weight of the glass plus resin was 5.7 lbs with a resin content of 21.9% by weight and the vessel internal volume was 1330 in³. The fiberglass vessel structural efficiency, PV/W, was:

$$PV/W = \frac{3940 \times 1330}{5.7} = .92 \times 10^6 \text{ in.}$$

This corresponds to a glass room temperature ultimate strength of 324 ksi as detailed in Appendix 6, Section 7.6.1. This compares very favorably with the strength developed by the NOL rings (268 to 295 ksi) and indicates that the winding pattern developed the full strength of the glass.

3.5.2.2 Resin Burn-Out Tests

Difficulties were experienced by

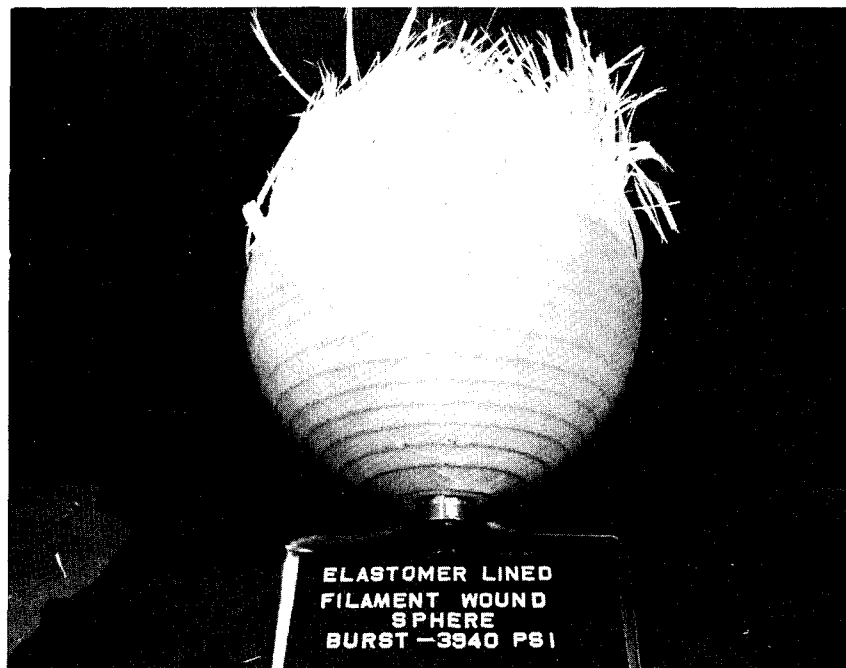


FIGURE 17

ELASTOMER LINED FILAMENT WOUND SPHERE AFTER BURST TEST

the fiber wrap vendor in monitoring and (controlling) the resin content of the GFR vessels. Resin content values were reported ranging from about 20-45%. Resin burn-out tests were used to verify vendor resin content and improved glass weighing technique and equipment were evolved to provide accurate monitoring of fiberglass weight after wrap and cure.

Samples were cut from the fiber wrap of S/N 14 and 15 GFR vessels subsequent to hydrostatic burst testing. These fiber wrap samples were subjected to resin burn-out tests at 1200°F by both ARDE and NASA using a NASA supplied test procedure. Resin content was determined as $\approx 20\%$ by both ARDE and NASA tests as compared to the 21 and 30% reported by the wrap vendor for S/N 14 and 15 respectively.

3.5.3 Modified GFR Liner Design Verification Unit Test

S/N 9 liner, previously rounded by hydrostatic stretching and cryogenic straining, described in 3.3.4 and Appendix 6, Section 7.6.2, was annealed and then processed according to the modified GFR vessel design. After successful processing, the liner was hydrostatically tested at room temperature to 1% biaxial strain without failure. Figure 18 gives the test pressure versus strain curve. Strain gages were used to monitor vessel deformation under pressure.

The strain achieved in the test was more than required to reach the target structural performance value for the GFR vessels at 3000 psi pressure. The modified design and fabrication processing was thus considered verified.

3.5.4 Tests of Pilot GFR Vessels

3.5.4.1 Test Description

Three (3) GFR pilot vessels, S/N 14, 15 and 16 were fabricated to the modified design detailed in Section 3.3.4 and hydrostatically "proof" and burst tested at room temperature using demineralized water as the pressurant. Fabrication processing is described in Section 3.4. Additional details of the test data are given in Table 3-7. Test methods are discussed in detail in Section 7.6.3 of the Appendix.

The GFR vessels were mounted in a rigid frame for hydrostatic testing. Both polar bosses were supported laterally in the frame while the lower boss was supported vertically by the frame. The upper polar boss

TABLE 3-7
GFR SPHERICAL VESSEL DATA

P/N	S/N	Metal Wt. (#)	Lamin Wt. (#)	Total Wt. (#)	Volume (in ³)		Liner I.D. (in)	Thickness (Mils)		Pressure (#/in ²)		Pre- strain V-V ₀ = ε; 3% (in/in)	Glass Pre- stress σ _{gi} ** (ksi)	Metal Liner Pre- stress σ _{ml} ** (ksi)	▲ $\frac{\sigma_{ml}}{\sigma_y}$	☒ $\frac{P \times V}{W}$	☒ $\frac{P \times V}{W}$	Vessel Type		
					Before Final Cryo- Stretch	After Final Cryo- Stretch		Metal t _m	Total Glass Struct t _g	Final Cryo- Stretch P _c	Oper. P _o								Burst P _b	
D3731	14	3.50	1.85	4.12	9.47	1231	1249*	13.40	21.9	57.0	3370 [⊕]	2700*	4000	.00573*	71.0*	-104*	.72*	.443	.656	Room temp.
D3731	15	3.31	1.96	4.94	10.21	1250	1268	13.46	20.9	75.8	3825	3000	3500	.00480	59.5	-108	.66	.462	.538	Hydro
D3731	16	3.42	1.85	4.83	10.10	1240	1261	13.50	21.6	72.6	3850	3000	3560	.00565	70.0	-118	.72	.461	.547	static test
D3731	17	3.32	1.90	4.97	10.19	1240.5	1259.8	13.40	20.6	72.4	3900	3000	3000	.00518	64.2	-113	.69			NASA Units
D3731	19	3.36	1.96	4.99	10.31	1194.8	1208.1	13.20	21.5	74.4	3900	3000	3000	.00371	46.1	-79.8	.49			Deliv.
D3731	21	3.49	1.96	5.01	10.46	1184.8	1199.7	13.18	22.4	74.6	4000	3000	3000	.00419	52.0	-86.5	.53			Units
D3731	22	3.42	1.59	5.16	10.17	1241.6	1258.3	13.40	21.2	72.2	4000	3000	3000	.00448	55.5	-94.5	.58			Heavy Wt.
D3731	23	3.39	1.93	5.23	10.55	1224.4	1241.7	13.33	21.2	73.0	4000	3000	3000	.00471	58.4	-100.5	.61			Boss
D3731	25	3.57	1.90	5.08	10.55	1230.5	1249.9	13.35	22.3	73.0	4000	3000	3000	.00525	65.1	-106.5	.65			
D3731	26	3.49	1.95	5.17	10.61	1208.6	1228.0	13.29	22.0	73.4	4000	3000	3000	.00535	66.3	-110.5	.67			
D3730	1	3.31	0.81	4.79	8.91	1220.3	1239.3	13.32	20.8	73.2	3900	3000	3000	.00520	64.5	-113.5	.68			NASA Deliv.
D3730	2	3.29	0.87	4.81	8.97	1234.4	1252.6	13.38	20.5	73.4	3900	3000	3000	.00492	61.0	-109.3	.67			Units Light
D3730	3	3.26	1.02	5.24	9.52	1209.7	1228.5	13.30	20.5	74.4	4000	3000	3000	.00519	64.3	-116.7	.71			Wt. Boss

Notes:

⊕ Fitting Leaked during cryostretch - further pressurization aborted (lower pressure than desired)

* (1) Reduced operating pressure due to lower yield point resulting from lower cryogenic stretch pressure (estimate 145 ksi room temperature yield point)

(2) Volume after 2700 psi pressurization was 1253.5 in³

(3) Prestrain prior to burst test was $\epsilon_i = \frac{1253.5 - 1231}{3 \times 1231} = .00573$

(4) Prestress values based on $\epsilon_i = .00573$

(5) 145 ksi σ_y used in σ_{ml}/σ_y value

** $\sigma_{gi} = E_g \epsilon_i = 12.4 \times 10^6 \epsilon_i$

▲ Based on 163 ksi σ_y (except as noted for S/N 14)

⊗ Weight used is membrane weight (total weight less boss weight) for comparison purposes with other data

S/N 9 HYDROTEST
(P/N 3728)

11/5/68
MS

FIG. 18

#1 } strain
#2 } gages
#3 }

○ □ Δ

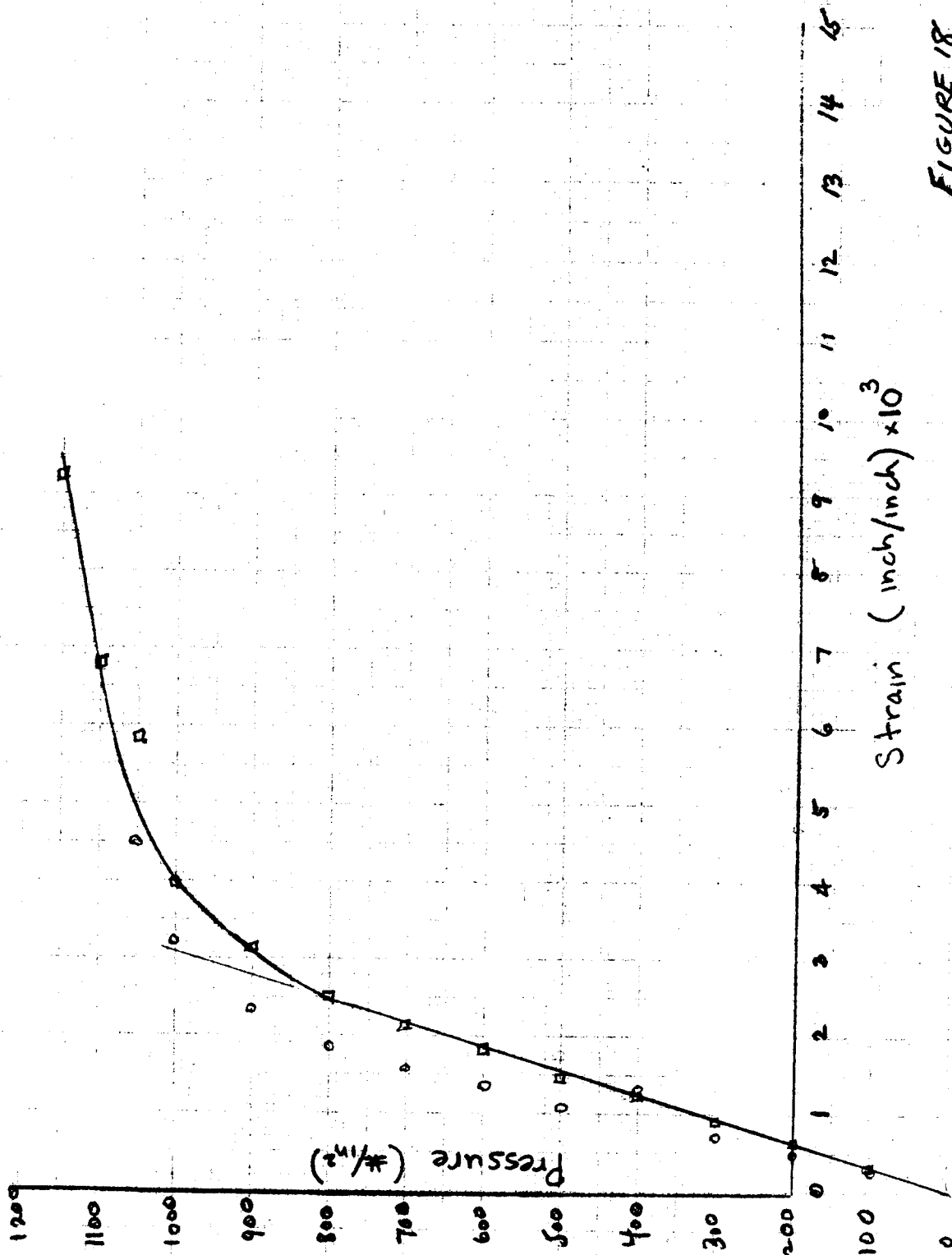


FIGURE 18

was free to move vertically. Displacement transducers, mounted on the rigid frame and in contact with the GFR spherical vessel, monitored vessel deflection under pressure. Vessel diametrical growth at the poles was monitored by a vertical displacement transducer connected to the upper polar boss. Vessel radial (lateral) growth at the equator was measured by a horizontal displacement transducer spring loaded to insure contact with the vessel. Hewlett Packard differential transformer type large displacement transducers (Linearsyn 585-DT-500) with a total displacement range of $\pm 1/2$ " were used. Vessel internal pressure was monitored by a strain gage type pressure transducer. The outputs from the pressure and displacement transducers were continuously recorded during testing. Figure 19 gives a schematic of the test set-up. A test vessel mounted in the rigid frame is shown in the photograph of Figure 20.

After visual, dimensional, weight and internal volume inspection, the vessels were pressurized to "proof" pressure and then unloaded to zero pressure. Vessel displacement and internal volume change measurements were used to determine if the vessel liner yielded. The vessels were then re-pressurized to burst pressure with pressure and displacements monitored.

3.5.4.2 Test of S/N 14 GFR Vessel

This vessel, designed for no liner yielding at 3000 psi, assuming 20% fiber wrap resin content, was downgraded to a 2700 psi pressure test. Fiberglass weight in the vessel after wrapping was about 11% less than anticipated. In addition, A LN₂ pressurant fitting leaked during final cryogenic stretching of S/N 14 vessel leading to termination of stretching at 3370 psig, a lower cryogenic stretch pressure than desired. This resulted in a lowering of liner room temperature yield point to a value below the 163 ksi design point.

S/N 14 vessel was pressurized to 2700 psi and then unloaded to zero psi. Pressure and internal vessel volume were monitored. Vessel displacements were not measured in this first test of the pilot GFR units. A liner average hoop strain of .12%, determined from the volume change measurement of .36% verified that the liner had not reached .2% offset yield. The S/N 14 vessel was re-pressurized until it burst at 4000 psi. The failure was in the liner in the boss region. The

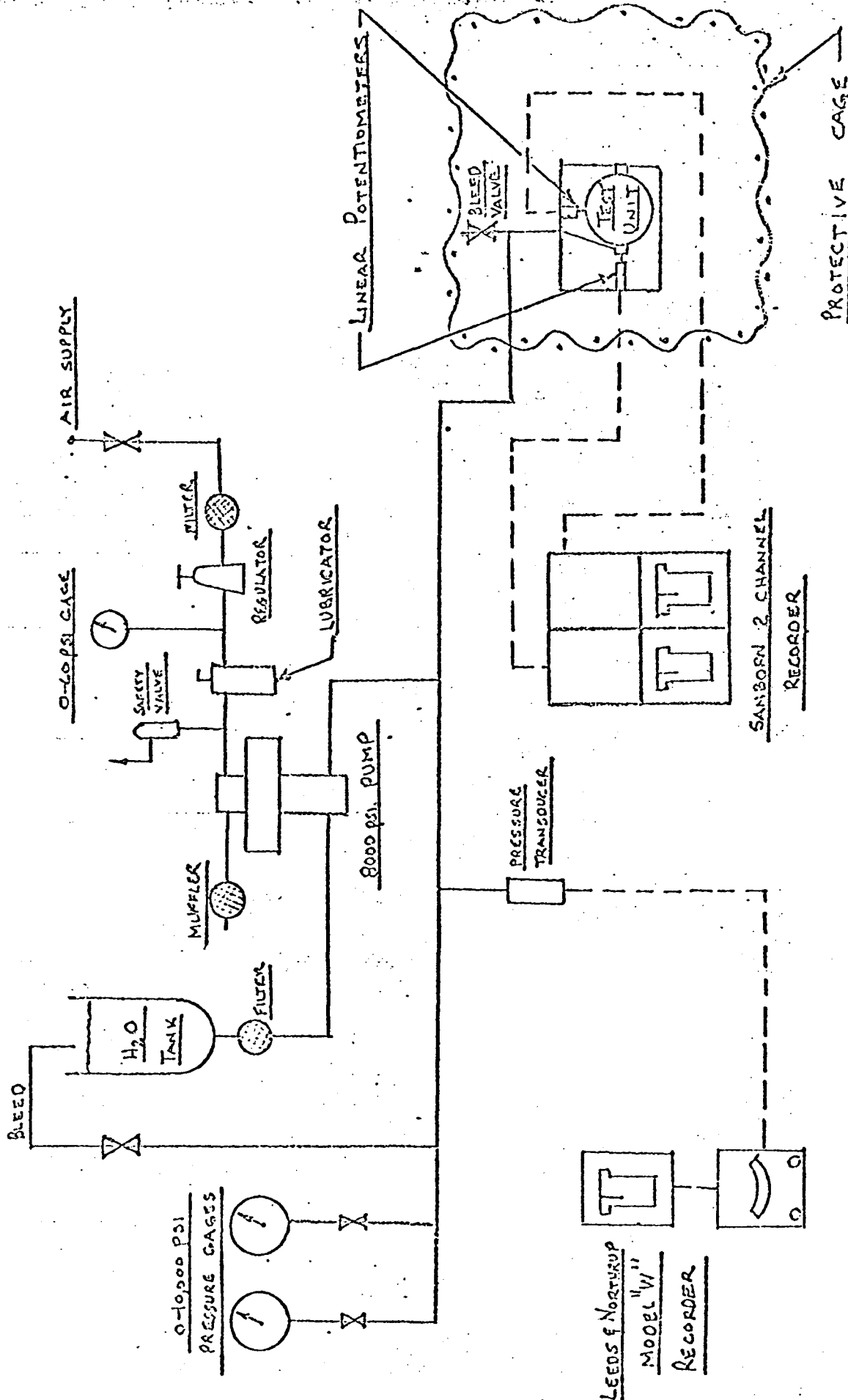


FIGURE 19
BURST PRESSURE TEST SET-UP

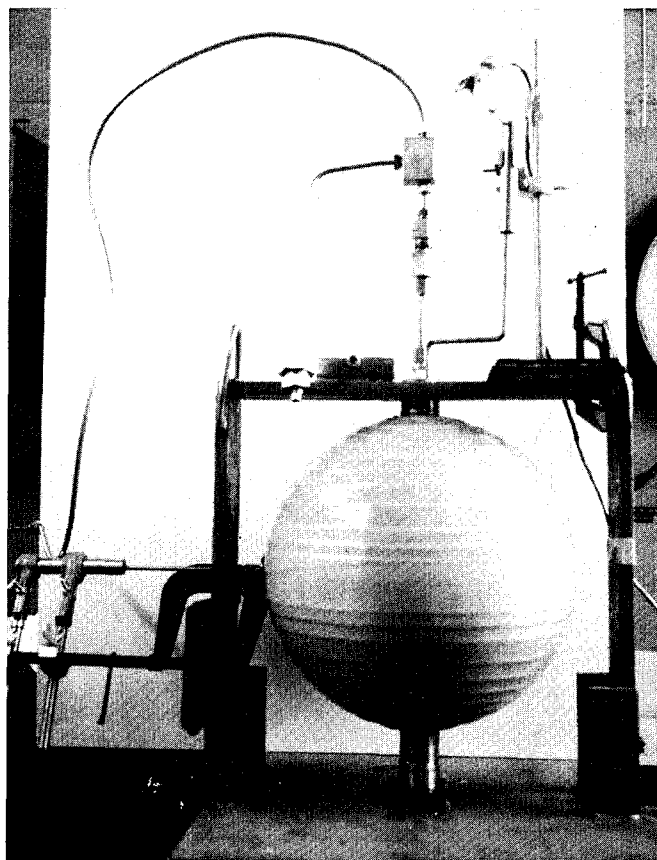


FIGURE 20

TEST SET-UP HYDROSTATIC TEST

fiberglass was intact.

S/N 14 GFR vessel (PV/W) values demonstrated by this test were $.656 \times 10^6$ (in.) and $.443 \times 10^6$ (in.) at 4000 psi burst pressure and 2700 psi operating pressure, respectively as shown in Table A-15. Fiberglass stress at 4000 psi pressure was 316 ksi as detailed in Section 7.6.3 of the Appendix. This high fiber stress achieved by the S glass without failure demonstrated the effectiveness of the spherical wrap pattern. The biaxial strain to failure was about 2% as computed from the fiberglass incremental stress between the unpressurized and 4000 psi burst pressure state. This relatively high biaxial elongation was achieved in S/N 14 vessel after processing and fabrication because the final cryogenic stretching operation was terminated due to a leaking fitting before design cryogenic stretch pressure could be reached. Therefore, the stainless steel liner room temperature yield point was reduced because of less cryogenic plastic strain and the elongation to rupture of the liner was increased. The GFR vessel design pressure capacity was thus lowered (2700 psi compared to 3000 psi design point) because of the lower yield point, while the burst pressure was increased since the metal, after yielding, had a higher strain capacity and could thus load up the fiberglass to a higher stress level.

The S/N 14 GFR vessel test results emphasize the importance of having a liner material with a high residual strain capacity after fabrication and processing in order to achieve a high burst pressure by working both materials of the GFR vessel at their ultimate strength capabilities. In addition, to provide high structural efficiency at operating and proof pressure, the liner material should have a high yield point. This requires one to apply a relatively high plastic strain to the liner during the final cryogenic stretch of the GFR vessel. To accomplish the design objectives (high structural efficiency at operating and proof pressures as well as burst pressures) the "ideal" liner material then must have sufficient residual biaxial elongation capacity (at least 2%) after being cryogenically strained sufficiently to produce a high room temperature yield point.

3.5.4.3 Test of S/N 15 and 16 GFR Vessels

S/N 15 and 16 GFR vessels were hydrostatically tested to 3000 psi, unloaded and then repressurized to burst pressure. Test data are summarized in Table A-15, Section 7.6.3 of the Appendix. No evidence

of liner yielding was observed based on measured internal volume changes at 3000 psi and zero pressure. Burst pressures achieved were 3500 and 3560 psi for S/N 15 and S/N 16 GFR vessels, respectively. Corresponding membrane structural efficiencies (PV/W values) demonstrated at 3000 psi and burst pressures were $.462 \times 10^6$ and $.538 \times 10^6$ for S/N 15 and $.461 \times 10^6$ and $.547 \times 10^6$ for S/N 16 GFR vessel.

The failures were in the liner adjacent to the boss weld on the membrane shell side of the joint. The fiberglass was intact. Figure 21 shows a close-up photograph of the liner of S/N 15 vessel failure region. An external view of S/N 15 GFR vessel after test is given on the photograph of Figure 22.

Pressure versus strain values are plotted on Figures 23 - 26. Measured radial displacement is greater at the poles than at the equator. This result was anticipated because the GFR vessels, as fabricated, were stiffer at the equator than at the poles.

Fiberglass and liner stresses at 3500 psi burst pressure were $\sigma_{gb} = 192$ and $\sigma_{mb} = 216$ ksi respectively for S/N 15 GFR vessel. Corresponding fiberglass and liner stress values at 3560 psi burst pressure for S/N 16 GFR vessel were $\sigma_{gb} = 198$ and $\sigma_{mb} = 223$ ksi, respectively. The stress calculations are given in Section 7.6.3 of the Appendix.

These results for S/N 15 and 16 units verified that the minimum liner membrane ultimate strength of 200 ksi was achieved in the fabricated vessels. However, the target ultimate strength of the fiberglass at burst pressure, $\sigma_{gb} = 330$ ksi was not achieved. The problem was that the strain to liner rupture in these vessels was insufficient to load up the glass to its "ultimate" load carrying capacity. Only about 1% strain to failure was achieved in these tests as seen from Figures 23 - 26. About twice this value, 2% strain to liner rupture, is required to reach the ultimate strength capacity of the fiberglass.

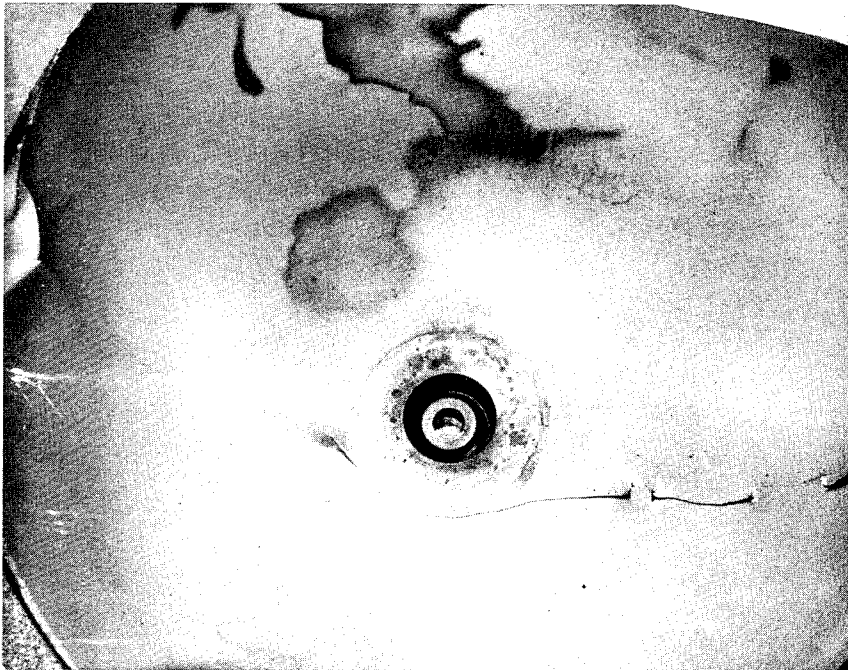


FIGURE 21

FAILURE REGION OF S/N 15 GFR VESSEL

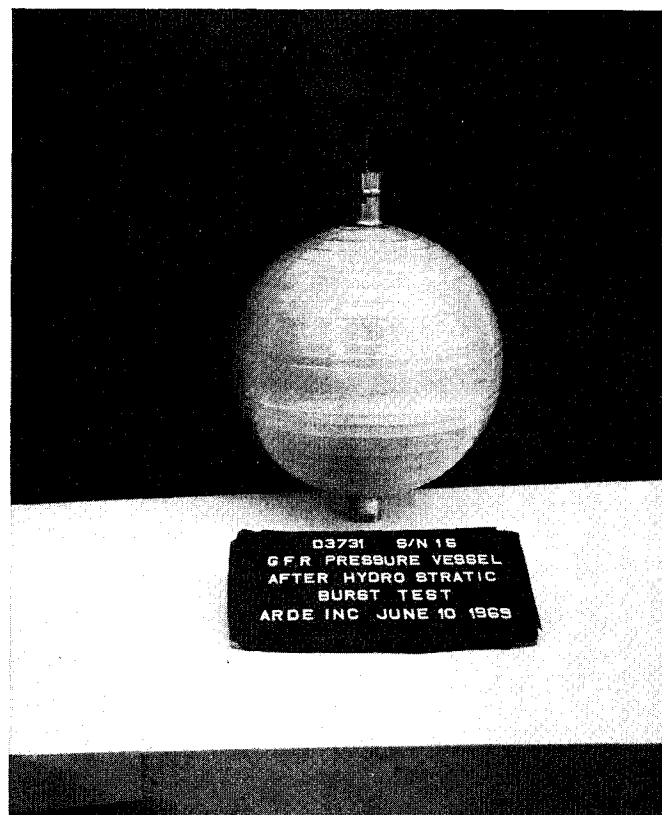


FIGURE 22

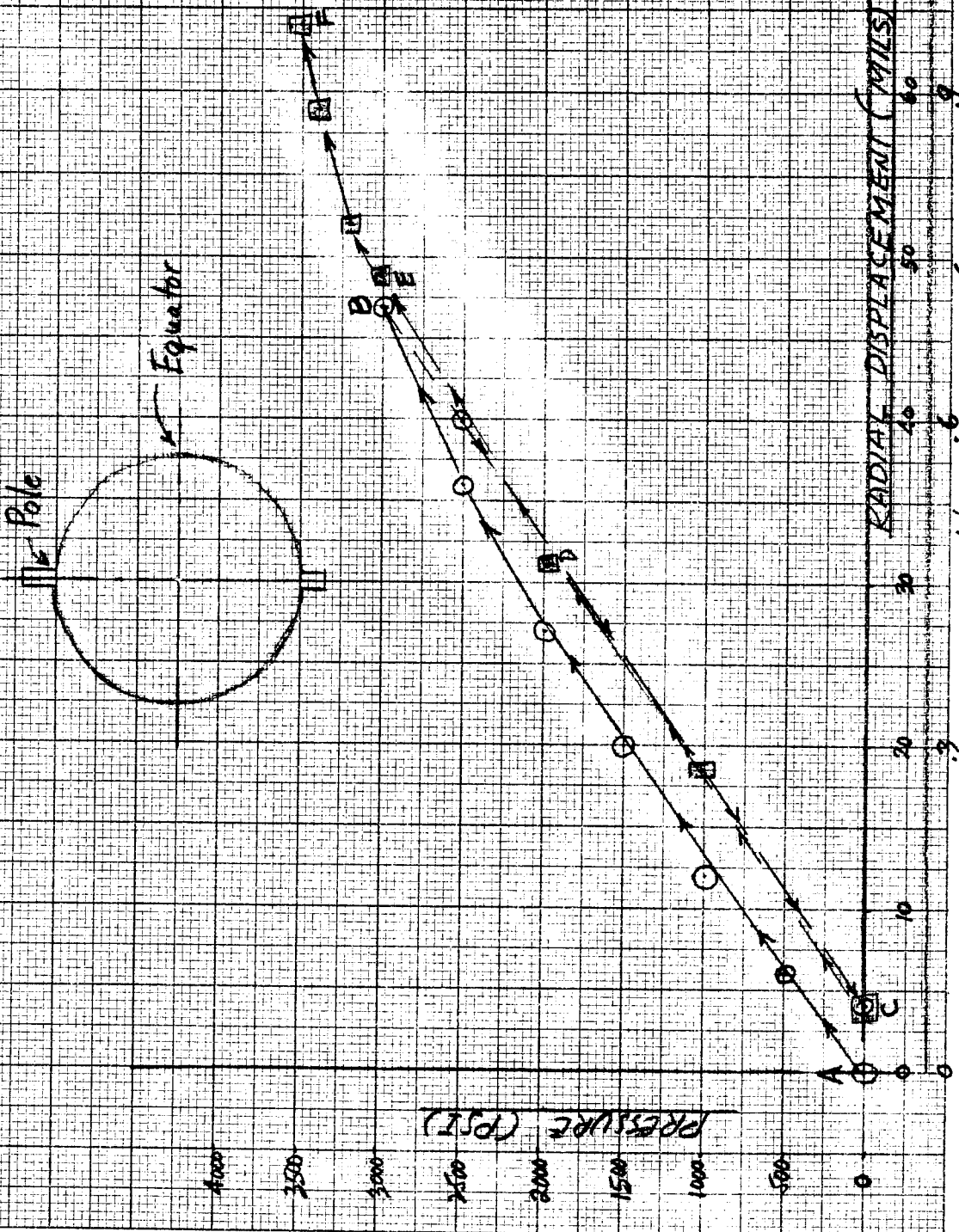
S/N 15 GFR VESSEL AFTER BURST TEST

FIG 23

SN 15 GFR VESSEL HYDROSTATIC TEST

Notes:

- 1) Radial Displacement measured at Equator.
- 2) Path ABC is loading to 3000 psi and unloading to zero.
- 3) Path CDEF is loading to 3500 psi burst pressure.



Hoop Strain (%)

FIG. 24

SN 15 GFR VESSEL HYDROSTATIC TEST

Notes:

- 1) Radial Displacement measured at poles.
- 2) Path ABC is loading to 2000 psi and unloading to zero.
- 3) Path CDEF is loading to 3500 psi burst pressure.

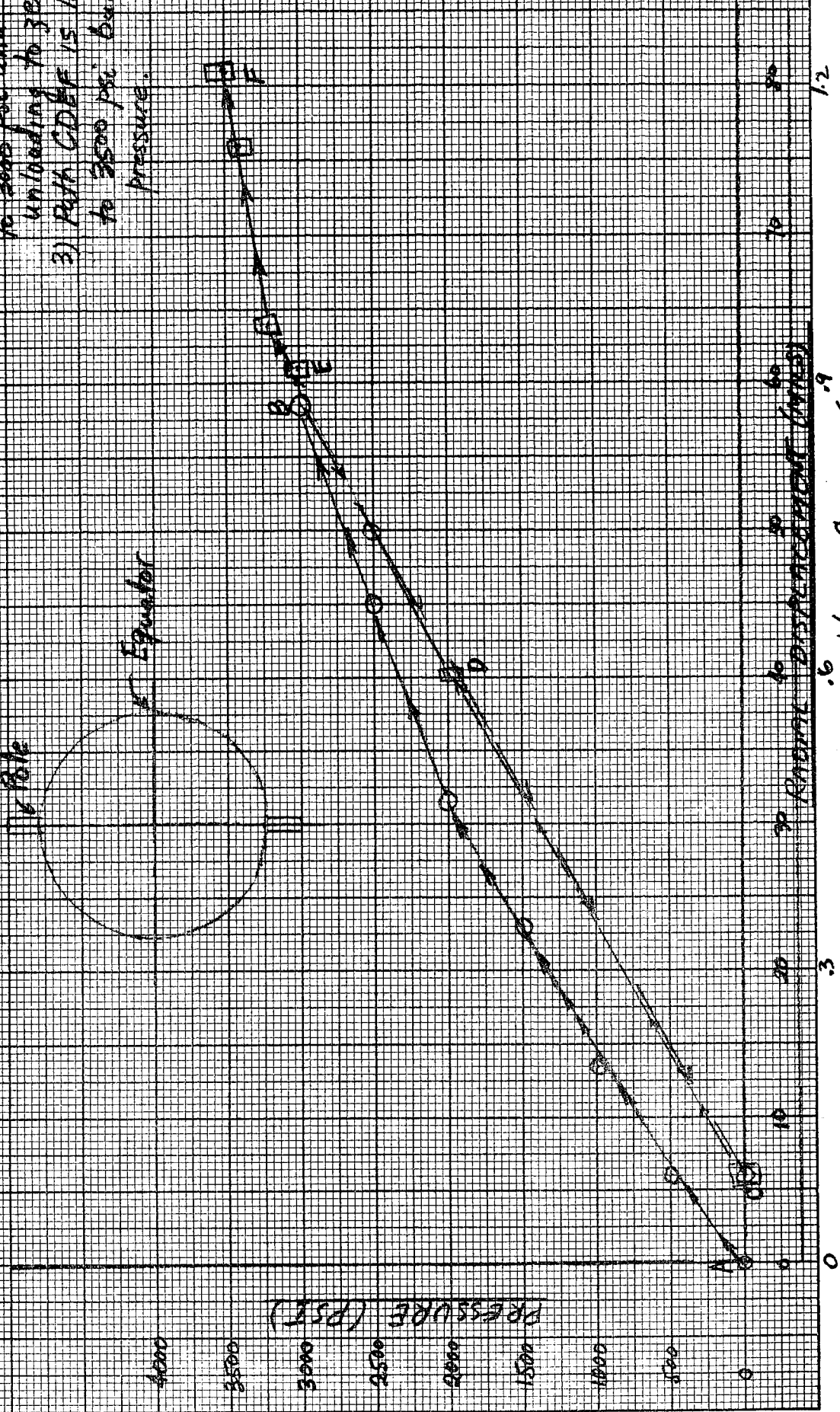
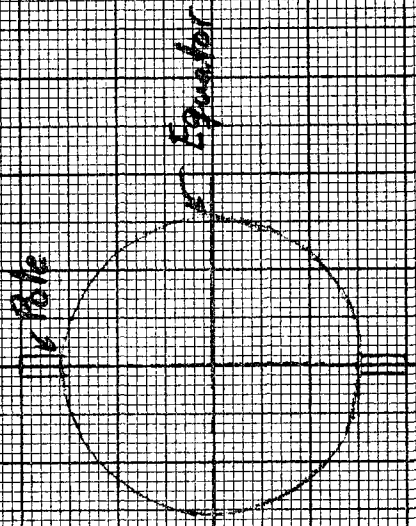


FIG 25 SN 16 GFR VESSEL HYDROSTATIC TEST

- Notes:
- 1) Radial displacement measured at equator
 - 2) \odot are points on curve of loading to 3000 psi and unloading to zero.
 - 3) \times are points on curve of loading from zero to 3560 psi burst pressure.

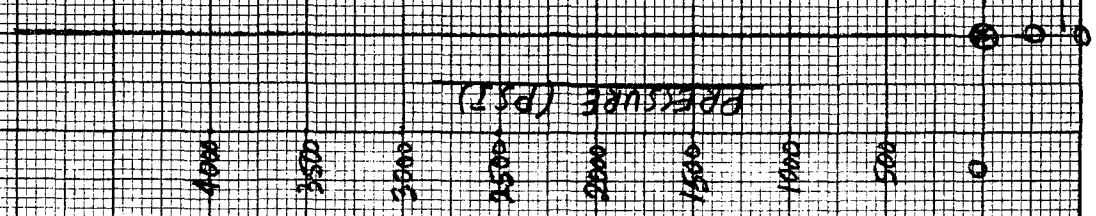
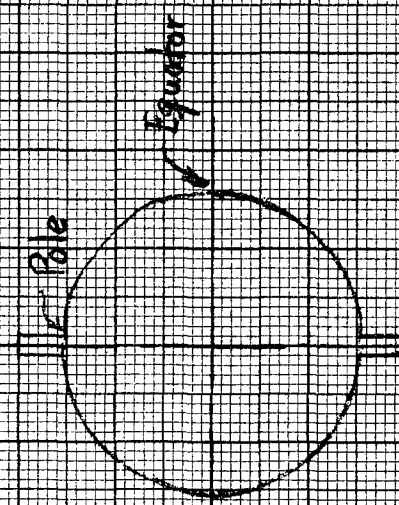
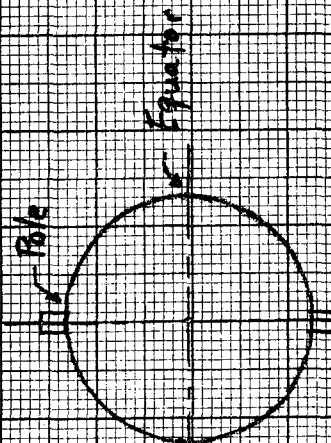


FIG. 26

SIN 16 GFR VESSEL HYDROSTATIC TEST

- Notes: 1) Radial displacement measured at poles.
- 2) O are points on curve of loading to 3000 psi and unloading to zero.
- 3) X are points on curve of loading from zero to 3500 psi burst pressure.



PRESSURE (PSI)

RADIAL DISPLACEMENT (MILS)

POLE STREAM (in)

4. GFR VESSEL PERFORMANCE EVALUATION

4.1 Present Configuration (Low Silicon Heat 50793 Liner)

4.1.1 Structural Performance

As described in the detailed discussion of Section 3, two (2) distinct GFR vessel configurations have been demonstrated on the program. One of these, S/N 14, with about 2% biaxial liner membrane elongation to failure, had a liner with a yield point lower than the selected GFR vessel design point value. This reduced the operating pressure to 2700 psi instead of 3000 psi, but increased the burst pressure to 1.5 times operating pressure, since the fiberglass was loaded up very close to its ultimate strength. The second configuration demonstrated, typified by S/N 15 and S/N 16 GFR vessels, had higher yield strength liners which met the design point value and permitted operation at 3000 psi without liner yielding. The biaxial membrane liner elongation to failure for these vessels was about 1%. This lowered the burst pressure to 1.2 times operating pressure since the glass was not stressed near its ultimate strength capacity because of the comparatively lower liner elongation to failure capability compared to S/N 14 GFR vessel.

Both types of vessels demonstrated that the liner minimum design ultimate strength of 200 ksi at room temperature was achieved. Further, the high structural efficiency of the spherical fiberglass wrap was verified by tests. A fiberglass stress of 316 ksi was achieved in the S/N 14 vessel test without fiber wrap failure and an ultimate stress of 324 ksi was reached in the fiberglass wrap evaluation vessel test.

The spherical configuration and stretch forming fabrication technique also permitted the attainment of lightweight bosses. The weight of two (2) lightweight bosses for the ARDEFORM GFR vessel was .81# (P/N D3730, S/N 1 Table A-15). This compares very favorably with a weight for two bosses plus boss fiber reinforcement of 3.44# for a smaller load per inch (pressure times radius) as detailed in referenced 1 and 2 for inconel X-750 oblate spheroid GFR vessels.

Listed in Table 4-1, for comparison purposes are the room temperature structural performance of S/N 14, 15 and 16 GFR spherical vessels as well as room temperature

performance factors of inconel X-750 and titanium
(5Al-2.5 Sn) oblate spheroid GFR vessels taken from references
1 and 2.

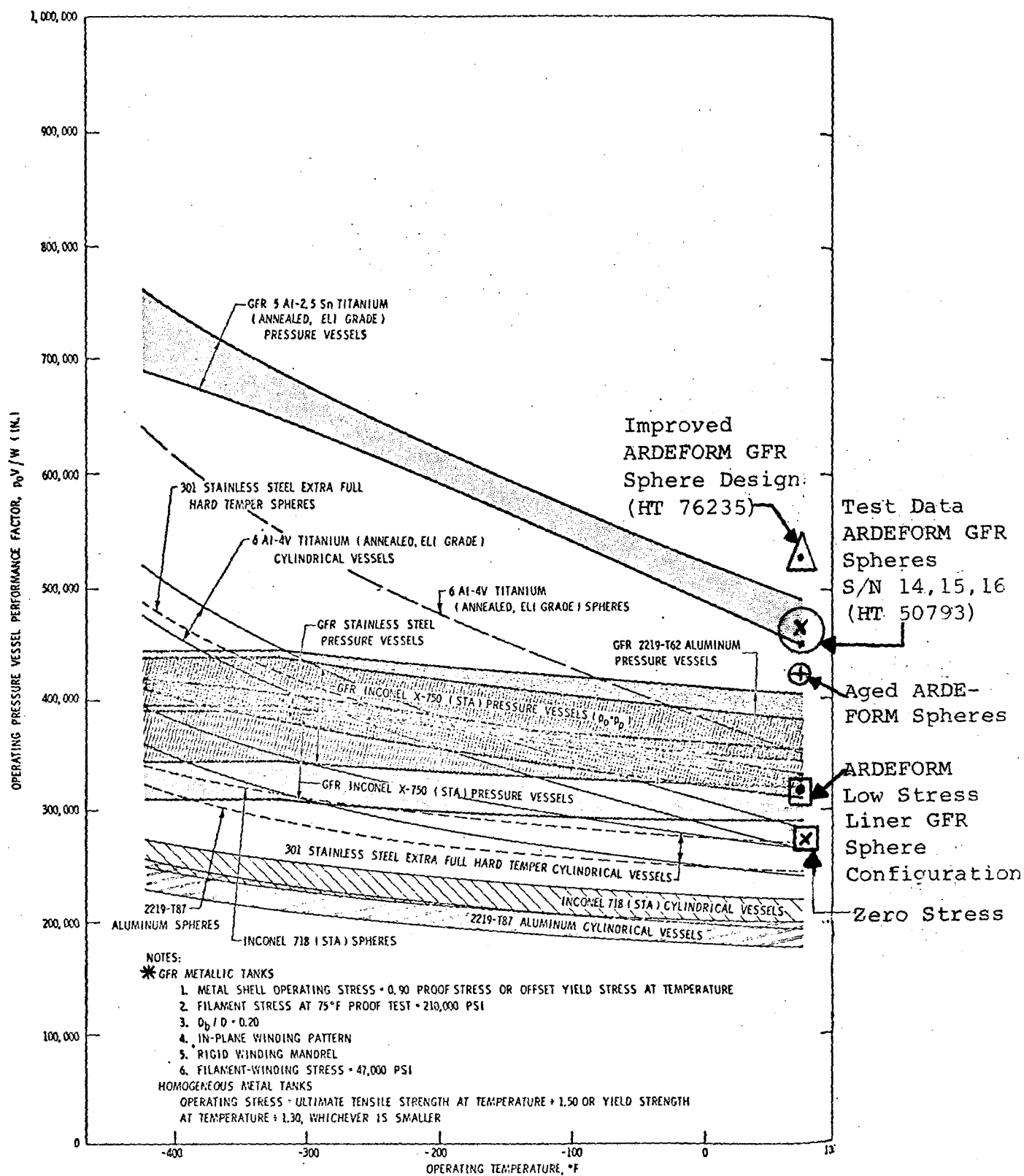
TABLE 4-1 GFR VESSELS - ROOM TEMPERATURE STRUCTURAL PERFORMANCE FACTORS

Vessel Type		$\frac{P_o V}{W} \times 10^{-6}$ (operating)	$\frac{P_b V}{W} \times 10^{-6}$ (burst)
Actual Test Results for ARDEFORM 301 spherical GFR Vessels	S/N 14	.443	.656
	S/N 15	.462	.538
	S/N 16	.461	.547
Actual Tests Inconel X-750 Oblate Spheroid GFR Vessels		.312 to .318 (Ref. 1 and 2)	.37 to .437 (Ref. 1 and 2)
Theoretically Projected values for Ti (5Al-2.5Sn) Annealed Oblate spheroid GFR vessels		.44 to .48 (Ref. 1 and 2)	

It is seen that the ARDEFORM 301 spherical GFR vessels had 40 to 50% higher structural performance at room temperature and operating pressure than the inconel GFR vessels and they demonstrated by actual test structural performance equal to that theoretically projected at room temperature for titanium (5Al-2.5 Sn) GFR vessels. For reference, the S/N 14, 15 and 16 ARDEFORM GFR spherical vessel results are plotted on Figure 27 herein which is taken from Figure 7 of Reference 2.

Aged ARDEFORM 301 stainless steel spherical vessel results are also plotted on Figure 27 for additional comparison. The assumption of References 1 and 2 for operating pressure stress of ultimate stress/1.5 or yield stress/1.3, whichever is smaller, has been used for the homogeneous material aged ARDEFORM vessels with 270 ksi ultimate strength. It is seen that the high performance factor of this homogeneous material configuration compares favorably with most vessel types.

Data on cryogenic testing of spherical



SUMMARY COMPARISON OF GFR, METAL AND HOMOGENEOUS METAL PRESSURE VESSEL PERFORMANCE LEVELS

(Taken from Figure 7 of Reference 2)

* (Less ARDEFORM) For ARDEFORM GFR Vessels See Text For
Design Conditions

FIGURE 27

ARDEFORM GFR vessels will be available shortly for further comparison. The ten (10) delivery GFR vessels on the present program are currently being tested and evaluated by NASA at LN₂ and LH₂ temperatures.

4.1.2 Fabrication Performance Evaluation

Problems resulting from weld distortion effects were resolved by "rounding" the vessels by hydrostatic and/or cryogenic stretching prior to cryogenic stretching for strengthening and final sizing. In addition, the cryogenic strain requirements were lowered. This has been detailed in Sections 3.3.4 and 3.4. Once this modified fabrication processing was established, three (3) GFR vessels were successfully fabricated and tested followed by successful fabrication of ten (10) out of twelve (12) GFR delivery type vessels. Total "scrap" was only about 13% which is exceedingly good performance for development type hardware fabrication and processing.

Difficulties were experienced in maintaining and controlling low resin content (20% level). Use of vacuum bag curing techniques should resolve this problem. Resin contents consistently in the range of 15 - 17% were obtained through use of this curing method as reported in reference 2. Achievement of this resin content level would increase the GFR vessel structural performance factor (PV/W) by about 2 to 3% compared to a 20% resin content GFR vessel performance.

4.2 Improved GFR Vessel Configurations

4.2.1 Increased Ductility Liners

Liner ductility available after cryogenic processing limits the performance of GFR vessels as discussed in detail in Section 3.5.4. The ARDEFORM 301 stainless steel liner material used in the present program (low silicon heat 50793) was selected for use primarily because of its high toughness at LH₂ temperature. For vessel operation at LN₂ temperature to room temperature, many different heats are available that have attractive elongation, strength and toughness properties over this temperature range. In addition, these heats can be readily fabricated into pressure vessels or GFR vessel liners. One such ARDEFORM 301 stainless steel material is heat 76235. It is projected that this heat will have superior elongation to rupture capability compared to low silicon heat 50793

(Particularly in the higher room temperature yield point range - 180 to 200 ksi).

The sphere design chart for heat 76235 is given on Figure 28. Spheres fabricated from this heat can be stretched cryogenically about 12 to 13%. The theoretical limit is where the nominal stress curve at LN₂ temperature, S₂, has a horizontal tangent corresponding to the sphere tensile instability limit (designated as 242 ksi on Figure 28). This high strain capability is generally an indication of good elongation properties. Vessel data under double cryogenic stretch conditions with intermediate fiberglass cure temperature "ageing" are needed to precisely define and verify the anticipated large (>2%) biaxial liner strain to rupture characteristics of heat 76235 at high yield point values.

Assuming at least 2% biaxial liner elongation to rupture for heat 76235 GFR spherical vessels at a liner yield point of 200 ksi and a fiberglass resin content of 20%, we theoretically project structural performance (PV/W values) at operating and burst pressure as, $.513 \times 10^6$ (in.) and $.770 \times 10^6$ (in.) respectively. The detailed calculations and design parameters are given in Appendix 7, Section 7.7.

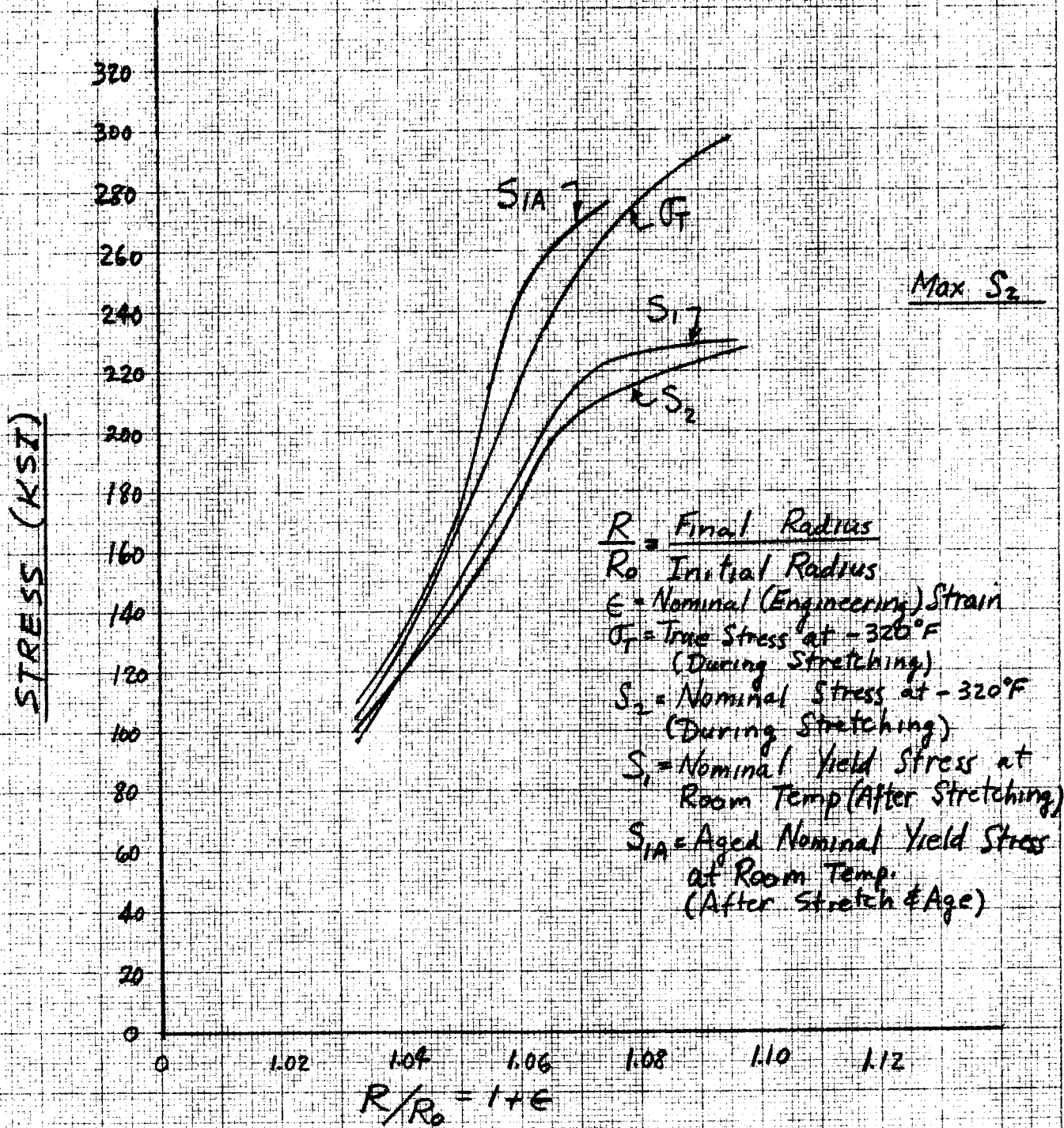
If the fiberglass resin content is reduced from 20% to 16%, the (PV/W) values increase to $.527 \times 10^6$ (in.) and $.791 \times 10^6$ (in.) at operating and burst pressure, respectively. This operating pressure (PV/W) value has been plotted on Figure 27 as a theoretical projection of ARDEFORM 301 stainless steel spherical GFR vessel performance capability at room temperature.

4.2.2 Low Stress Liner Configurations

If the metal liner of the GFR vessel is at low tension (or in compression) at operating pressure, "crack propagation" problems would be eliminated. This fact offers attractive options for hydrogen storage and gunfire applications, for example.

When LH₂, under long term storage conditions warms up and GH₂ forms, severe degradation of tank material properties followed by premature vessel failure takes place because of "attack" by the hydrogen gas. Aluminum is apparently the only metallic material unaffected by this phenomenon. It appears that ARDEFORM stainless steel

FIG. 28
SPHERE DESIGN CHART
BASED ON VESSEL TEST DATA
(Heat 76235)



spherical GFR vessels with better (PV/W) values at operating pressure than aluminum can be designed and built within the framework of demonstrated state-of-the-art. Moreover, the burst to operating pressure ratio of the GFR spherical vessel should be higher than an aluminum configuration.

GFR spherical vessels with low liner stress and good structural performance at operating pressure should be a promising candidate for high pressure gas storage vessels subject to gunfire requirements. The low liner stress improves liner fragmentation and fatigue resistance. In addition, the fiberglass has the ability to absorb energy and to contain metal liner fragments, if they occur at rupture.

As an example of the "low stress" liner configuration, consider the GFR spherical vessel design with 16% resin content discussed in Sections 4.2.1 and 8.7. Selecting, for example, a liner stress at operating pressure as a tension of 25% of yield point (or 50 ksi), the vessel would have to be operated at 1790 psi pressure as detailed in Appendix 7, Section 7.8. Its (PV/W) value at operating pressure would then be $.315 \times 10^6$ (in.) with a burst to operating pressure ratio of $\frac{4500}{1790} = 2.51$. This room temperature (PV/W) value is plotted on Figure 27 for comparison purposes. It is about 30% better than 2219-T87 aluminum spheres and compares favorably with many other vessel configurations. This concept of low stress can be applied for those cases of poor material compatibility by designing the liner to operate at "zero" stress levels or at a computed PoV/W of $.264 \times 10^6$ in.

5. CONCLUSIONS AND RECOMMENDATIONS

5.1 The program objective has been accomplished. High performance ARDEFORM 301 stainless steel spherical GFR vessel configurations have been demonstrated by room temperature hydrostatic tests of 13 1/2" nominal diameter vessels designed for 3000 psi operating pressure. Considerable weight savings over homogeneous material vessels and other GFR configurations have been proven by comparison of results obtained with previously published data. Test PV/W) values for the ARDEFORM 301 stainless steel spherical GFR vessels ranged from .44 to .46 x 10⁶ (in.) at operating pressure and .54 to .66 x 10⁶ (in.) at burst pressure. These test-verified structural performance factors were 30% higher than those given for titanium 5Al-2.5 Sn homogeneous spheres as well as 40 to 50% higher than previous test results reported for inconel X-750 (STA) oblate spheroid GFR vessels and were equal to those theoretically projected for 5Al-2.5 Sn titanium GFR oblate spheroids. Achievement of the structural performance theoretically predicted for titanium GFR vessels is somewhat speculative because of anticipated elongation capability problems with titanium weldments. This lends additional impact to the spherical GFR vessel test results obtained in this program.

Based on theoretical projections, operating pressures at -320°F and -423°F can be 26 and 32% higher, respectively, than the 3000 psi room temperature value. These predicted structural performance increases will be checked by cryogenic testing and evaluation by NASA. Ten (10) ARDEFORM 301 spherical GFR vessels have been delivered for this purpose.

5.2 The design and fabrication processing of the ARDEFORM 301 stainless steel spherical GFR vessels have been verified by test, fabrication and delivery of vessels. Once this processing was defined, three (3) GFR vessels were successfully fabricated and tested followed by the successful fabrication of ten (10) out of twelve (12) delivery vessels. The "scrap factor" demonstrated (13%) is quite small, especially for a research and development limited hardware quantity program.

5.3 The spherical configuration and the cryogenic stretch forming processing facilitates achievement of lightweight bosses. The fabricated and tested weight of two (2) lightweight bosses for the ARDEFORM 301 stainless steel

GFR spherical vessel was 0.81# compared to a weight for two (2) bosses of 3.44# for the inconel X-750 oblate spheroid GFR vessels tested in a previous program at a smaller pressure load per inch.

5.4 Weld distortion problems in the thin (20 mil) 301 stainless steel liner shells at the boss regions were eliminated by vessel rounding using hydrostatic stretching at room and/or LN₂ temperatures. This method, together with ARDEFORM unfixtured welding techniques, could also be successfully applied to thin liner fabrication and boss attachment problems in other materials.

5.5 The high structural efficiency of the ARDE spherical fiber wrap pattern has again been demonstrated by tests. Membrane hoop stress values of 316 ksi without failure and 324 ksi at rupture were achieved in spherical vessel burst tests indicating that essentially the full ultimate strength of the fiberglass was achieved in a spherical configuration.

5.6 No definitive test data were obtained on the buckling of spherical GFR vessels due to premature failure of early model test vessels. However, a "lower bound" compression value of 72% of tensile yield stress (or 118 ksi compression) at a diameter to thickness ratio (D/t) of 650 may be deduced from the successfully fabricated GFR vessels which did not exhibit evidence of buckling. Test data for actually buckled vessels at various D/t ratios are obviously needed.

5.7 A pronounced Baushinger effect was noted in the tension-compression cycling tests. This result was not surprising considering that the liner was yielded both in tension and compression initially and then cycled at $\pm 90\%$ of the initial tensile yield stress. A preliminary value of $\pm 65\%$ of initial tensile yield stress for maximum cyclic stress is estimated based on the test data obtained for these severe loading conditions. Although a severe (and interesting) condition, yielding the liner initially in both tension and compression followed by cycling is not realistic for ARDEFORM 301 stainless steel liners. The plastic deformation, which raises the liner tensile and compressive yield points and provides the pre-stress at release of load, is applied during the GFR vessel fabrication process. The liner, with its increased yield points, behaves elastically thereafter at initial compression

stress to operating and proof pressure tensile stress levels. There is no need to plastically deform the liner again, except to determine burst stress. Test data for completely elastic cycling is obviously needed in order to define permissible cyclic stress limits for ARDEFORM 301 stainless steel liners.

5.8 Use of proven vacuum bag cure techniques should control and maintain fiberglass wrap resin content at or below 20%.

5.9 Although the demonstrated performance of the ARDEFORM 301 stainless steel GFR spherical vessels was exceedingly good, the structural efficiencies achieved were limited by the liner strain to rupture available after cryogenic processing and fabrication. Two percent (2%) minimum bi-axial strain to rupture is needed for increased performance ARDEFORM GFR spherical vessels. The low silicon heat selected for use (Heat 50793) was chosen primarily for its excellent toughness at LN_2 temperatures. There are many ARDEFORM 301 stainless steel heats available which have excellent properties and superior elongation characteristics compared to Heat 50793 in the LN_2 to room temperature range. One such heat is Heat 76235. Significant structural performance increases are projected using this heat for the GFR vessel liner. At room temperature, for example, (PV/W) increases anticipated range from 15 - 20% increase at operating pressure and 20 - 45% increase at burst pressure compared to GFR spherical vessel test results obtained in this program. The improved ductility liner GFR spherical vessel structural performance potential is 10 - 20% higher than that projected for GFR oblate spheroid 5Al-2.5 Sn titanium vessels considered as the best GFR vessel configuration in a previous program study. Evaluation of ARDEFORM 301 stainless steel spherical GFR vessels using Heat 76235 is recommended to verify the projected improved structural performance for use in applications in the LN_2 to room temperature range.

5.10 A GFR vessel with the metal liner under "low stress" at operating pressure (small tension or compression) offers attractive options for many applications. The low operating liner stress eliminates crack propagation problems and increases fatigue life while the GFR configuration provides good structural efficiency with a high burst to

operating factor of safety. Moreover, the ability to vary the prestress to provide operating stresses at many places along the stress-strain curve offers important options for other than lightweight consideration, e.g., replace difficult to fabricate monolithic structures, improve compatibility. These design trade-offs should be studied and evaluated experimentally.

5.11 Packaging considerations often dictate the use of cylindrical vessels instead of spheres. Application of ARDEFORM 301 stainless steel GFR vessel technology to cylindrical shapes is recommended to provide high performance vessels for current and projected applications.

5.12 ARDEFORM 301 stainless steel GFR vessels have demonstrated high structural performance and the potential exists for even further improvements. In order to apply this technology to a wider range of applications and to evaluate vessel configurations in greater depth, more basic data on ARDEFORM 301 materials (particularly fracture mechanics information) is required at various temperatures for different fluids. It is recommended that this data be obtained by means of an appropriate experimental program.

6. REFERENCES

- 1) Morris, Darms, Landes and Campbell, Parametric Study of Glass-Filament-Reinforced Metal Pressure Vessels, NASA CR 54-855, Aerojet-General Corporation under Contract NAS3-6292, April 1966.
- 2) E. E. Morris, Glass-Fiber Reinforced Metallic Tanks for Cryogenic Service, NASA CR72224, Aerojet-General Corporation prepared under Contract NAS3-6292, June 1967.
- 3) Timoshenko and Gere, Theory of Elastic Stability, Second Edition, McGraw-Hill Book Co., New York, 1961.
- 4) M. A. Krenzke and T. J. Kiernan, The Effect of Initial Imperfections on the Collapse Strength of Deep Spherical Shells, Research and Development Report 1757, David Taylor Model Basin Structural Mechanics Lab., Washington, D.C., February 1965.
- 5) M.P. Hanson, H. T. Richards, and R. O. Hickel, Preliminary Investigation of Filament-Wound Glass-Reinforced Plastics and Liners for Cryogenic Pressure Vessels, NASA TND-2741, Lewis Research Center, National Aeronautics and Space Administration, Cleveland, Ohio, March 1965.
- 6) J. M. Toth, Jr., W. C. Sherman, and D. J. Soltysiak, Investigation of Structural Properties of Fiber-Glass Filament-Wound Pressure Vessels at Cryogenic Temperatures, NASA CR-54393, Douglas Aircraft Company Report SM-48845, prepared under Contract NAS3-2562, September 1965.
- 7) R. W. Frischmuth, Jr., Investigation of Thin Films as Floating Liners for Fiber-Glass Cryogenic Propellant Tanks, NASA TND-3205, Lewis Research Center, January 1966.
- 8) R. W. Frischmuth, Jr. and P. T. Hacker, Investigation of Bonded Plastic Tape for Lining Filament-Wound Fiber-Glass Cryogenic Propellant Tanks, NASA TND-3206, Lewis Research Center, January 1966.

- 9) R. W. Frischmuth, Jr., Experimental Investigation of Glass Flakes as Liner for Fiber-Glass Cryogenic Propellant Tanks, NASA TMX-1193, Lewis Research Center, January 1966.
- 10) R. W. Buxton and R. N. Hanson, Design Improvements in Liners for Glass Fiber Filament-Wound Tanks to Contain Cryogenic Fluids, NASA CR 54-854, Aerojet-General Report 3141 prepared under Contract NAS3-4189, January 1966.

7. APPENDICES

7.1 Appendix 1 - Material Certification Data (Heat 50793)

Material certification data for the low silicon heat number 50793 consisted of the following information:

- a) Incoming inspection data, including chemical and gas analysis.
- b) Tensile specimen tests.
- c) Heat evaluation pressure vessel data.

Tables A-1 and A-2 list the as received material inspection data. Tensile test data, together with the theoretical biaxial curves derived from the uniaxial tensile results, as well as those predicated on vessel data are given on Figures A-1 to A-7. Table A-3 gives the plasticity relations used for transforming uniaxial tensile test data (true stress versus true strain) to biaxial true stress versus true strain data and for converting true stresses and strains to nominal (or engineering) values.

Comparison of actual vessel data with predictions based on tensile test results and plasticity theory (i.e. Figures A-5 and A-6 with A-7) shows that agreement is good. Correlation between uniaxial and biaxial stress-strain states is thus once more demonstrated.

Figures A-8 and A-9 show uniaxial tensile data for double cryogenic stretch conditions simulating vessel fabrication processing. Thermal treatments between first and second stretches consist of 24 hours at room temperature or 2 hours at 150°F followed by 4 hours at 300°F to simulate a resin cure cycle. Comparison of Figure A-8 with Figure A-1 shows essentially the same total strain and maximum stress indicating no deterioration in physical properties due to the double stretch and 24 hour room temperature aging. On the other hand, intermediate elevated temperature aging (2 hours at 150°F followed by 4 hours at 300°F) in conjunction with double cryogenic stretch has a significant effect on material properties as shown by comparison of Figure A-1 and A-9. There is an increase in tensile strength and a reduction in total strain.

7.2 Appendix 2 - Biaxial Coupon Data

7.2.1 Biaxial Coupons

Biaxial coupons were cut from S/N 1, 3 and 4

TABLE A-1 (SHEET 1 OF 2)
ARDEFORM MATERIAL INSPECTION RECORD

5-16-68

P.O.No. _____ Date Recd. _____ Vendor Lathrop Matl.Spec. AES 256

Heat No. 50793 No. of Pieces _____ Size Ordered _____ Weight _____

Certificate of Conformance No. _____ Serial Numbers _____

Characteristic	Results	Inspect.	MRB
1. Surface Finish.			
2. Packaging			
3. Sheet Thickness Per Matl. Spec.			
4. Sheet Length & Width Per Matl. Spec.			
No. of Sheets	Accept		
No. of Sheets	Reject		
5. Chemistry Target per Spec.	(Cert. of Conf.) Ladle Analysis	<i>J. Meyer</i>	
C .025 to .045	.03		
Mn .10 MAX	.01		
Si .10 MAX	.07		
Cr 18.30 To 18.70	(18.16)		
Ni 7.10 To 7.50	(7.37)		
Mo .15 to .35	.27		
N .02 To .04	.04		
P } D Smith	.15		
S } D Smith			
	Gas Analysis		
H 2 MAX	2.0 PPM		
O 60 MAX	37 PPM		
Check Analysis Vendor			
Gas Analysis Vendor			
6. Hardness RB 90 MAX	RB 84	<i>Jm</i>	
7. Grain Size		<i>Jm</i>	
Ave. Allowable 5	5		
Ind. Max. Allowable 4	5		

Mount L-4

Reviewed By R Nag

TABLE A-1 (SHEET 2 OF 2)

Characteristic			Results	Inspect.	MRB
8. Inclusions					
Type A	Thin	Allowable 1	0	<i>[Signature]</i>	
	Heavy	0	0		
Type B	Thin	1	0	<i>Wey</i>	
	Heavy	0	0		
Type C	Thin	1	0	<i>[Signature]</i>	
	Heavy	0	0		
Type D	Thin	1	1	<i>[Signature]</i>	
	Heavy	1	0		
T1 C N x y 2	Thin				
	Heavy				
9. Carbide Precip.					
Free of			Carbides Present	<i>[Signature]</i>	
10. Radiographic Inspection					
11. Remarks					

TABLE A-2 (SHEET 1 OF 2)
ARDEFORM MATERIAL INSPECTION RECORD

P.O.No. _____ Date Recd. 6/21/68 Vendor Lafayette Matl.Spec. 256
 Heat No. 50793 No. of Pieces _____ Size Ordered .005" thick Weight _____
 Certificate of Conformance No. _____ Serial Numbers _____

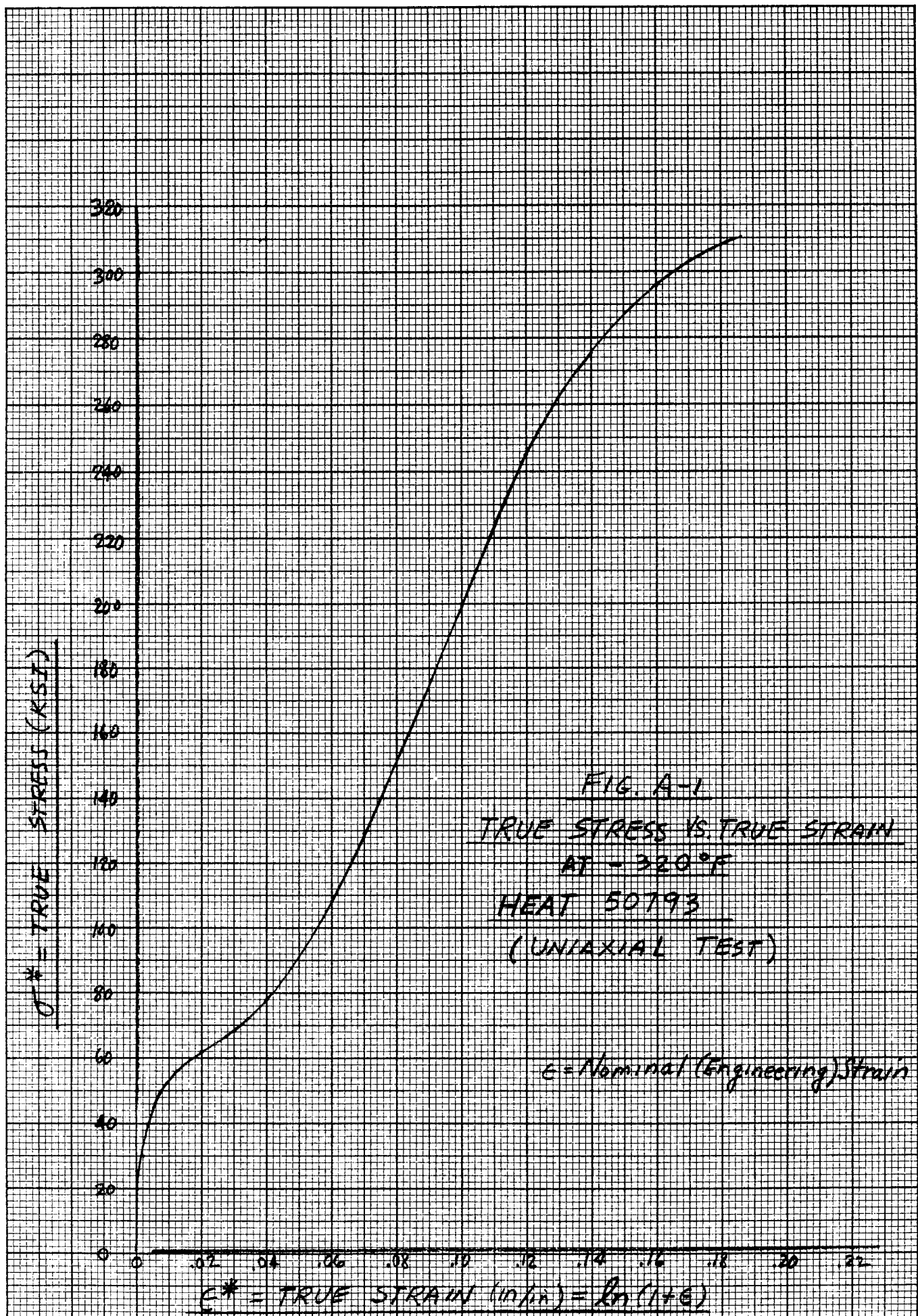
Characteristic	Results	Inspect.	MRB
1. Surface Finish.			
2. Packaging			
3. Sheet Thickness Per Matl. Spec.			
4. Sheet Length & Width Per Matl. Spec.			
No. of Sheets	Accept		
No. of Sheets	Reject		
5. Chemistry Target per Spec.	(Cert. of Conf.)		
	Ladle Analysis	Check Analysis	
C .005 to .045	.03		
Mn 1.0 MAX	.01		
Si .10 MAX	.07		
Cr 18.30 to 18.70	18.76		
Ni 2.10 to 2.50	2.57		
Mo .015 to .035	.27		
N } 2.75 to 2.95 or 0.04	.04		
P } .015 MAX			
S } .015			
	Gas Analysis		
H 2 MAX	2.0		
O 60 MAX	37		
Check Analysis Vendor			
Gas Analysis Vendor			
6. Hardness RB 90 MAX	300-67.5 Conv. RB 96		
7. Grain Size			
Ave. Allowable 6	6		
Ind. Max. Allowable 4	5		

Mount L-9

Reviewed by [Signature]
 1.12.1968

TABLE A-2 (SHEET 2 OF 2)

Characteristic			Results	Inspect.	MRB
8. Inclusions					
Type A	Thin	Allowable /	0	J meyer J	
	Heavy	0	0		
Type B	Thin	/	0		
	Heavy	0	0		
Type C	Thin	/	0		
	Heavy	0	0		
Type D	Thin	/	1	✓ J	
	Heavy	/	0		
Tl C N x y 2	Thin				
	Heavy				
9. Carbide Precip.					
Free of			Carbides Present	✓ J	
10. Radiographic Inspection					
Remarks					



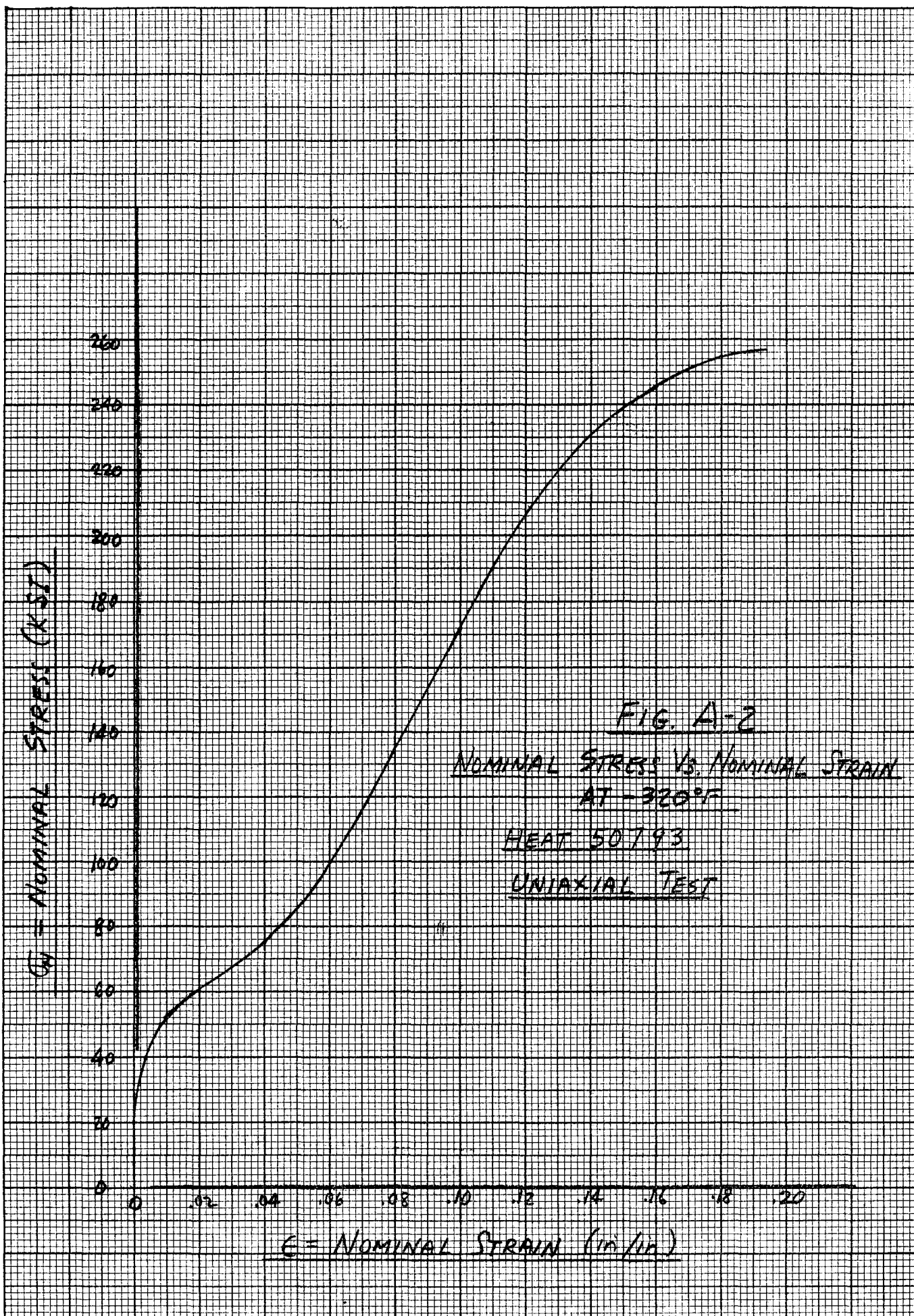


FIG. A-3
 ROOM TEMPERATURE RESPONSE
 HEAT 50793
 (UNIAXIAL)

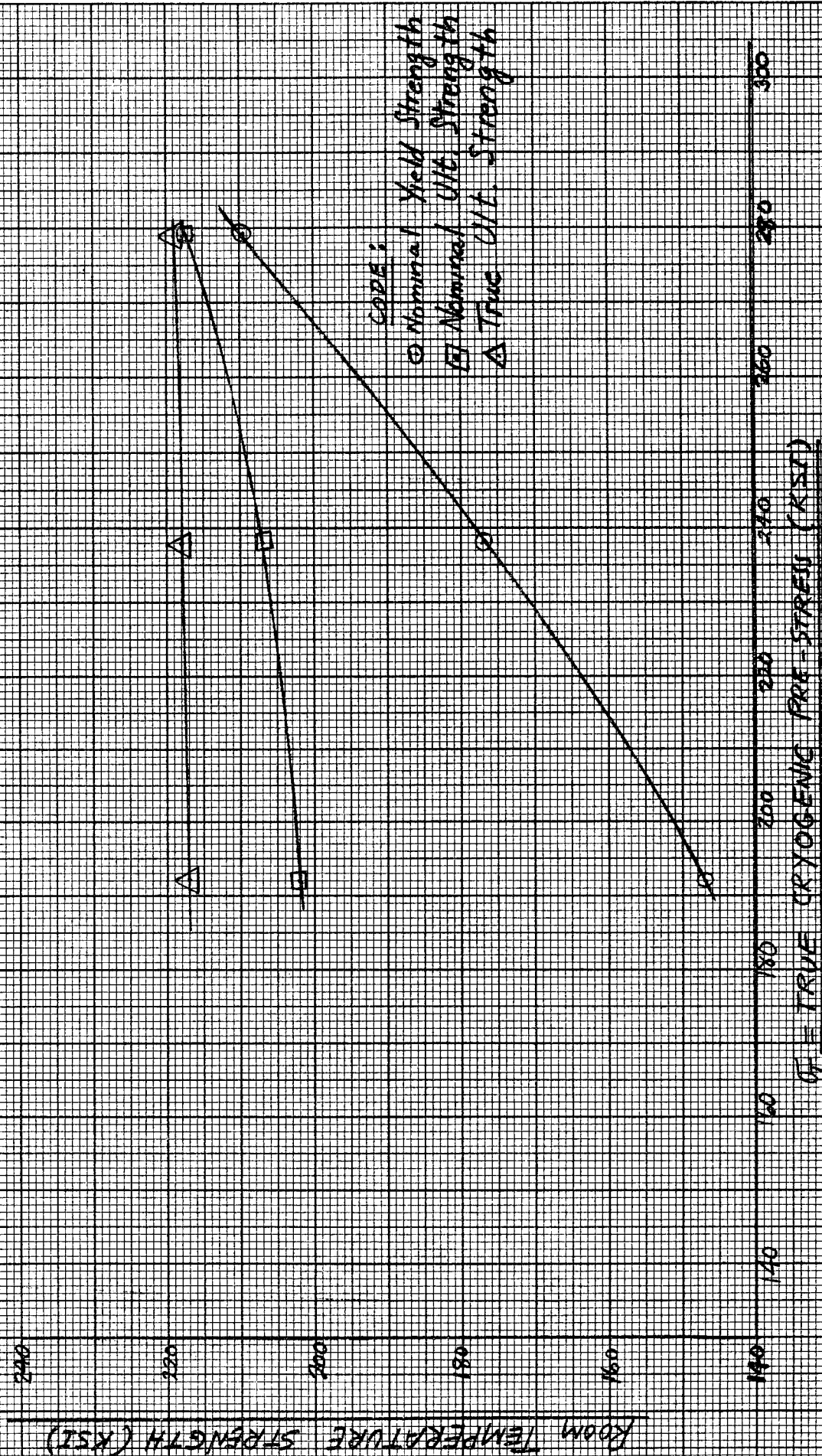
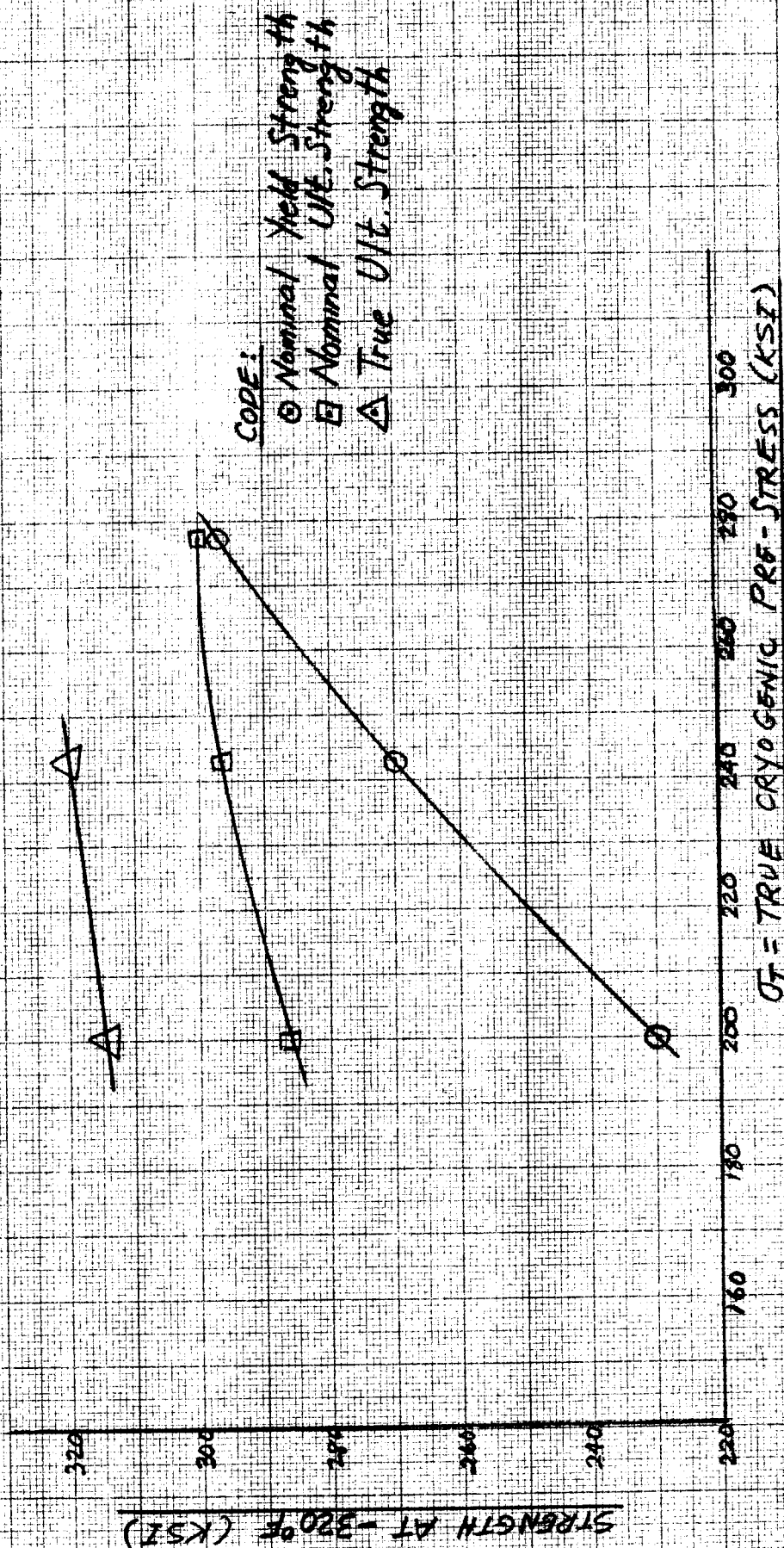


FIG. A-4
RESPONSE AT -320°F
HEAT 50793
(UNIAXIAL)



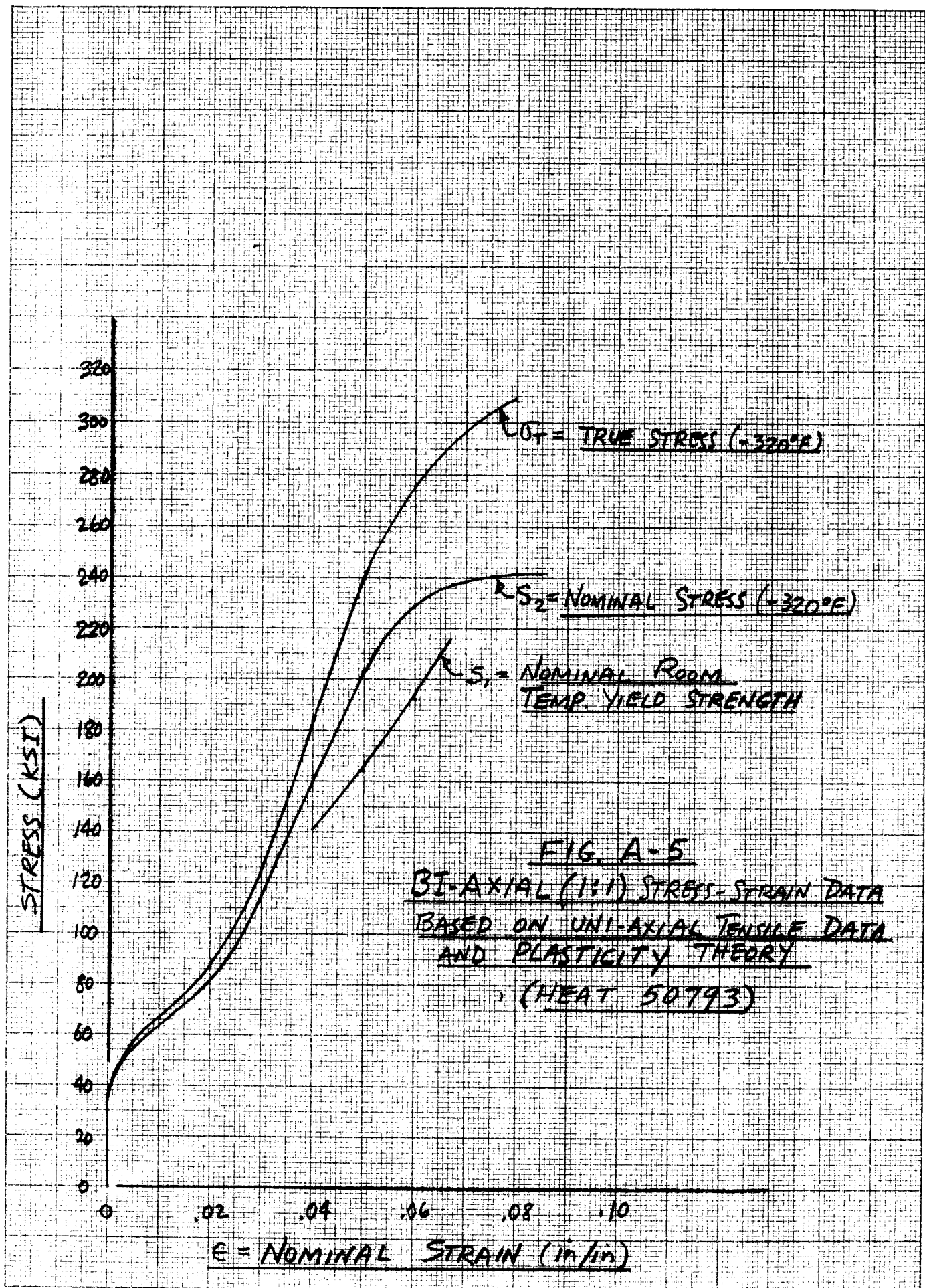


FIG A-6
SPHERE DESIGN CHART
BASED ON UNI-AXIAL DATA & PLASTICITY THEORY
(HEAT 50793)

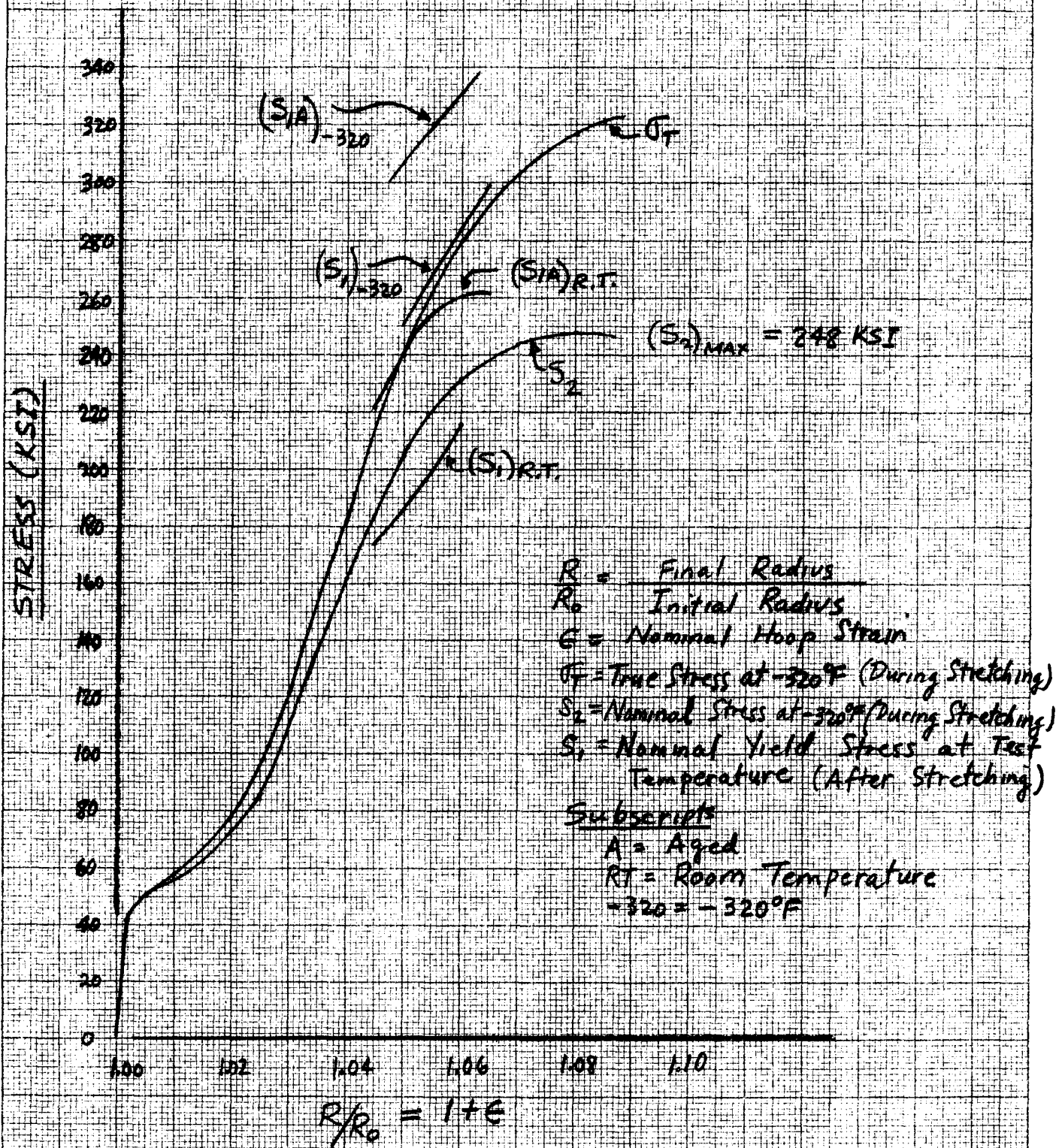


FIG. A-7
SPHERE DESIGN CHART
BASED ON VESSEL DATA
(HEAT 50793)

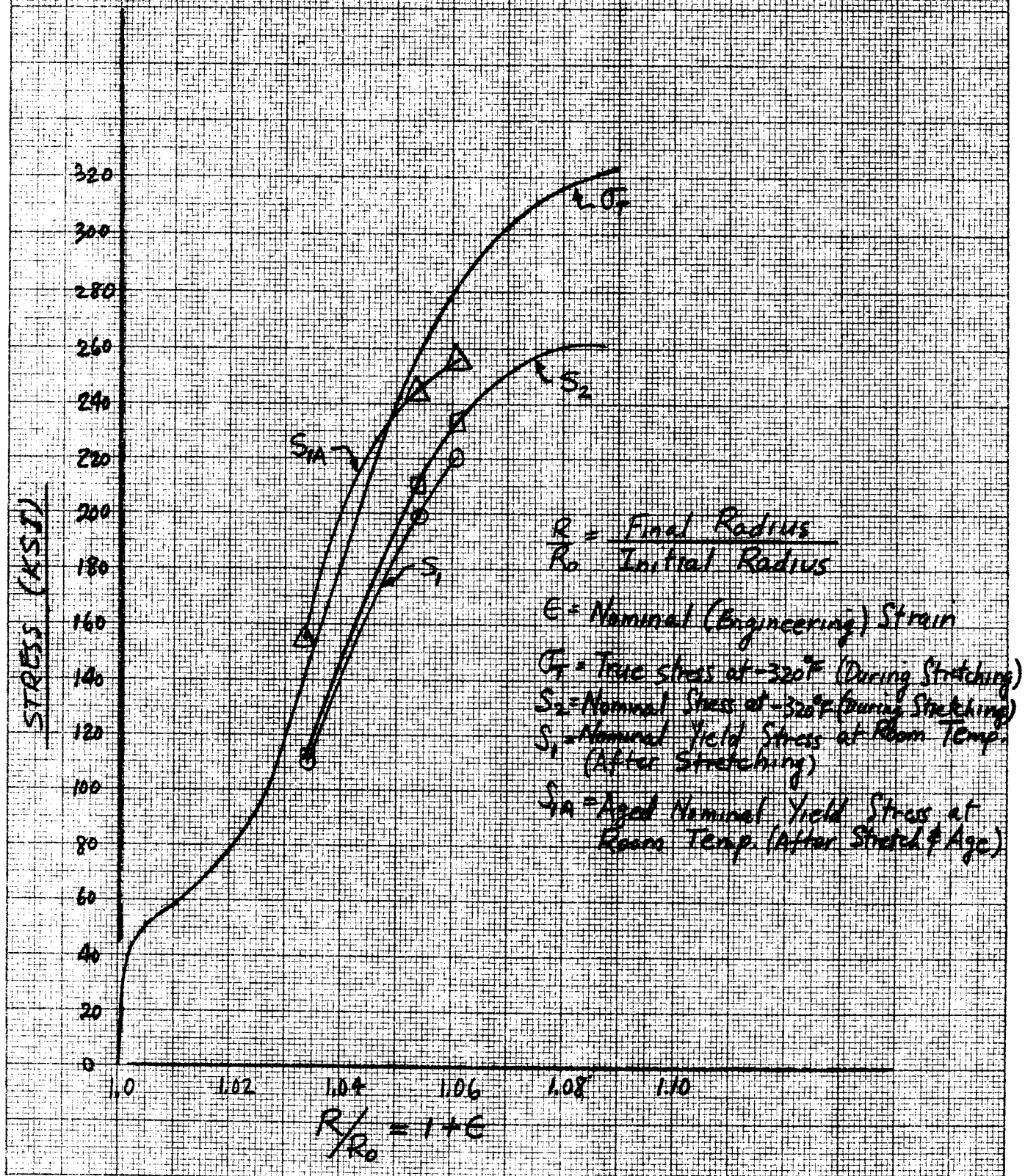


TABLE A-3

PLASTICITY RELATIONS APPLIED TO TENSILE COUPONS
AND INTERNALLY PRESSURIZED SPHERES AND CYLINDERS

Line No.	Type of Member	Tensile Coupon		Sphere	Cylinder
		Loading	Axial	Pressure	Pressure
1	Given principal stresses, in terms of Maximum Principal Stress,	σ_1 σ_2 σ_3	σ_1 0 0	σ_1 σ_1 0	σ_1 $\frac{1}{2}\sigma_1$ 0
2	Stress invariant in terms of maximum principal stress, $\sigma^* = \sqrt{\frac{1}{2}[(\sigma_1 - \sigma_2)^2 + (\sigma_2 - \sigma_3)^2 + (\sigma_3 - \sigma_1)^2]}$		σ_1	σ_1	$\frac{\sqrt{3}}{2} \sigma_1$
3	Principal stresses in terms of stress invariant,	σ_1 σ_2 σ_3	$\sigma^* = \sigma_N(1+\epsilon)$ 0 0	$\sigma^* = \sigma_N(1+\epsilon)^3$ $\sigma^* = \sigma_{2N}(1+\epsilon)^3$ 0	$\frac{2}{\sqrt{3}} \sigma^*$ $\frac{1}{\sqrt{3}} \sigma^*$ 0
4	Invariant stress-strain relation		$\sigma^* = D\epsilon^*$	$\sigma^* = D\epsilon^*$	$\sigma^* = D\epsilon^*$
5	Strain invariant relation		$\sqrt{\frac{2}{3}} \sqrt{\epsilon_1^2 + \epsilon_2^2 + \epsilon_3^2}$		
6	Principal strains in terms of stress invariant $D\epsilon_1 = \sigma_1 - .5(\sigma_2 + \sigma_3)$ $D\epsilon_2 = \sigma_2 - .5(\sigma_3 + \sigma_1)$ $D\epsilon_3 = \sigma_3 - .5(\sigma_1 + \sigma_2)$		σ^* $-.5\sigma^*$ $-.5\sigma^*$	$.5\sigma^*$ $.5\sigma^*$ $-\sigma^*$	$\frac{1}{2}\sqrt{3} \sigma^*$ 0 $-\frac{1}{2}\sqrt{3} \sigma^*$
7	Principal strains in terms of invariant strain, $\epsilon_1 = \ln L/L_0$ or $\epsilon_1 = \ln R/R_0$ $\epsilon_2 = \ln w/w_0$ $\epsilon_3 = \ln t/t_0$		ϵ^* $-.5\epsilon^*$ $-.5\epsilon^*$	$.5\epsilon^*$ $.5\epsilon^*$ $-\epsilon^*$	$\frac{1}{2}\sqrt{3} \epsilon^*$ 0 $-\frac{1}{2}\sqrt{3} \epsilon^*$

$\sigma^*, \sigma_1, \sigma_2, \sigma_3$ are true stresses (load \div actual area)
 σ_N, σ_{2N} are nominal stresses, (load \div initial area)
 $\epsilon^*, \epsilon_1, \epsilon_2, \epsilon_3$ are true strains (logarithmic)
 ϵ = engineering (nominal) strain, uniaxial or hoop strain as appropriate

L_0, R_0, t_0, w_0 = initial values of length, radius, thickness, width

L, R, t, w = final value of length, radius, thickness, width

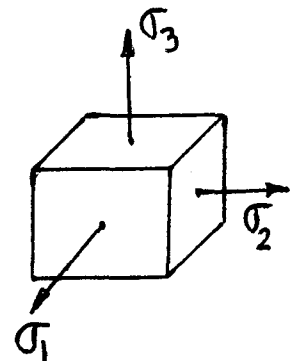


FIG A-8

STRESS - STRAIN CURVE (UNI-AXIAL)

DOUBLE CRYOGENIC STRETCH

INTERMEDIATE ROOM TEMP. AGE

(HEAT 50793)

S/N 125

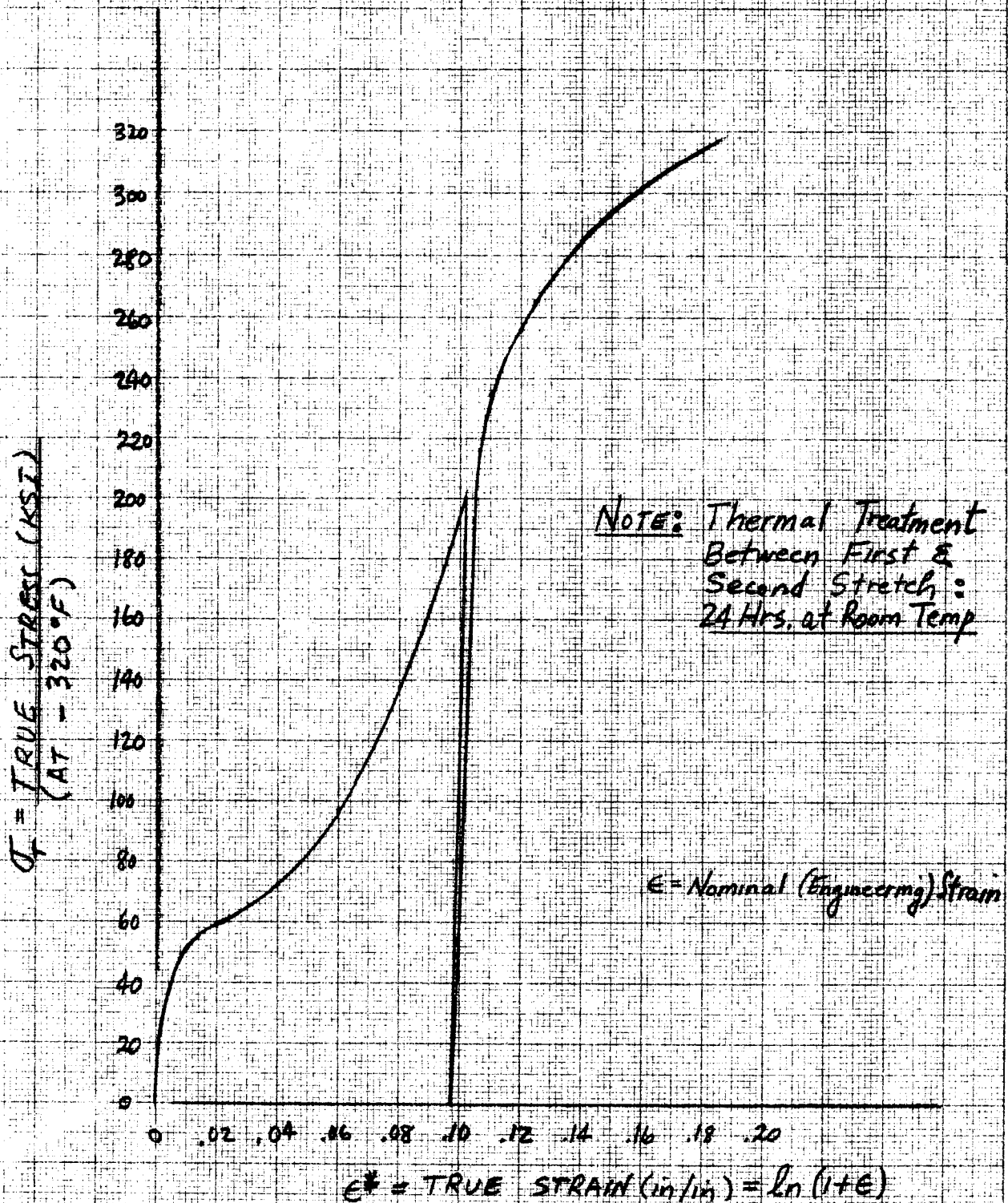
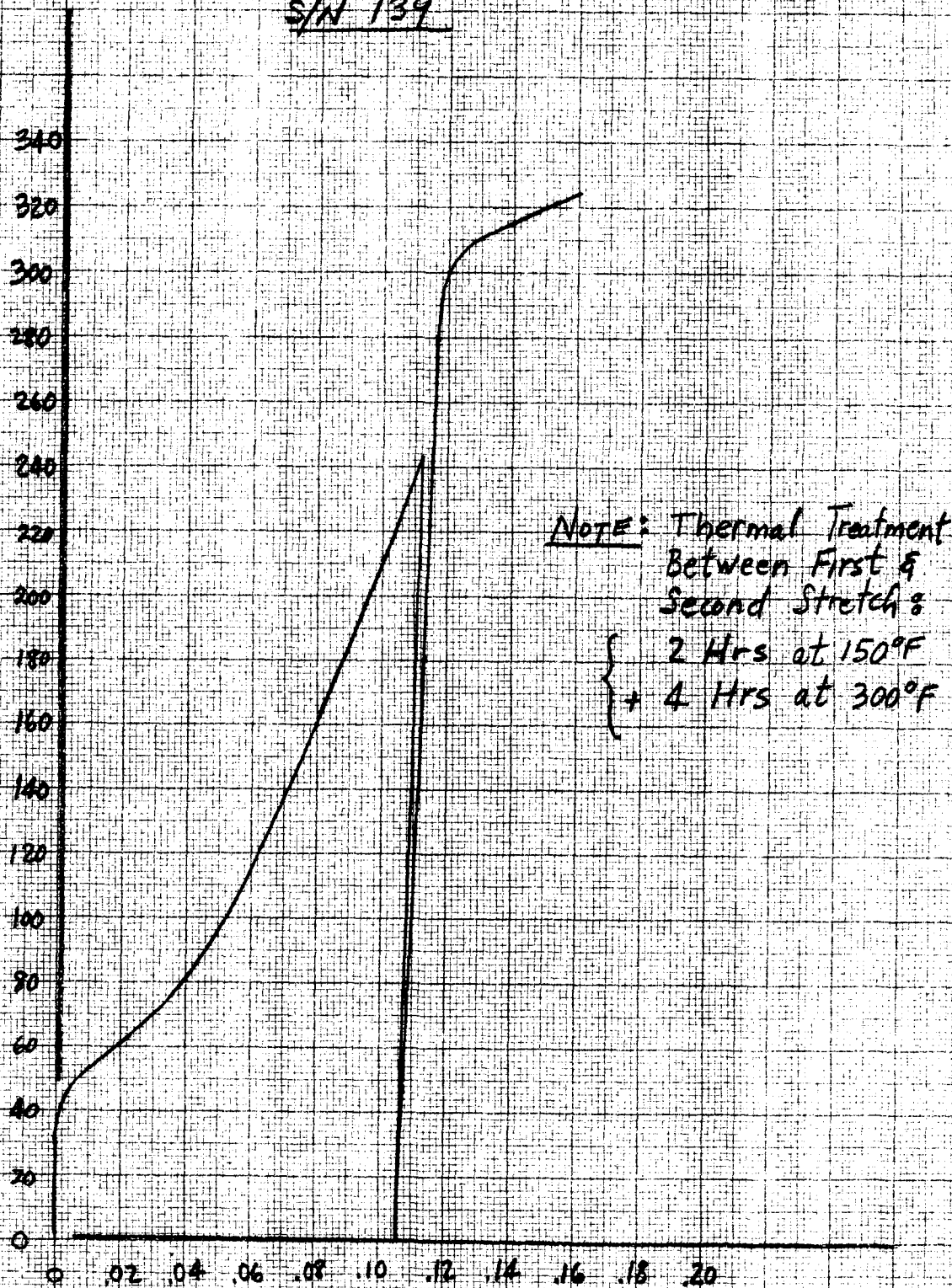


FIG A-9
STRESS-STRAIN CURVE (UNI-AXIAL)
DOUBLE CRYOGENIC STRETCH
INTERMEDIATE THERMAL AGE
(HEAT 50793)
S/N 139

$\sigma_T = \text{TRUE STRESS (KSI)}$
 (AT -320°F)



$\epsilon^* = \text{TRUE STRAIN (in/in)} = \ln(1+E)$

spheres described in Table A-4. Specimen dimensions are given on Figure A-10; thicknesses correspond to those given in Table A-4. Special grip plates, as shown in the photographs on Figure A-11, were attached to the tensile specimen ends as required to facilitate testing and to prevent failure in the specimen grip region.

7.2.2 Biaxial Coupon Test Data Summary

Tables A-5 through A-8 and Figures A-12 through A-18 summarize the tensile test data. Yield points were determined as .2% offset values. Axial and transverse strain gages were used to monitor strains for Poisson's ratio measurements. Extensometers in conjunction with X-Y recorders were used to obtain the load strain curves generated by loading the specimens in a tensile testing machine. Cryostats were employed to facilitate complete submergence of the test specimens in LN₂ or LH₂ for the cryogenic tests.

7.3 Appendix 3 - Tension-Compression Uniaxial Test Data

Tension-compression room temperature test data for low silicon Heat 50793 is summarized in Table A-9. Figures A-19 and A-20 depict the cyclic loading used in these uniaxial tests. The cyclic loading consisted of an initial plastic tensile loading followed by tension - compression cycling at $\pm 90\%$ of the initial .2% offset tensile yield point. Typical variation of .2% offset tensile and compressive yield points and total strain with number of cycles is shown on Figures A-21 through A-24 herein.

As discussed in Section 3.3, a considerable Bauschinger effect was found. Substantial reduction in .2% offset tensile and compressive yield points as well as an increase in total strain with increased number of cycles was found. For example, cyclic tension - compression testing of S/N 108 specimen (Figure A-24) resulted in reductions of about 1/3 in .2% tensile and compressive yield points after 100 cycles with an increase of about 17% in total strain.

7.4 Appendix 4 - Coefficient of Thermal Contraction and Density Data

Prestrained tensile specimens fabricated from low silicon heat 50793 were used in these tests. Values of thermal contraction versus temperature are given in the

TABLE A-4 BIAXIAL COUPON SPHERES

<u>Sphere</u>	<u>S/N 1</u>	<u>S/N 3</u>	<u>S/N 4</u>
First Cryogenic Stretch (-320°F)	$\bar{\sigma}_T = 305 \text{ ksi}$	$S_2 = 175 \text{ ksi}$	$S_2 = 175 \text{ ksi}$
Room Temperature Age (Several Days)	---		---
150°F (2 hrs.) + 300°F (4 hrs.)	---	---	
Second Cryogenic Stretch (-320°F)	---	$\bar{\sigma}_T = 264 \text{ ksi}$	$\bar{\sigma}_T = 260 \text{ ksi}$
Final Sphere Diameter	22.3 in.	22.8	22.9
Final Sphere Thickness	.026 in.	.026	.027
Tensile Specimen S/N*	1-220 to 1-225, 216, 226, 227, 253A, 254A, and 257A to 263A	230 to 235 and 237 to 239	243 to 251

Notes:

- * Letter A in tensile specimen S/N signifies an annealed specimen. These specimens were annealed at $1950 \pm 25^\circ\text{F}$ subsequent to cryogenic stretch and tensile coupon machining.

S_2 = Nominal stress at -320°F

$\bar{\sigma}_T$ = True stress at -320°F

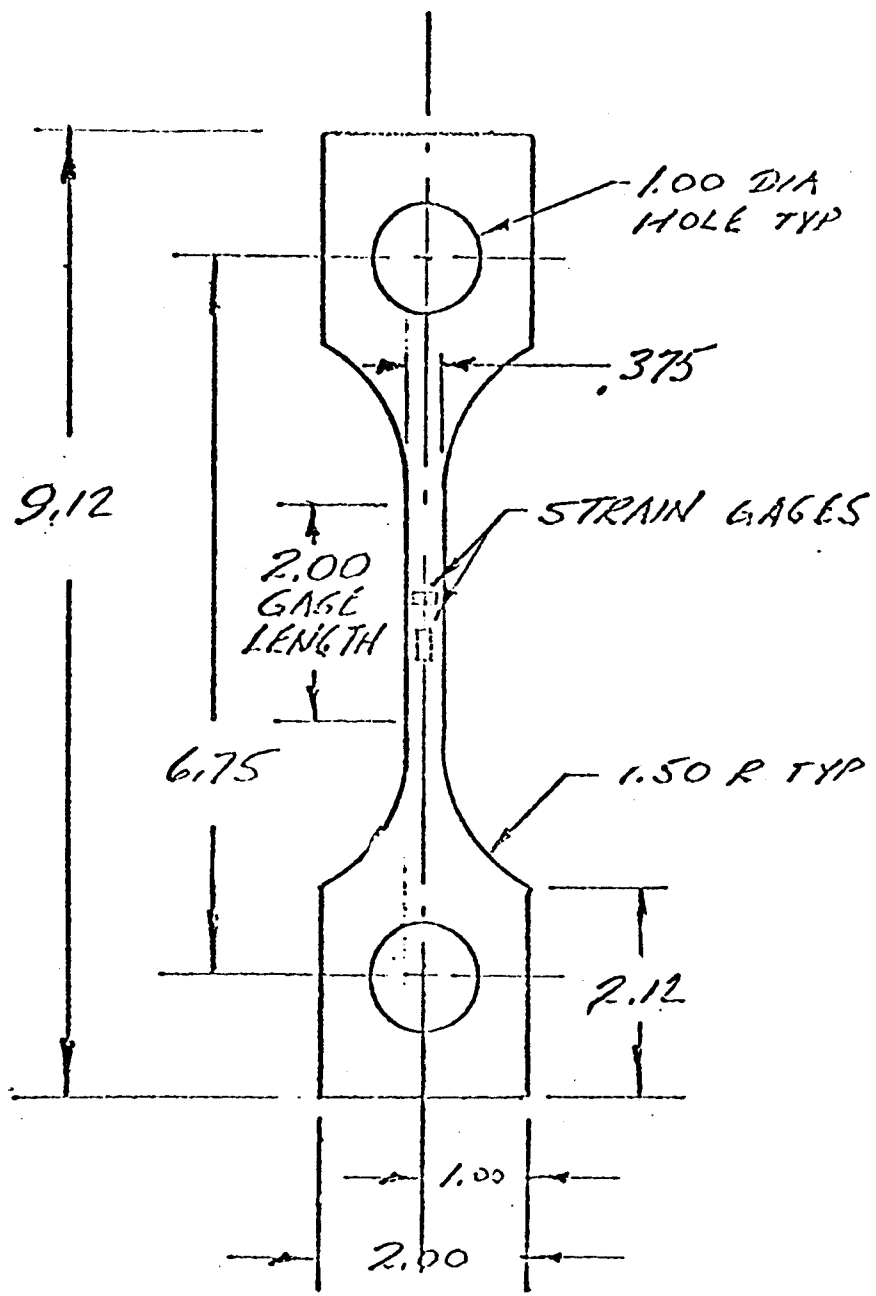


FIG. A-10
BI-AXIAL TENSILE
SPECIMEN DIMENSIONS

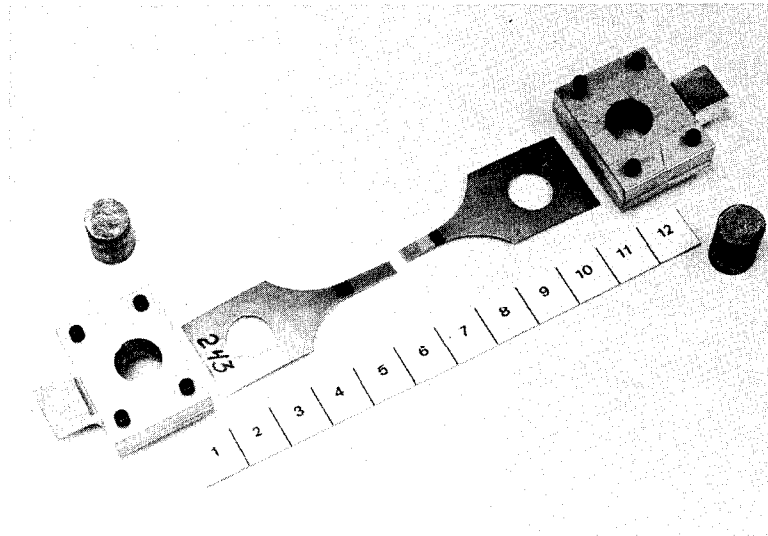


FIGURE A-11 TEST SPECIMEN AND SPECIAL GRIPS

Vessel S/N 3

TABLE A-5
SUMMARY OF BIAXIAL COUPON DATA
DOUBLE CRYOGENIC STRETCH - ROOM TEMP. AGING
TRUE CRYOGENIC PRE-STRESS = 264,000 PSI

Specimen S/N	Test Temp. (°F)	Area (In ²)	Yield Load (lb.)	Yield Stress (ksi)	Ult. Load (lb.)	Ult. Stress (ksi)	Elongation %	Modulus of Elasticity (psi) x 10 ⁶	Poisson's Ratio
237	R.T.	.01029	1935	188	2160	210	3	21.3	.294
238	R.T.	.01074	2060	192	2240	209	4	23.3	.290
239	R.T.	.01042	1920	184	2290	220	2	21.9	.296
233	-320	.01115	----	---	3270	293	11	22.7	.278
234	-320	.01015	----	---	3000	296	8	22.0	.338
235	-320	.01042	2760	265	3070	295	9	22.5	.240
230	-423	.0102	3125	306	3460	339	1.8	28.3	.32
231	-423	.0095	----	---	----	---	1.7	----	.32
232	-423	.0096	3025	315	3420	356	1.7	27.3	.31

Vessel S/N 4

TABLE A-6
SUMMARY OF BIAxIAL COUPON DATA
DOUBLE CRYOGENIC STRETCH - THERMAL AGING BETWEEN STRETCHES
TRUE CRYOGENIC PRE-STRESS = 260,000 PSI

Specimen S/N	Test Temp. (°F)	Area (in ²)	Yield Load (lb.)	Yield Stress (ksi)	Ult. Load (lb.)	Ult. Stress (ksi)	Elongation %	Modulus of Elasticity (psi) x 10 ⁶	Poisson's Ratio
246	R.T.	.01064	1855	174	2250	211	7	20.3	.295
247	R.T.	.01123	1900	169	2425	216	8	21.3	.264
248	R.T.	.01088	1875	172	2330	214	8	20.8	.290
249	-320	.01151	2520	219	3400	295	14	22.6	.266
250	-320	.01124	2620	233	3280	292	11	23.9	.280
251	-320	.01147	-----	---	3330	290	13	22.7	.305
243	-423	.0120	3075	256	3660	305	1.7	27.7	.33
244	-423	.0110	3260	296	3400	309	1.7	27.7	.29
245	-423	.0110	3175	280	3490	317	1.7	26.7	.32

Vessel S/N 1

TABLE A-7
 SUMMARY OF BIAxIAL COUPON TESTS
 SINGLE CRYOGENIC STRETCH
 TRUE CRYOGENIC PRE-STRESS = 305,000 PSI

Specimen S/N	Test Temp. (°F)	Area (in ²)	Yield Load (lb.)	Yield Stress (ksi)	Ult. Load (lb.)	Ult. Stress (ksi)	Elongation (%)	Modulus of Elasticity (psi x 10 ⁶)	Poisson's Ratio
1-220	R.T.	.00985	1920	195	2080	211	3	21.1	.278
1-221	R.T.	.01065	2000	188	2290	215	5	23.4	.265
1-222	R.T.	.01110	1950	176	2270	205	5	21.3	.278
1-223	-320	.009296	-----	---	2840	306	6	25.5	.284
1-224	-320	.01120	2770	247	3270	292	9	28.9	.295
1-225	-320	.01032	-----	---	3070	297	5	22.6	.272
216	-423	.00988	3210	325	3360	339	1.2	30.2	.33
226	-423	.01102	3320	301	3700	336	1.3	26.8	.36
227	-423	.00952	3080	324	3410	358	1.1	29.3	.32

Vessel S/N 1

TABLE A-8
SUMMARY OF BIAxIAL COUPON TESTS
ANNEALED SPECIMENS

Specimen S/N	Test Temp. (°F)	Area (in ²)	Yield Load (lb.)	Yield Stress (ksi)	Ult. Load (lb.)	Ult. Stress (ksi)	Elongation %	Modulus of Elasticity (psi) x 10 ⁶	Poisson's Ratio
260A	R.T.	.01289	458	35.5	1540	119	30	22.6	.240
261A	R.T.	.01211	415	32.3	1460	121	28	32.8	.340
262A	R.T.	.01150	374	32.5	1350	117	33	29.8	.262
257A	-320	.01185	520	43.9	3100	262	26	23.7	.324
258A	-320	.01272	572	45.0	3270	257	18	26.2	.280
259A	-320	.01172	530	45.2	3010	257	23	21.7	.292
253A	-423	.013	648	50.0	3250	250	17.7	30.8	.35
254A	-423	.011	520	47.0	2500	227	12.8	16.1	.37
263A	-423	.012	595	50.0	3000	250	14.3	21.6	.31

FIG. A-12

BIAXIAL COUPON TEST DATA

DOUBLE CRYOGENIC STRETCH-THERMAL AGING*

[TRUE CRYOGENIC PRE-STRESS = 200,000 PSI]

* 2 HRS. @ 150°K
64 HRS. @ 300°K

- YIELD STRENGTH
- ULTIMATE STRENGTH
- POISSON'S RATIO
- △ MODULUS OF ELASTICITY

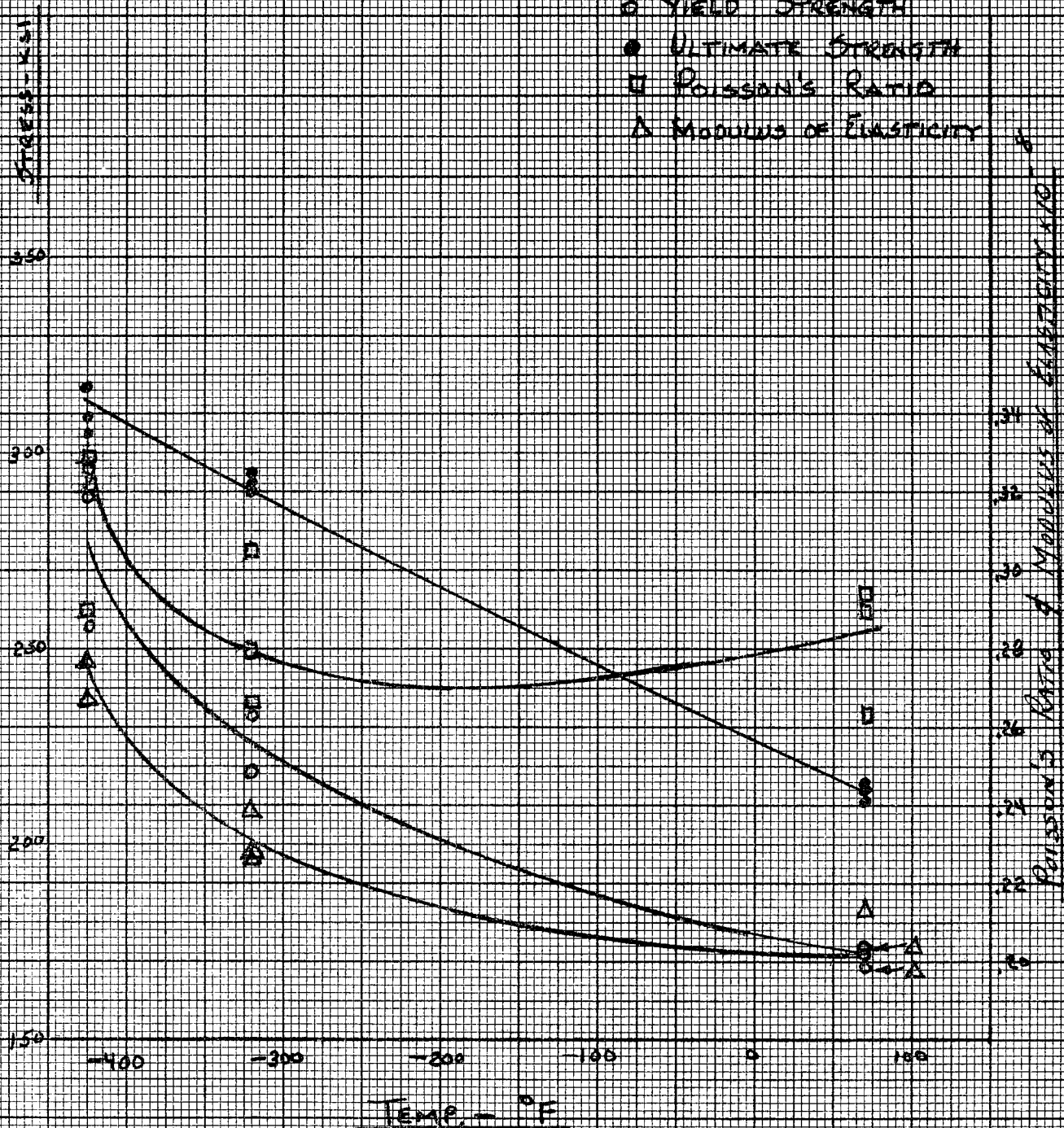


FIG. A-13
BIAXIAL COUPON TEST DATA
DOUBLE CRYOGENIC STRETCH - ROOM TEMP. AGE
 [TRUE CRYOGENIC PRE-STRESS = 264,000 PSI]

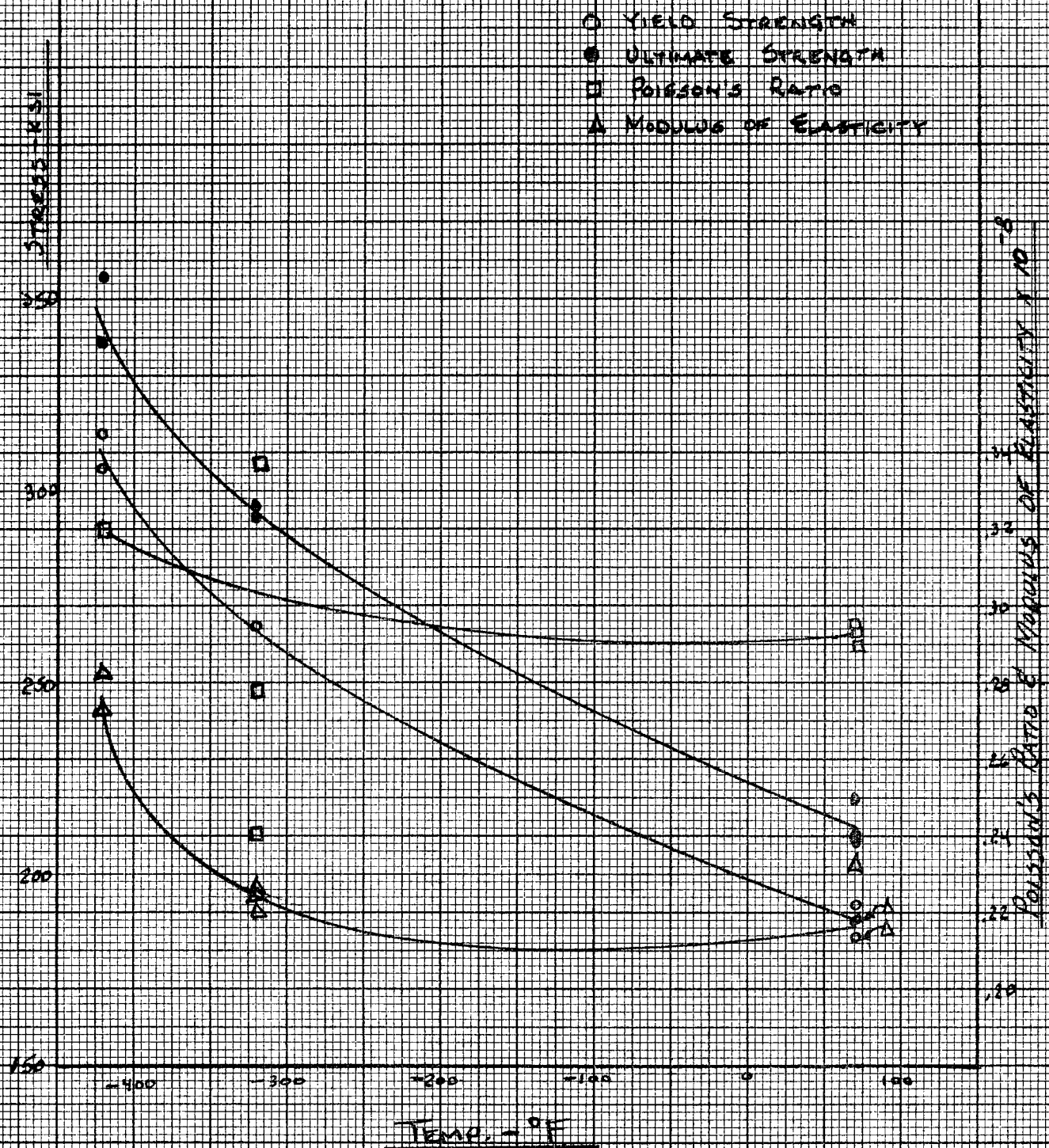


FIG. A-14 BIAXIAL COUPON TEST DATA SINGLE CRYOGENIC STRETCH

[TRUE CRYOGENIC PRESTRESS = 305,000 PSI]

- YIELD STRENGTH
- ULTIMATE STRENGTH
- POISSON'S RATIO
- △ MODULUS OF ELASTICITY

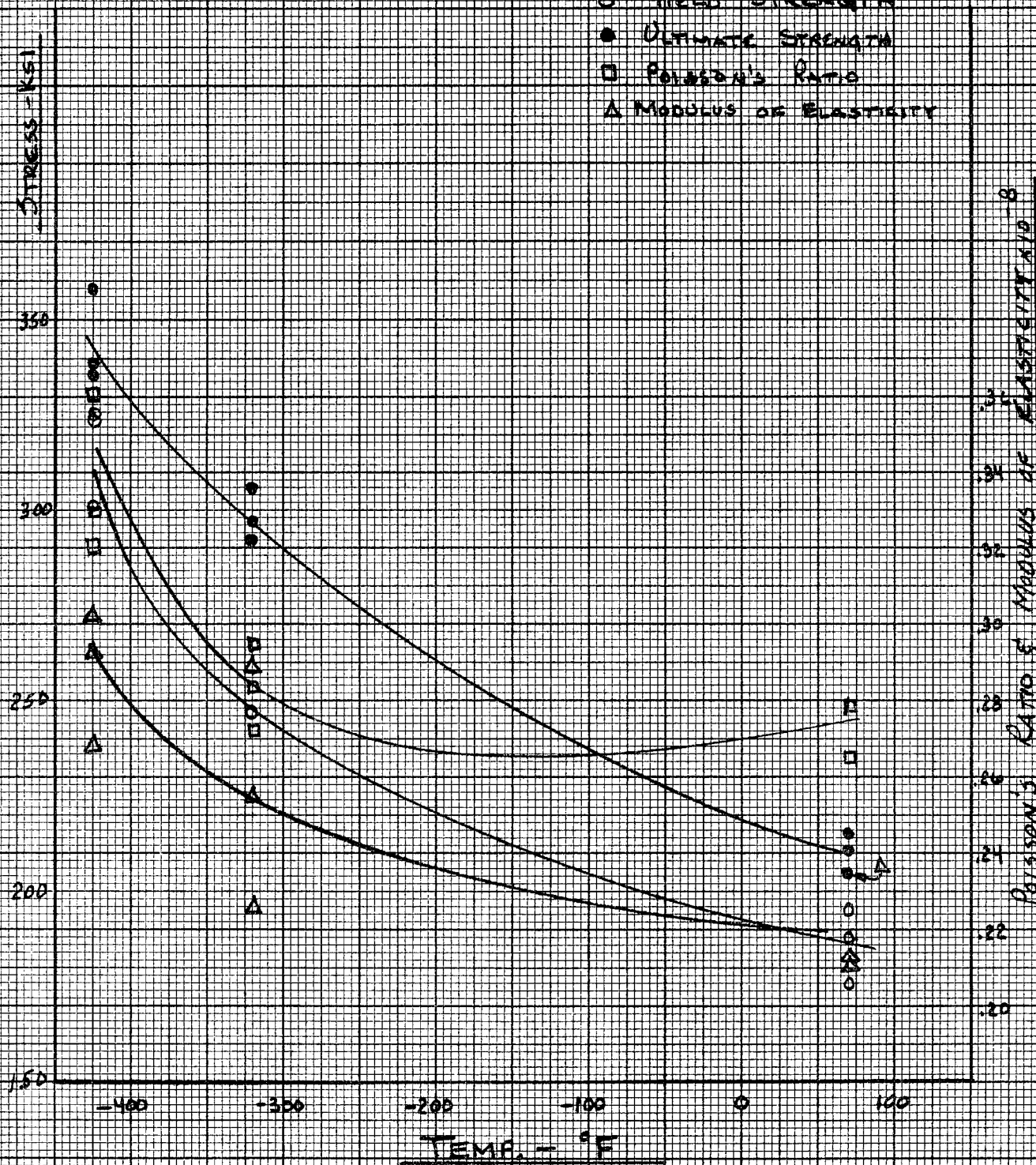


FIG. A-15

BIAXIAL COUPON TEST DATA
ANNEALED SPECIMENS

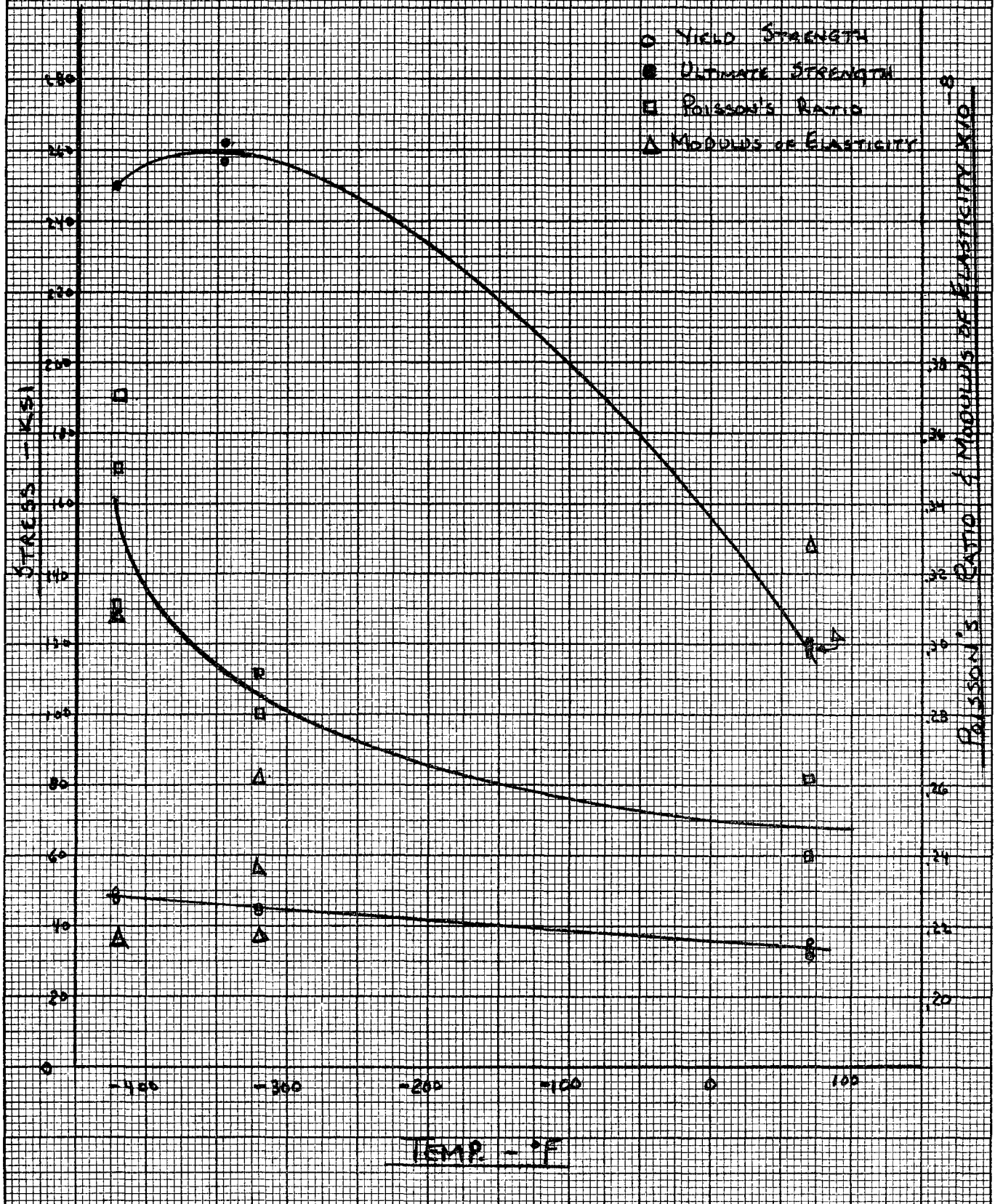


FIG. A-16

TRUE STRESS VS TRUE STRAIN

DOUBLE CRYSTALLINE STRETCH - THERMAL AGE

TEST TEMP. = -423°K

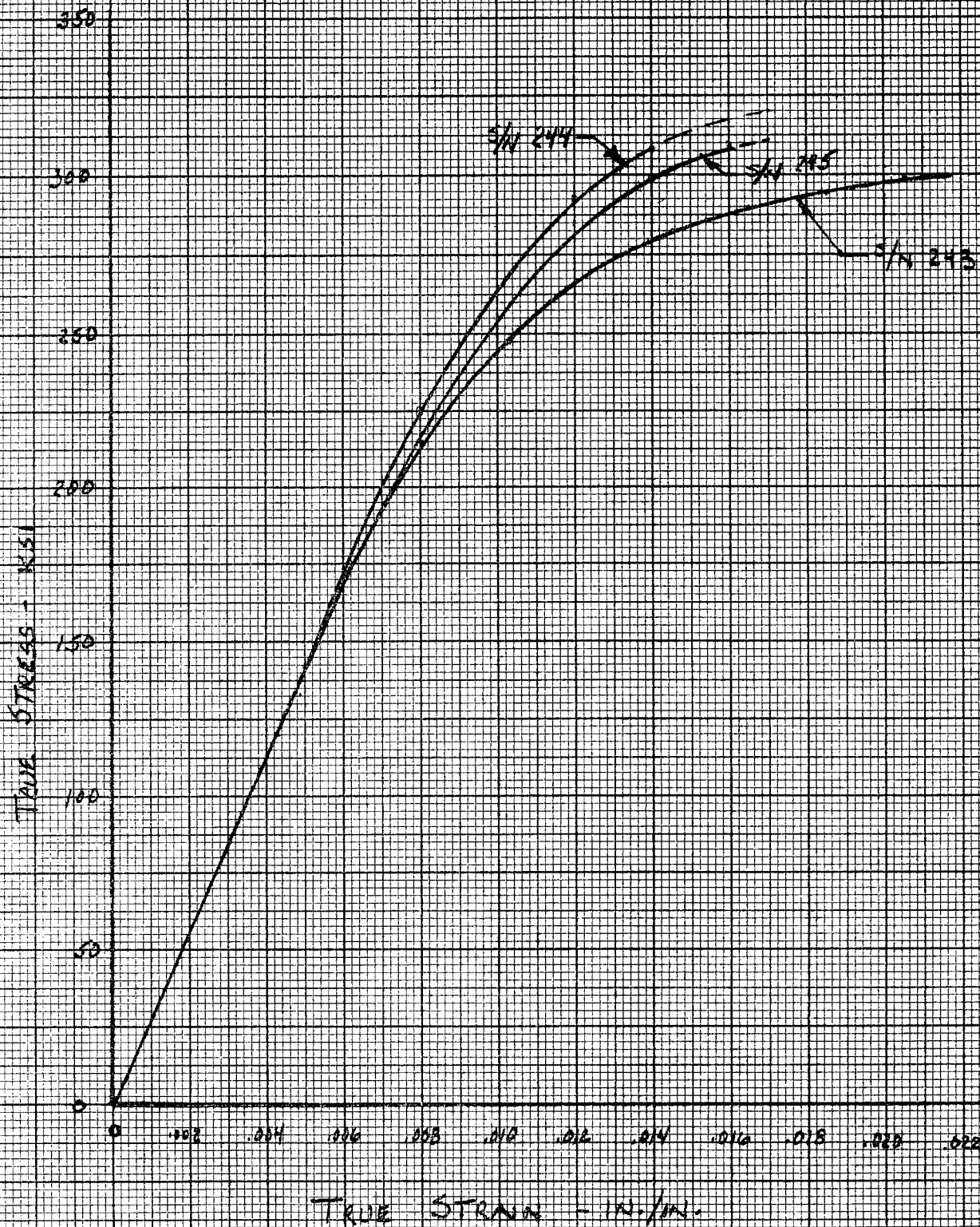


FIG. A-17
TRUE STRESS VS TRUE STRAIN
DOUBLE CRYSTALLINE STRETCH - ROOM TEMP. AGE
TEST TEMP. = -423°F

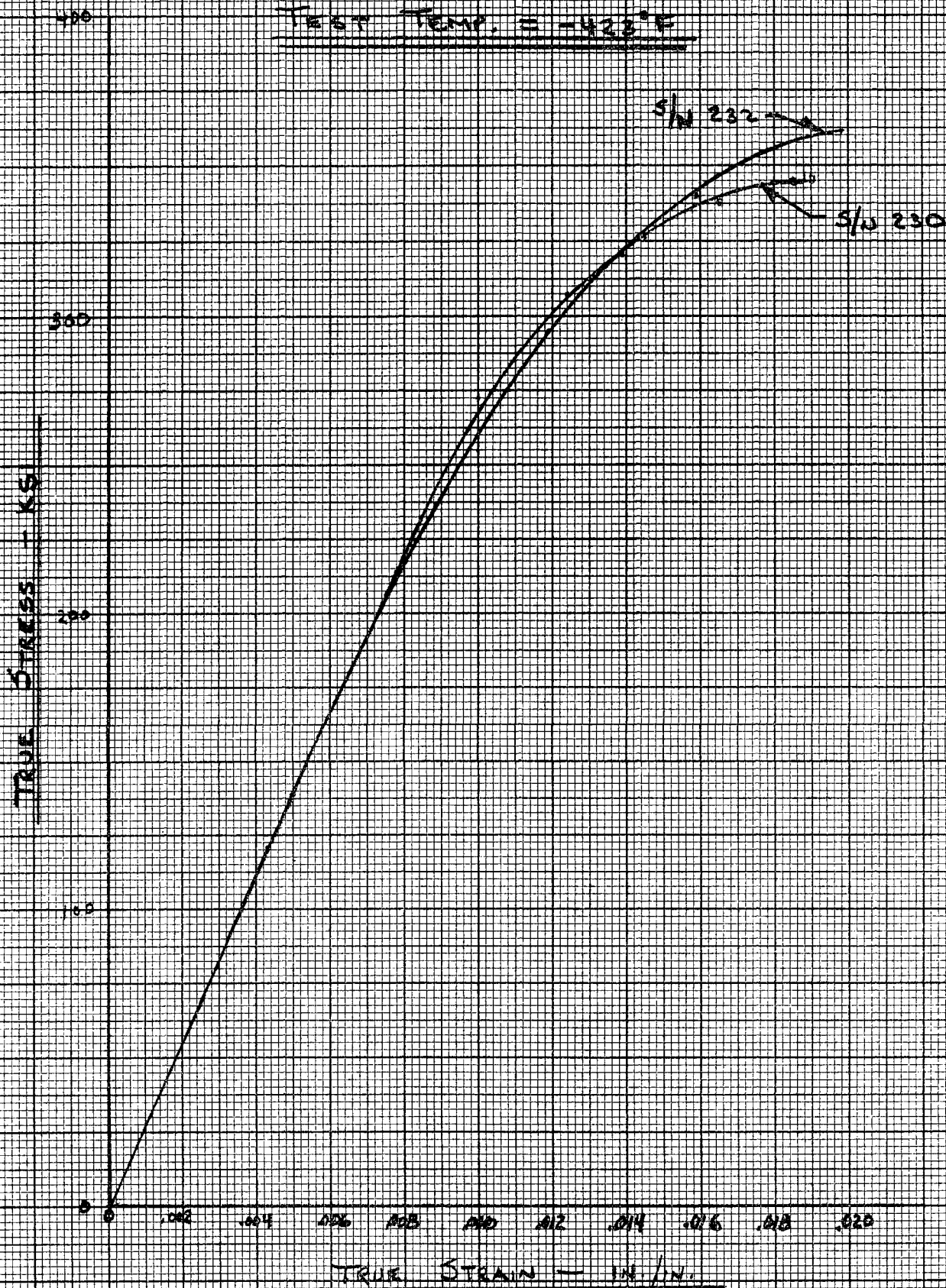


FIG. A-18
TRUE STRESS VS TRUE STRAIN
SINGLE CRYOGENIC STRETCH
TEST TEMP. = -423°F

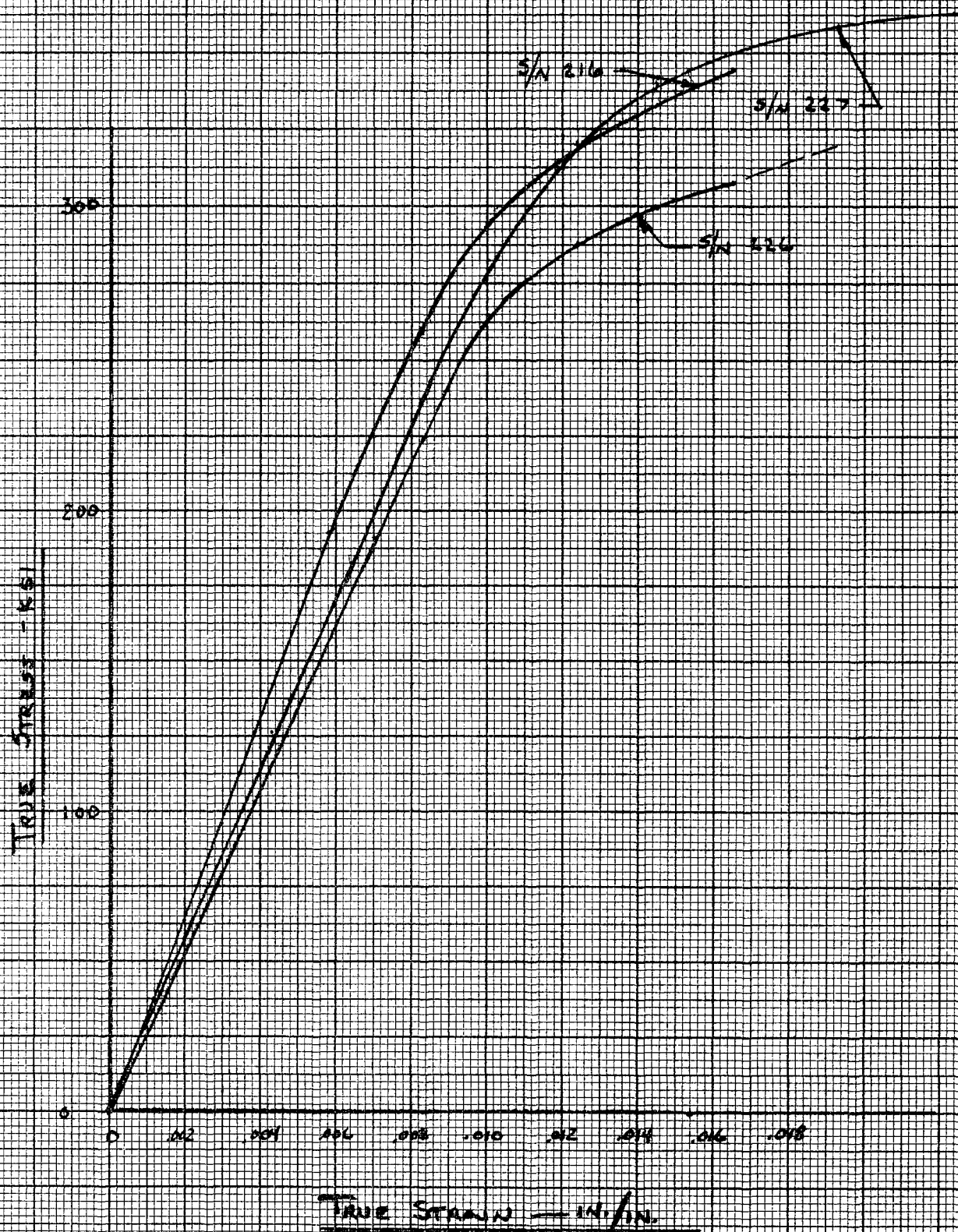


TABLE A-9
TENSION-COMPRESSION COUPON TEST DATA SUMMARY

S/N	σ_M (Pre-Strain)		Aging Treatment Prior to 2nd Stretch	Cross-Section Area Prior to Test (in ²)	2% Tensile Yield Load (lb.)	Initial Tensile Yield Stress σ_{yt} (ksi)	Cyclic Stress (ksi)	Number of Cycles	Yield Point Ratio σ_{yc}/σ_{yt}	Initial Compression Yield σ_{yc}	Remarks
	1st Stretch	2nd Stretch									
113	N/A	N/A	N/A	.06299	2100	33.3	30.0	100	---	---	
116	N/A	N/A	N/A	.06476	2060	31.8	27.8	100	---	---	
117	N/A	N/A	N/A	.06299	2100	33.3	30.5	100	---	---	
118	N/A	N/A	N/A	.06175	2080	33.7	30.4	100	---	---	
119	N/A	N/A	N/A	.06400	2240	35.0	31.6	100	---	---	
102	244	N/A	N/A	.05486	13000	237	214	~36			Specimen Necked Out-Side Gage Section
103	243	N/A	N/A	.05536	12000	217	195	100	---	---	
111	243	N/A	N/A	.05730	12900	227	199	100	---	---	
112	243	N/A	N/A	.05263	12450	237	207	70	---	---	Specimen Necked Test Stopped
104	214	280	R.T. Age	.0579	13200	228	205	6	.68	155	Specimen Buckled
114	216	280	R.T. Age	.0568	12900	227	205	39	.70	159	Fractured Outside Gage Section
120	214	280	R.T. Age	.0551	12600	229	194	100	.71	163	
123	214	283	R.T. Age	.05583	13100	235	201	74+	.73	171	Specimen Fractured
101	184	278	2 hrs. @ 150°F - 4 hrs. @ 300°F	.05753	12450	217	191	100	.67	145	
105	185	281	"	.05726	13170	230	205	20	.67	154	Buckled at Grips
106	181	282	"	.05713	13170	231	205	100	.65	150	
108	182	281	"	.06006	13240	221	205	100	.67	148	
110	181	283	"	.05833	13800	237	211	88	---	---	Fractured Outside Gage Length

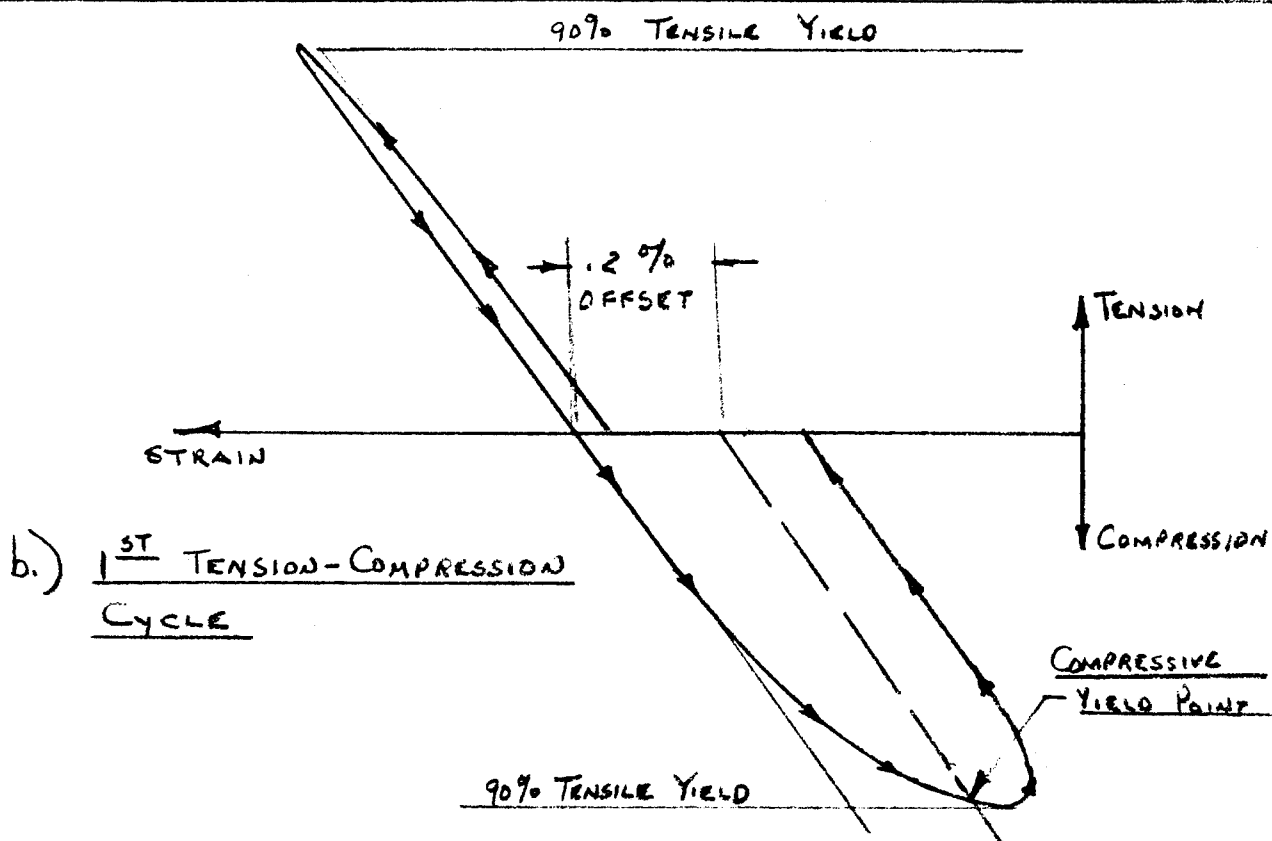
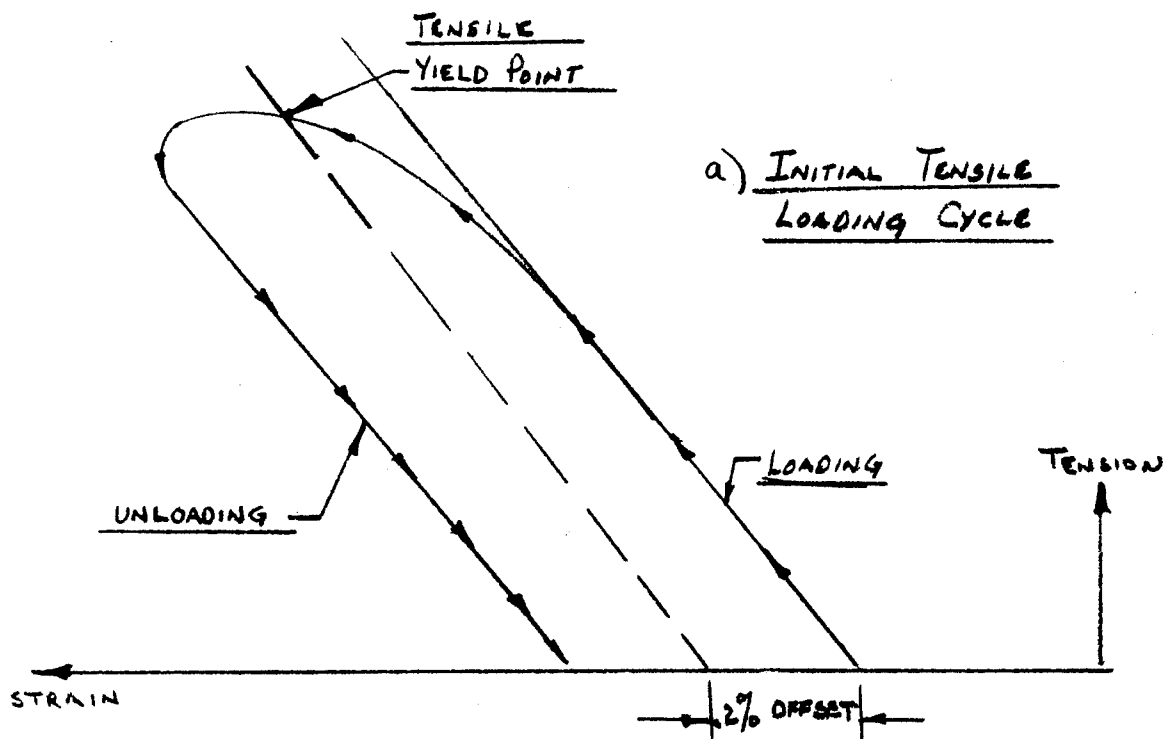


FIG. A-19

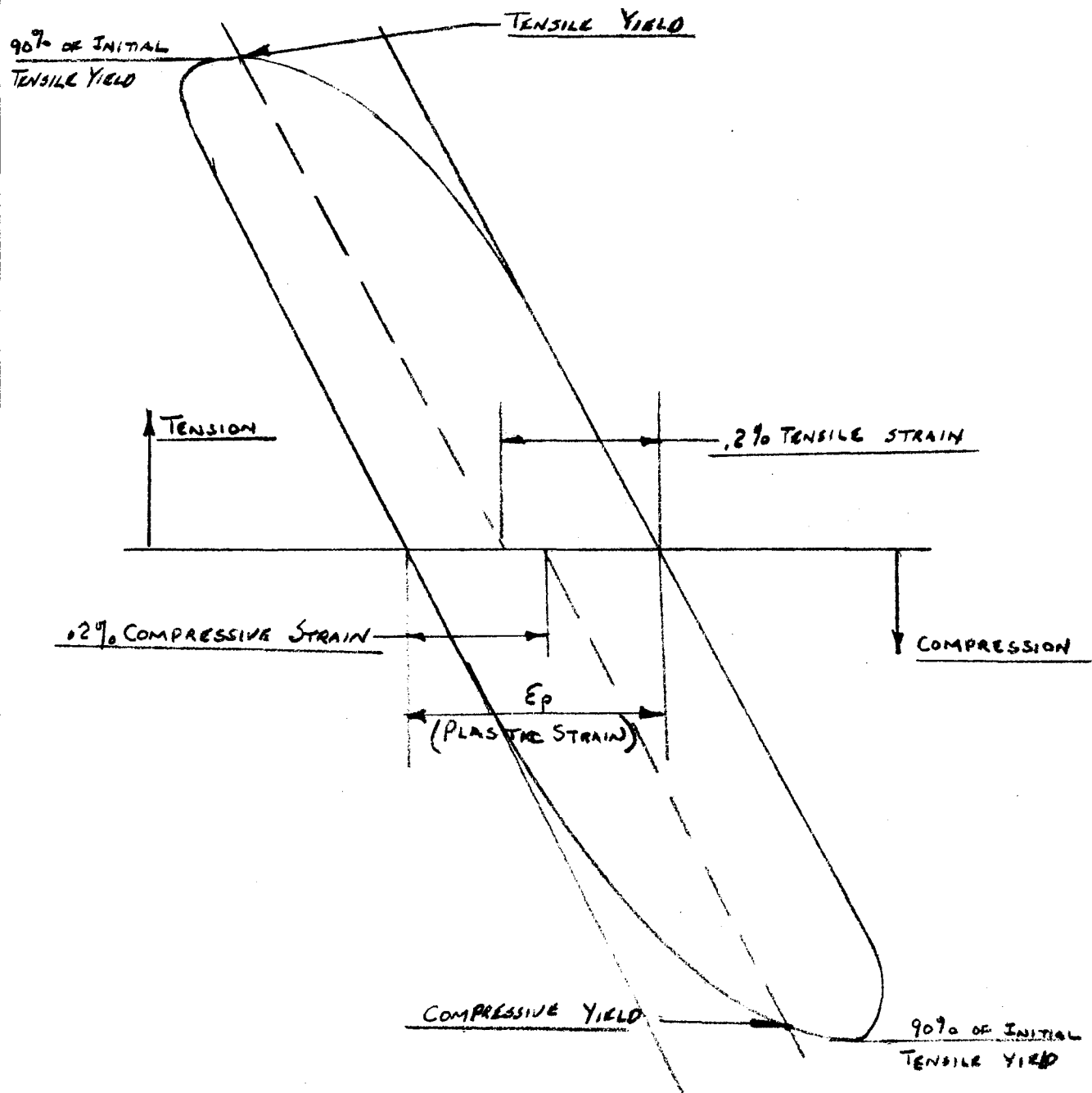


FIG. A-20

TYPICAL LOADING CYCLE

FIG. A-21

TENSION - COMPRESSION TEST

S/N 101 - Age 2 Hrs @ 150°F + 4 Hrs @ 300°F

(Heat 50793)

Initial Tensile Yield = 217 KSI
Cyclic Stress = 191 KSI

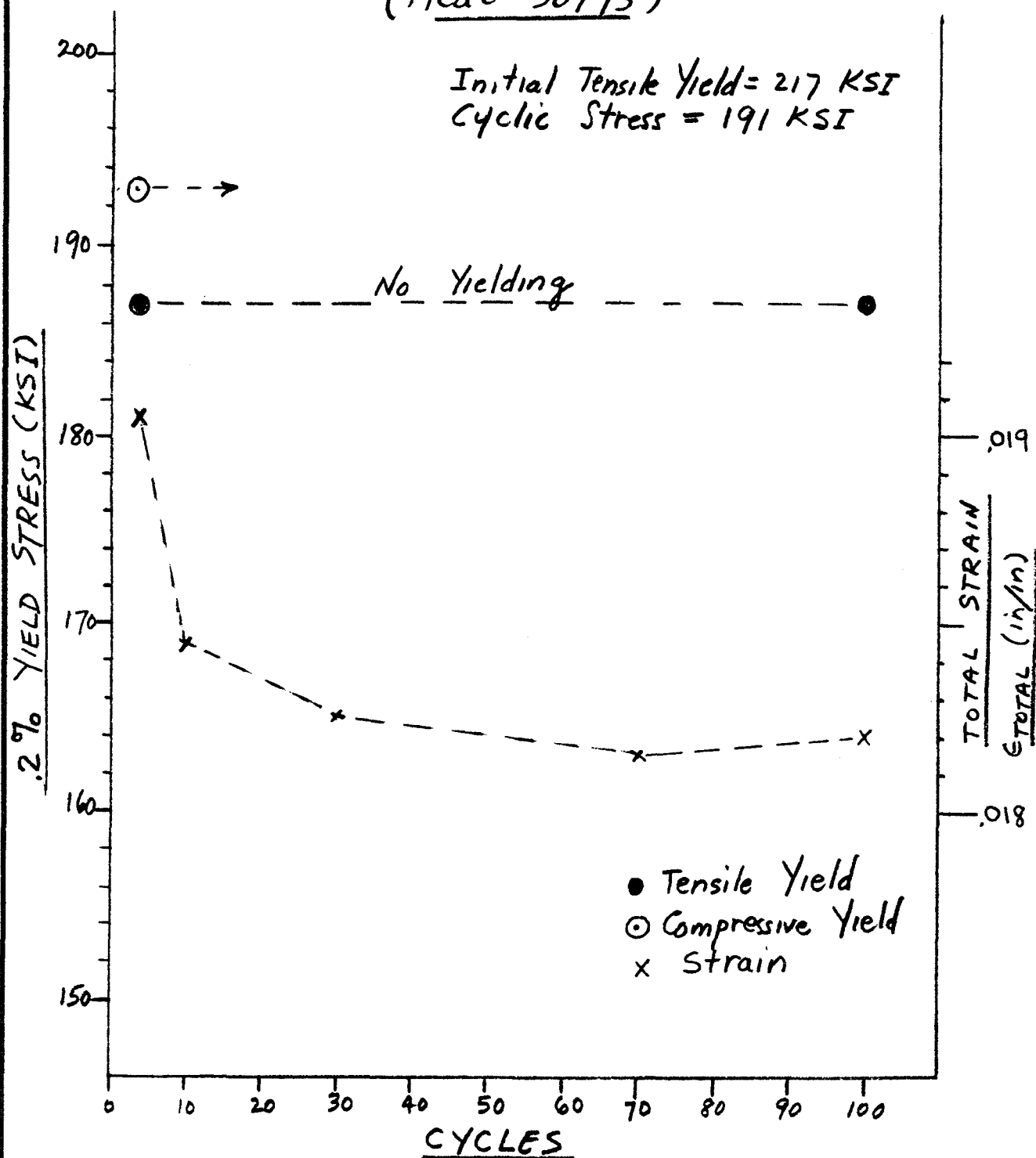
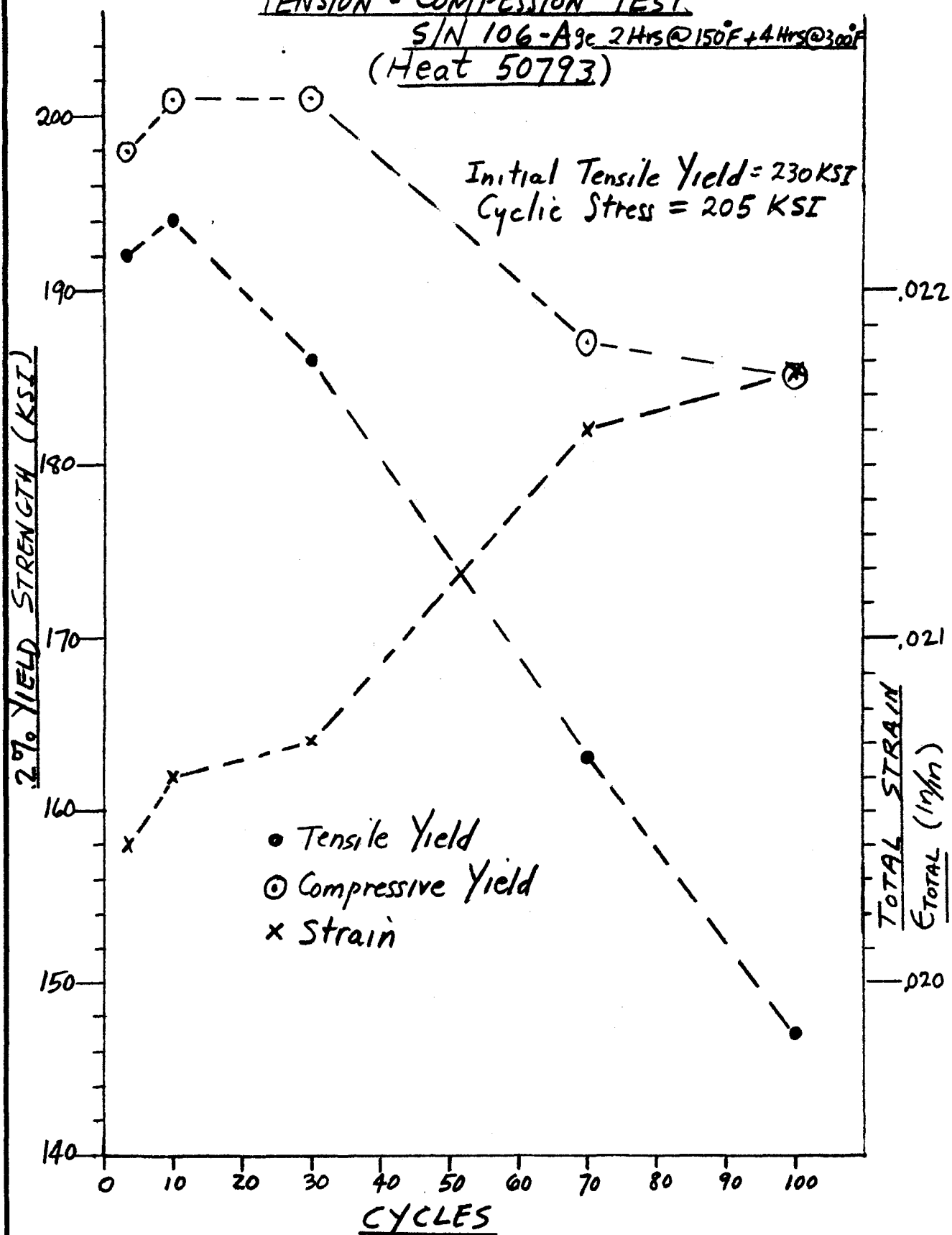


FIG A-22
TENSION - COMPRESSION TEST

S/N 106-Age 2 Hrs @ 150°F + 4 Hrs @ 300°F
(Heat 50793)



A-35

FIG. A-23
TENSION - COMPRESSION TEST

S/N 108 - Age 2 Hrs @ 150°F + 4 Hrs @ 300°F
(Heat 50793)

Initial Tensile Yield = 229 KSI
Cyclic Stress = 205 KSI

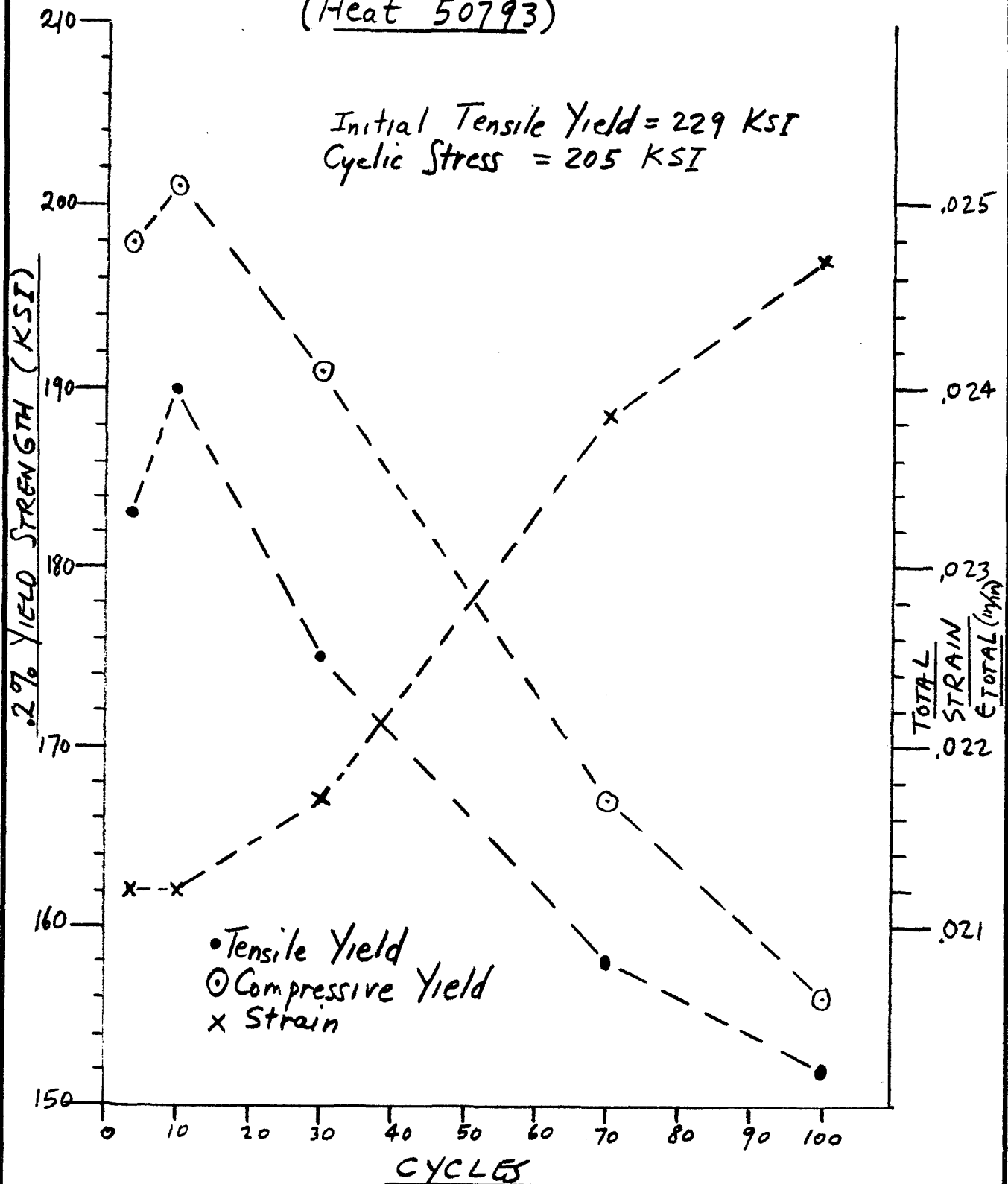
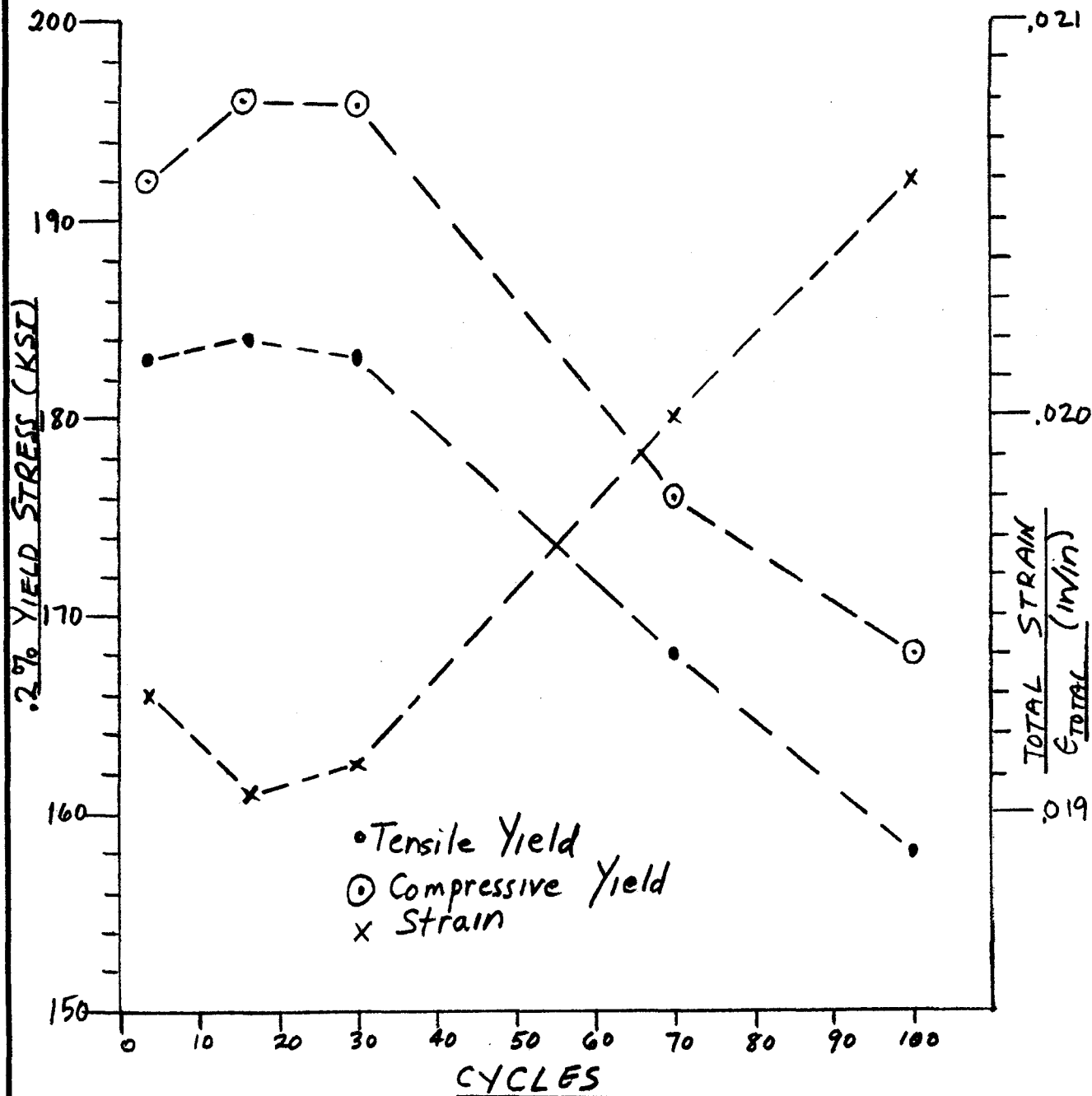


FIG. A-24
TENSION-COMPRESSION TEST
S/N 120 - Room Temp. Age
(Heat 50793)

Initial Tensile Yield = 229 KSI
 Cyclic Stress = 194 KSI



A-37

National Bureau of Standards Test Report, reproduced on the following pages. The ferromagnetic property of the transformed material (not typical of "standard" austenitic 301 stainless steel) is discussed in ARDE's comment to the Bureau of Standards.

Using the aforementioned Bureau of Standards' test data, coefficients of thermal contraction between room temperature and LN₂ and LH₂ temperatures were computed as follows:

$$\alpha \text{ (RT to } -320^{\circ}\text{F)} = \frac{.001775}{388} = 4.59 \times 10^{-6} \text{ in/in } ^{\circ}\text{F}$$

$$\alpha \text{ (RT to } -423^{\circ}\text{F)} = \frac{.001864}{491} = 3.78 \times 10^{-6} \text{ in/in } ^{\circ}\text{F}$$

Material density was determined from weight and volume measurements on a machined test piece cut from a tensile coupon. A density value of .2704 #/in³ was obtained. Approximately a 5% volume increase occurs during transformation of this low silicon heat from austenite to essentially martensitic structure. This would explain the low value of density compared to the "Standard" .285 #/in³ value for steel.

7.5 Appendix 5 - Vessel Design

ARDEFORM test data for low silicon Heat 50793, discussed in Section 3 and herein in Sections 7.1 through 7.4, together with S994 glass information were used to establish the material properties employed in the design effort. The specific materials properties used are called out in the appropriate sections of this appendix.

7.5.1 Parametric Design Curves

Reference 1 gives a buckling equation for overwrapped cylinders (which they also assume valid for oblate spheroids)

$$\frac{\sigma_{cr}}{E_s} = 106,000 (t/D)^3 \quad (7.1)$$

The classical theoretical elastic buckling relation for a long thin homogeneous material cylinder subject to lateral pressure is, reference 3,

U.S. DEPARTMENT OF COMMERCE
NATIONAL BUREAU OF STANDARDS
WASHINGTON, D.C. 20234

NATIONAL BUREAU OF STANDARDS
REPORT OF TEST

on

A Cryogenic Pre-Strained 301 Stainless Steel Specimen

Submitted by

Arde, Inc.
580 Winters Avenue
Paramus, New Jersey 07652

The thermal expansion of the pre-strained specimen of "301" stainless steel was determined by the Pizeu method described in the ASTM Tentative Method of Test for Linear Thermal Expansion of Rigid Solids with Interferometry, ASTM Designation: E289-65T. Three pieces, 0.997 cm in length, cut from the center of the pre-strained tensile specimen were used to separate the optical flats. The green line ($\lambda_v = 0.5462 \mu\text{m}$) of a natural mercury lamp was used to obtain interference. The length at each temperature was measured with a precision of ± 0.04 fringe ($\pm 0.01 \mu\text{m}$). A platinum-resistance thermometer was used to measure temperature with an accuracy better than $\pm 0.1^\circ\text{F}$. All measurements were made in a helium atmosphere at low enough pressure so that changes in the index of refraction were not significant but high enough to support good heat transfer. Each measurement of length was made at a constant temperature after the specimen had reached thermal equilibrium.

The values obtained for the thermal expansion of the specimen are shown in the table on page 2 of this report.

Test No. 212.21/198064
Date: March 10, 1969

Report of Test continued
A cryogenic Pre-Strained 301
Stainless Steel Specimen

Page 2

<u>Temperature</u>	<u>Linear Thermal Expansion</u>
71.7 °F	0.0000 percent
68	-0.0021 *
-28.0	-0.0555
-129.8	-0.1079
-227.1	-0.1503
-316.4	-0.1772
-423	-0.1864 *
-426.2	-0.1864

*Interpolated values.

Although this specimen is reported to be 301 stainless steel, the thermal expansion as determined in this test is not typical of that type of stainless steel. If the material is in fact a stainless steel, this test indicates that it is a 400 type. This is also confirmed by the fact that the specimen is ferromagnetic.

For the Director,

Original signed by
J. S. Beers

J..S. Beers
Acting Chief, Length Section
Metrology Division, IBS

Test No. 212.21/198064
Date: March 10, 1969



SALES, ENGINEERING
19 INDUSTRIAL AVENUE,
PHONE (201) 529-3700

March 27, 1969

U. S. Dept. of Commerce
National Bureau of Standards
Washington, D. C. 20234

Attention: Mr. J. S. Beers
Acting Chief, Length Section
Metrology Division, IBS

Subject: Cryogenically Prestrained 301
Stainless Steel Specimens

Reference: Thermal Expansion Tests, Test
Number 212.21/198064, 3/10/69

Gentlemen:

Per referenced test report and your observations regarding the type of material tested, I think the following might be of general interest to your office.

Arde Inc's process is one where annealed "301" stainless steel is plastically deformed (cold worked) at -320°F in order to cause a transformation which in turn results in high strength levels. The strengthened product can be used as is or can be further strengthened by aging at 800°F for 20 hours.

Transformation from austenite to martensite is characterized by a change in lattice structure without a change in chemical composition. Upon completion of the process, the material is indeed magnetic.

You will notice that I have put 301 in quotes. Utilization of this terminology is generally correct. However, we have modified and tightened up the chemistry in order to achieve a proper balance between toughness, weldability, strength and corrosion resistance. The material you tested has been modified to insure high toughness at -423°F .

U.S. Dept. of Commerce

= 2 =

March 27, 1969

Thank you for assistance in providing most valuable test data.

Very truly yours,

ARDE, INC.



A. Cozewith

bap

$$\frac{\sigma_{cr}}{E} = \left(\frac{1}{1 - \nu^2} \right) * (t/D)^2 \quad (7.2)$$

We can thus define from equations 7.1 and 7.2 an "improvement factor", F, produced by the stiffening effect of the fiber overwrap, as

$$F = \frac{106,000 (t/D)^3}{(t/D)^2} (1 - \nu^2) = 106,000 (1 - \nu^2) (t/D) \quad (7.3)$$

The lower bound elastic buckling stress for homogeneous material spheres, taking into account imperfections, is, reference 4,

$$\frac{\sigma_{cr}}{E} \approx .2 (t/D) \quad (7.4)$$

In the absence of any data, we assume the improvement factor for spheres due to the fiber overwrap is the same as for cylinders. Using equation 7.3, we obtain for the overwrapped sphere the critical compressive stress value,

$$\frac{\sigma_{cr}}{E} = .2 (t/D) F = .2 (t/D)^2 (106,000) (1 - \nu^2)$$

or

$$\left(\frac{\sigma_{cr}}{E} \right) = 21,200 (1 - \nu^2) (t/D)^2 \quad (7.5)$$

Based on an analysis of the biaxial coupon test data and density test with transformed material, metal liner material properties listed in Table A-10 below were selected.

TABLE A-10 - SELECTED LINER MATERIAL PROPERTIES

<u>Temperature</u>	<u>E x 10⁻⁶ (psi)</u>	<u>ν</u>	<u>(#/in³)</u>
R. T.	21.5	.29	.270
-320°F	22.7	.29	.270
-423°F	27.7	.32	.270

The design curves of Figures 1 and 2 were constructed using these materials properties in equations 7.1 and 7.5.

7.5.2 Parametric Vessel Design

The design calculations for the parametric vessel design are detailed herein. The materials properties employed are given below in Table A-11. The values are based on analysis of test data discussed in previous sections of this appendix.

The stress-strain diagram used in the analysis and for the purpose of defining terms is sketched on Figure A-25.

At Operating Pressure, P_o , and Room Temperature

Hoop (or meridional) equilibrium requires that,

$$(\sigma_{go}) \frac{(t_g)}{2} + \sigma_{mo} t_m = \frac{P_o R}{2}$$

Using the operating liner stresses, in Table A-11 we find,

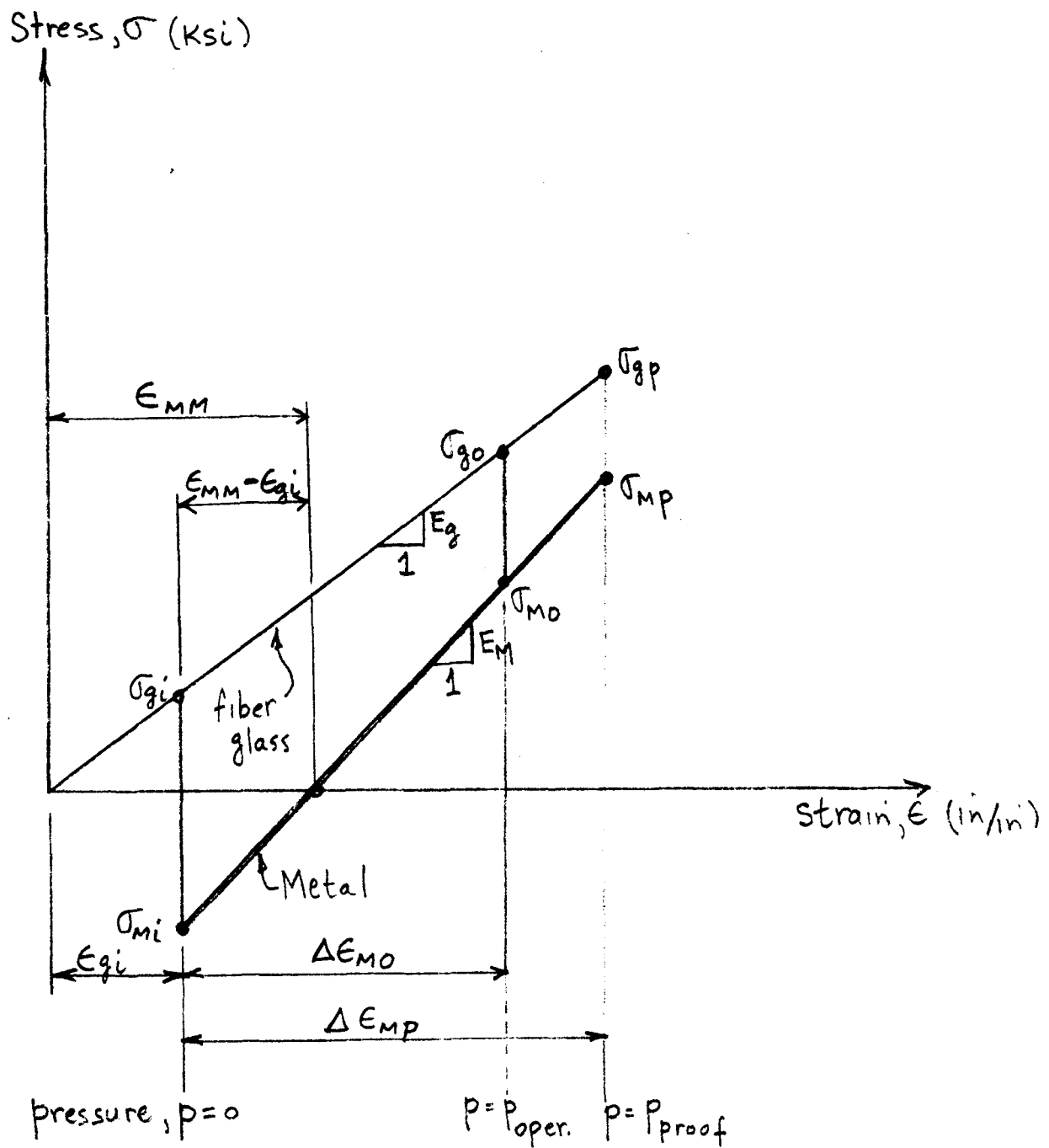
$$100 t_g + 180 t_m = \frac{P_o R}{2} \quad (7.6)$$

Here, t_m = metal liner thickness (mils)
 t_g = total effective structural
fiber glass thickness (mils)
 R = Sphere radius (in.)

TABLE A-11

MATERIAL PROPERTIES FOR PARAMETRIC VESSEL DESIGN

Metal Liner	RT	-320°F	-423°F
Allowable Operating Tensile Stress (ksi), σ_{M0}	$\left(\begin{matrix} 180 = .9x \\ \sigma_{yrt} \end{matrix} \right)$	$1.41 \times 180 = 254$	$1.65 \times 180 = 297$
Allowable Max. Operating Compressive Stress (ksi), σ_{Mi}	$-.65 (180) = -117$	$-1.41 \times 117 = -165$	$-1.65 \times 117 = -193$
Young's Modulus, $E_M \times 10^{-3}$ (ksi)	21.5	22.7	27.7
Poisson's Ratio, ν	.29	.29	.32
Coefficient of Contraction	---	4.59	3.78
$\alpha \left(\begin{matrix} \text{between} \\ R.T. \text{ and } T \end{matrix} \right) (in/in^{\circ}F) \times 10^6$			
<u>S-994 Glass</u>			
Allow Operating Tensile Stress (ksi), σ_{g0}	200	297	297
$E_g \times 10^{-3}$ (ksi)	12.4	13.6	13.6
$\alpha \left(\begin{matrix} \text{between} \\ R.T. \text{ and } T \end{matrix} \right) (in/in^{\circ}F) \times 10^6$	---	2.01	2.01



STRESS-STRAIN DIAGRAM
(Parametric Vessel Design)

FIGURE A-25

The factor of 1/2 is used with total fiber-glass structural thickness t_g since 1/2 of the fibers carry hoop load and 1/2 of the fiber resist meridional load.

The room temperature metal spherical liner elastic strain increment $\Delta \epsilon_{mo}$ from operating pressure to zero pressure is computed from Hooke's Law as (see Figure A-25)

$$\Delta \epsilon_{mo} = \frac{\sigma_{mo} - \sigma_{mi}}{E_m} (1 - \nu_m) = \frac{(180 + 117)(1 - .29)}{21.5 \times 10^3} = 9.8 \times 10^{-3} \text{ in/in} \quad (7.7)$$

which yields the corresponding fiberglass stress increment $\Delta \sigma_g$ as

$$\Delta \sigma_g = (E_g) (\Delta \epsilon_{mo}) = 12.4 \times 10^3 \times 9.8 = 121.5 \text{ ksi}$$

The initial fiberglass stress (at $p = 0$) σ_{gi} is then given by,

$$\sigma_{gi} = \sigma_{go} - \Delta \sigma_g = 200 - 121.5 = 78.5 \text{ ksi} \quad (7.8)$$

At $p = 0$, and Room Temperature

Hoop (or meridional) equilibrium considerations require,

$$\sigma_{gi} (t_g/2) + \sigma_{mi} t_m = 0 \text{ or,}$$

$$(78.5/2) t_g - 117 t_m = 0 \text{ and thus,}$$

$$t_m = .335 t_g \quad (7.9)$$

Substituting (7.9) in (7.6) gives,

$$100 t_g + 180 (.335 t_g) = \frac{P_o R}{2} = 160.3 t_g \quad (7.10)$$

as the room temperature operating pressure membrane load per inch.

The "mismatch" strain at room temperature (for metal liner unstressed) is computed as (see Figure A-25)

$$\begin{aligned} \epsilon_{mm} &= \epsilon_{gi} - \frac{\sigma_{mi}(1 - \nu_m)}{E_m} = \frac{\sigma_{gi}}{E_g} - \frac{\sigma_{mi}(1 - \nu_m)}{E_m} \\ (\epsilon_{mm})_{RT} &= \frac{78.5}{12.4 \times 10^3} - \frac{(-117)(.71)}{21.5 \times 10^3} = 10.21 \times 10^{-3} \text{ (in/in)} \end{aligned} \quad (7.11)$$

At p = 0 and -320°F

The reduction in mismatch strain $\Delta(\epsilon_{mm})$ due to the thermal contraction from room temperature to -320°F is found from,

$$\begin{aligned}\Delta\epsilon_{mm} &= -\Delta(\alpha T) = -(\Delta\alpha)(\Delta T) = -10^{-6}(4.59 - 2.01) \{70 - (-320)\} \\ \Delta\epsilon_{mm} &= -2.58 \times 390 \times 10^{-6} \cong -1.01 \times 10^{-3} \text{ in/in}\end{aligned}\quad (7.12)$$

The mismatch strain at -320°F is then from 7.11 and 7.12

$$(\epsilon_{mm})_{-320} = (10.21 - 1.01) \times 10^{-3} = 9.20 \times 10^{-3} \text{ in/in} \quad (7.13)$$

From equilibrium requirements at zero pressure,

$$\begin{aligned}(\sigma_{gi})_{-320} t_g/2 + (\sigma_{mi})_{-320} t_m &= 0 \quad \text{or,} \\ (\epsilon_{gi})_{-320} (E_g)_{-320} t_g/2 - (E_m)_{-320} \left\{ \frac{.0092 - (\epsilon_{gi})_{-320}}{(1 - \nu_m)} \right\} t_m &= 0\end{aligned}$$

Utilizing 7.9, we obtain

$$t_g \left(\frac{13.6 \times 10^3}{2} \right) (\epsilon_{gi})_{-320} = \frac{22.7 \times 10^3}{.71} \left\{ .0092 - (\epsilon_{gi})_{-320} \right\} t_m = .335 t_g$$

Solving for $(\epsilon_{gi})_{-320}$ the fiber prestrain at -320°F gives,

$$(\epsilon_{gi})_{-320} = 5.62 \times 10^{-3} \text{ in/in} \quad (7.14)$$

The fiber and metal prestresses at -320°F are then,

$$(\sigma_{gi})_{-320} = (E_g)_{-320} (\epsilon_{gi})_{-320} = 13.6 \times 10^{-3} \times 5.62 = 76.3 \text{ ksi} \quad (7.15)$$

and

$$\begin{aligned}(\sigma_{mi})_{-320} &= \frac{-(E_m)_{-320}}{1 - \nu_m} \left\{ (\epsilon_{mm})_{-320} - (\epsilon_{gi})_{-320} \right\} = \\ &= \frac{-22.7 \times 10^3}{.71} \left\{ 9.20 - 5.62 \right\} \times 10^{-3}; \\ (\sigma_{mi})_{-320} &= -114.5 \text{ ksi}\end{aligned} \quad (7.16)$$

At $P = P_0$ and -320°F

The strain and stress increments are,

$$(\Delta \epsilon_{mo})_{-320} = \left\{ \frac{(\sigma_{mo} - \sigma_{mi})(1-\nu)}{E_m} \right\}_{-320} = \frac{(254 + 114.5)(.71)}{22.7 \times 10^3} = 11.52 \times 10^{-3} \text{ in/in}$$

$$(\Delta \sigma_q)_{-320} = (E_q \Delta \epsilon_{mo})_{-320} = 13.6 \times 10^3 \times 11.52 \times 10^{-3} = 156.5 \text{ ksi}$$

$$(\sigma_q)_{-320} = 76.3 + 156.5 = 232.8 \text{ ksi} < 297 \text{ allowable} \quad (7.17)$$

From equilibrium at operating pressure using 7.9 and 7.17 we obtain,

$$(P_0 R/2)_{-320} = t_q/2 (232.8) + 254 (t_m = .335 t_q)$$

$$(P_0 R/2)_{-320} = 201.4 t_q \quad (7.18)$$

From 7.18 and 7.10 the ratio of -320°F to room temperature operating pressures is,

$$\frac{(P_0)_{-320}}{(P_0)_{RT}} = \frac{201.4 t_q}{160.3 t_q} = 1.26 \quad (7.19)$$

and since $(P_p)_{RT} = (1.1 P_0)_{RT}$ we have,

$$\frac{(P_0)_{-320}}{(P_p)_{RT}} = \frac{1.26}{1.1} = 1.15 \quad (7.20)$$

At $p = p$ Proof and -320°F

Using the same calculation procedure as above, one finds,

$$(\Delta \epsilon_{mp})_{-320} = \left\{ \frac{(\sigma_{mp} - \sigma_{mi})(1-\nu_m)}{E_m} \right\}_{-320} = \left\{ \frac{(1.1 \times 254) + 114.5}{22.7 \times 10^3} \right\} (.71) = 12.3 \times 10^{-3}$$

$$(\Delta \sigma_{qp})_{-320} = E_q (\Delta \epsilon_{mp})_{-320} = 13.6 \times 10^3 \times 12.3 \times 10^{-3} = 167 \text{ ksi} \quad \text{and}$$

$$(\sigma_{qp})_{-320} = (\sigma_{qi})_{-320} + (\Delta \sigma_{qp})_{-320} = 76.3 + 167 = 243.3 \text{ ksi} \quad (7.21)$$

$$(P_p R/2)_{-320} = \left(\frac{t_q}{2} \right) (243.3) + (1.1 \times 254) (t_m = .335 t_q) \approx 215.2 t_q \quad \text{and}$$

$$\frac{(P_p)_{-320}}{(P_0)_{RT}} = \frac{215.2 t_q}{160.3 t_q} = 1.34 \quad (7.22)$$

Similar calculations utilizing -423°F materials properties given in Table A-11 yield the results,

$\frac{(P_0)_{-423}}{(P_0)_{RT}}$	$= 1.32$	$\frac{(P_0)_{-423}}{(P_p)_{RT}}$	$= 1.20$
$\frac{(P_p)_{-423}}{(P_0)_{RT}}$	$= 1.42$		

The computed pressure ratios at the prescribed temperatures are tabulated in Table 1 in Section 3.3.2.

7.5.3 Initial GFR Spherical Vessel Designs

Typical design calculations for an initial GFR spherical vessel configuration are given below. The design parameters employed are detailed in Table A-12 herein.

7.5.3.1 Determination of Initial and Final Liner Dimensions

$$\text{Final Liner I.D.} = D_{mf} = \left(\frac{6V}{\pi} \right)^{1/3} = \left(\frac{6 \times 1200}{\pi} \right)^{1/3} = 13.2''$$

For 200 ksi spherical liner RT yield point, total plastic biaxial strain $\cong .055$ in/in (see Figure A-7).

$$\text{Liner Preform Diameter} = \frac{13.2}{1.055} = 12.5'' = D_{mi} \\ (\text{initial diameter})$$

Liner Preform Thickness = 25 mils average = t_{mi} (existing (initial thickness) formed heads).

For constant metal volume before and after strain,

$$\pi D_{mf}^2 t_{mf} = \pi D_{mi}^2 t_{mi} \quad \text{or, } (t_{mf}/t_{mi}) = \left(\frac{D_{mi}}{D_{mf}} \right)^2 = \left(\frac{1}{1.055} \right)^2; \\ t_{mf} = \frac{.025}{(1.055)^2} = 22.5 \text{ Mils} \quad (\text{final liner thickness})$$

7.5.3.2 Computation of Fiberglass Thickness

Equilibrium at $P = P_0$, $T = R$. T. requires,

$$P_0 R/2 = \frac{(3000)(6.6)}{2} = \sigma_{g0} t_{g/2} + \sigma_{m0} t_m$$

$$9900 \text{ #/in} = 200 t_{g/2} + 180 \times 22.5$$

$$t_g = 58.5 \text{ Mils (Total effective structural thickness)}$$

$$t_g (\text{composite}) = \frac{t_g}{\text{Volume fraction}} = \frac{58.5}{.65} = 90 \text{ Mils Fiber-}$$

glass - composite resin thickness.

7.5.3.3 Computation of Prestress at Room Temperature and Zero Pressure

Equilibrium:

$$\sigma_{gi} t_{g/2} + \sigma_{mi} t_m = 0 = \sigma_{gi} \left(\frac{58.5}{2} \right) + \sigma_{mi} (22.5) \\ \sigma_{mi} = -1.3 \sigma_{gi} \quad (7.23)$$

TABLE A-12

DESIGN PARAMETERS FOR INITIAL GFR SPHERICAL VESSEL CONFIGURATIONS

Vessel Internal Volume, $V = 1,200 \text{ in}^3$
 Operating Pressure, $P_o = 3,000 \text{ psi}$

<u>Operating Stress Level (ksi)</u>	RT	-320°F
Metal, $\sigma_{mo} = (.9 \times \text{yield point})$	= 180	---
Fiber Glass, $\sigma_{go} = (.6 \times \text{ultimate})$	= 200	297
<u>Young's Modulus (ksi x 10⁻³)</u>		
Metal, E_m	= 21	23
Fiber Glass, E_g	= 12.4	13.6
<u>Poisson's Ratio</u>		
Metal ν_m	= .29	.29
<u>Coefficient of Thermal Contraction</u> (between R.T. and -320°F) in/in °F x 10 ⁶		
Metal, α_m	=	4.59
Fiber Glass, α_g	=	2.01
<u>Density (#/in³)</u>		
Metal, $\rho_m = (.270)$		
Composite Fiberglass, $\rho_{gc} = (.074)$		
<u>Volume Fraction Fiberglass</u> (.65, corresponding to 20% resin content)		

Equal Strain Increments of Metal and Fiberglass at Room Temperature

(Between $P = P$ operating and $P = 0$)

$$\Delta \epsilon_m = \frac{180 - \sigma_{mi}}{(21.71) \times 10^3} = \Delta \epsilon_g = \frac{(200 - \sigma_{gi})}{12.4 \times 10^3} \quad (7.24)$$

Substituting (7.23) in (7.24) gives the prestresses,

$$\begin{aligned} \sigma_{gi} &= 81 \text{ ksi} \\ \sigma_{mi} &= -1.3(81) = -105 \text{ ksi} \end{aligned} \quad (7.25)$$

These initial stress values are low enough to prevent glass creep, liner buckling or compressive yielding as well as prevent fatigue failure in less than the 100 cycle design point.

7.5.3.4 Computation of Cryogenic State of GFR Vessel

The mismatch strain at $p = 0$ and -320°F , ϵ'_{mm} , is computed as (see Section 7.5.3.3 and Figure A-26).

$$\begin{aligned} (\epsilon'_{mm}) &= \epsilon_{mm} - \Delta(\alpha r) = \left\{ \frac{\sigma_{gc}}{E_g} - \frac{(\sigma_{mc} - \sigma_{mi})}{E_m / (1 - \nu_m)} \right\} - \{1.01 \times 10^{-3}\} \\ (\epsilon'_{mm}) &= \left[\frac{200}{12.4} - \left\{ \frac{180 - (-105)}{21.71 \times 10^3} \right\} \right] - 1.01 \times 10^{-3} = 9.01 \times 10^{-3} \text{ in/in} \end{aligned}$$

Equilibrium at $p = 0$, $T = -320^\circ\text{F}$ requires,

$$\begin{aligned} \sigma_{gi} \left(\frac{t_g}{2} \right) + \sigma_{mi} \frac{t_m}{3} = 0 &= (E_g \epsilon'_o) \frac{t_g}{2} - \left(\frac{E_m}{1 - \nu_m} \right) \left\{ \frac{20901}{- \epsilon'_o} \right\} \frac{t_m}{3} = 0 \\ \epsilon'_o \left(\frac{13.6}{2} \right) (58.5) \times 10^3 - \left(\frac{23}{71} \right) (100901 - \epsilon'_o) \times 22.5 \times 10^3 &= 0 \end{aligned}$$

Solving for initial prestrain at

-320°F , ϵ'_o , yields,

$\epsilon'_o = 5.83 \times 10^{-3}$ in/in which gives fiberglass initial stress σ'_{gi} as,

$$\sigma'_{gi} = E_g \epsilon'_o = 13.6 \times 10^3 \times 5.83 \times 10^{-3} = 79.3 \text{ ksi}$$

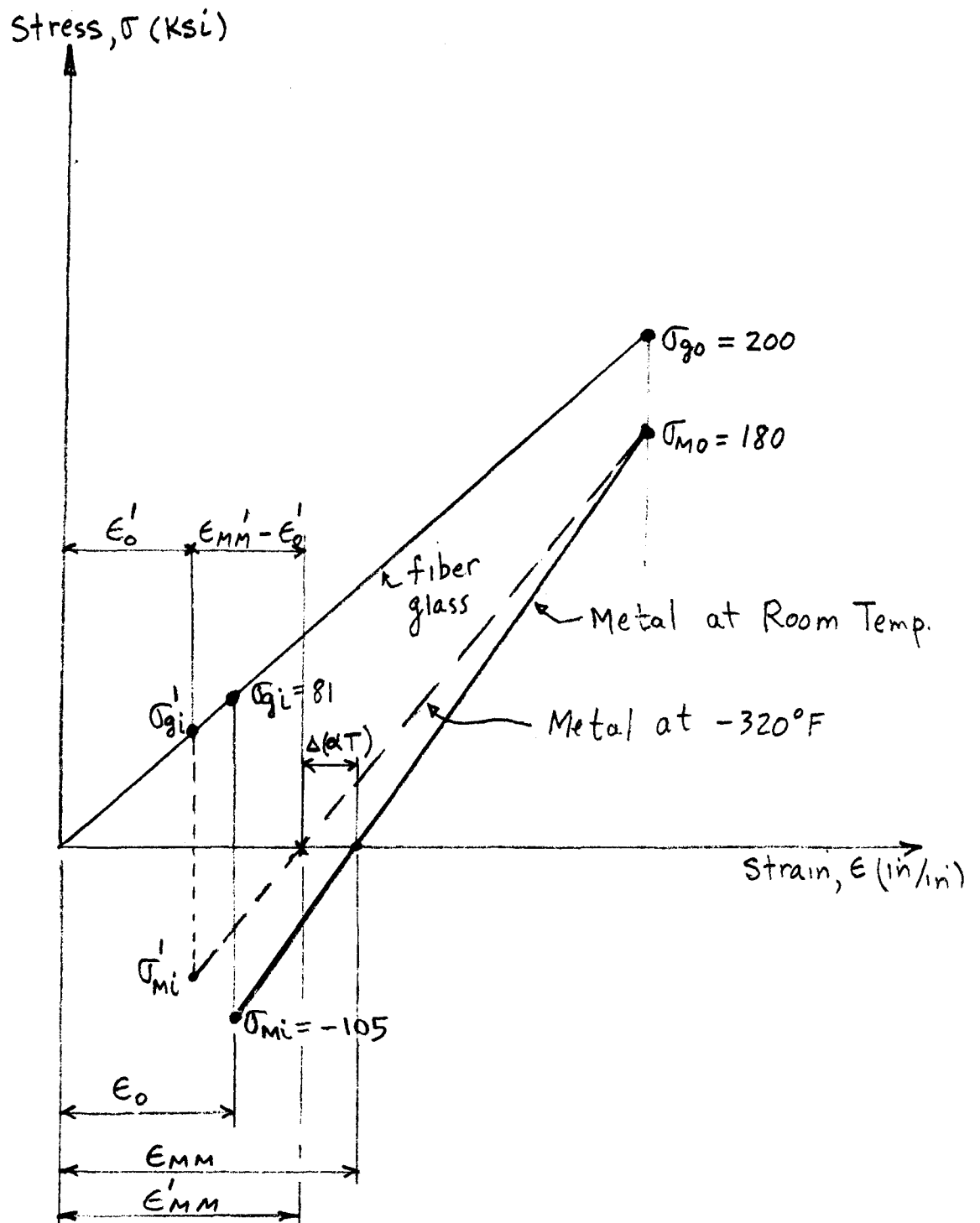
From the equilibrium equation one

finds,

$$\sigma'_{mi} = -\sigma'_{gi} \left(\frac{t_g/2}{t_m} \right) = -\left(\frac{79.3}{2} \right) \left(\frac{58.5}{22.5} \right) = -103.1 \text{ ksi}$$

A true cryogenic stress at -320°F of $\sigma_T = 262 \text{ ksi} = \sigma_{mc}$ is required to give a 200 ksi liner yield point at room temperature (see Figure A-7). The incremental liner strain at -320°F , $\Delta \epsilon'_m$, then is,

$$\begin{aligned} \Delta \epsilon'_m &= \frac{\sigma'_{mc} - \sigma'_{mi}}{E'_m / (1 - \nu'_m)} = \frac{262 - (-103.1)}{(23.71) \times 10^3} = 11.25 \times 10^{-3} \text{ in/in} \\ &= \frac{\sigma_{gc} - 79.3}{E_g} = \frac{\sigma_{gc} - 79.3}{13.6 \times 10^3} \end{aligned}$$



STRESS-STRAIN DIAGRAM
(Initial GFR Spherical Vessel Configuration)

FIGURE A-26

A-53

which yields the fiberglass stress at -320°F as $\sigma_{gc} = 232.3 \text{ ksi}$. The total strain at -320°F , $\epsilon_T = \epsilon_0' + \Delta\epsilon_m' = .0583 + .01125 = .01708 \text{ in/in}$ as seen from Figure A-27.

The equivalent uniaxial liner strain during the second cryogenic stretch forming is then,

$$\epsilon_2' \text{ (uniaxial)} = \frac{.01708}{.5} \approx .034 \text{ in/in}$$

as set forth in the formulations of Table A-3. The total equivalent uniaxial liner strain is $.055 = .110 \text{ in/in}$ which yields an equivalent uniaxial liner $.5$ strain of

$\epsilon_1' = .110 - .034 = .076 \text{ in/in}$ for the first cryogenic stretch forming operation. The nominal biaxial strain in the spherical liner for this state is then, $\epsilon = \frac{R}{R_0} - 1 =$

$.5(.076) = .038 \text{ in/in}$. The nominal stress S_2 at this liner cryogenic strain level is, $S_2 = 140 \text{ ksi}$ as given on Figure A-7.

The cryogenic stretch pressures are then found as indicated below.

$$P_{c1} = \frac{4 S_2 t_{mi}}{D_{mi}} = \frac{4 \times 140 \times 25}{12.5} = 1120 \text{ psi, for the}$$

first cryogenic stretch of the liner alone and

$$P_{c2} = \frac{4}{D_{mf}} \{ \sigma_{mc} t_{mf} + \sigma_{gc} t_{g/2} \} = \frac{4}{13.2} \{ 262 \times 22.5 + 232.3 \times \frac{58.5}{2} \}$$

$P_{c2} = 3850 \text{ psi}$, for the second cryogenic stretch of the liner plus fiberglass overwrap.

The structural efficiency parameter at operating pressure is computed as,

$$P_0 V/W = \frac{P_0 \frac{4}{3} \pi R^3}{4 \pi R^2 \{ P_m t_m + P_{gc} t_{gc} \}} = \frac{P_0 R/3}{P_m t_m + P_{gc} t_{gc}}$$

$$P_0 V/W = \frac{\frac{1}{3} (3000 \times 6.6) \times 10^3}{(.27 \times 22.5 + .074 \times 90)} = .518 \times 10^6 \text{ (in)}$$

7.6 Appendix 6 - Vessel Testing

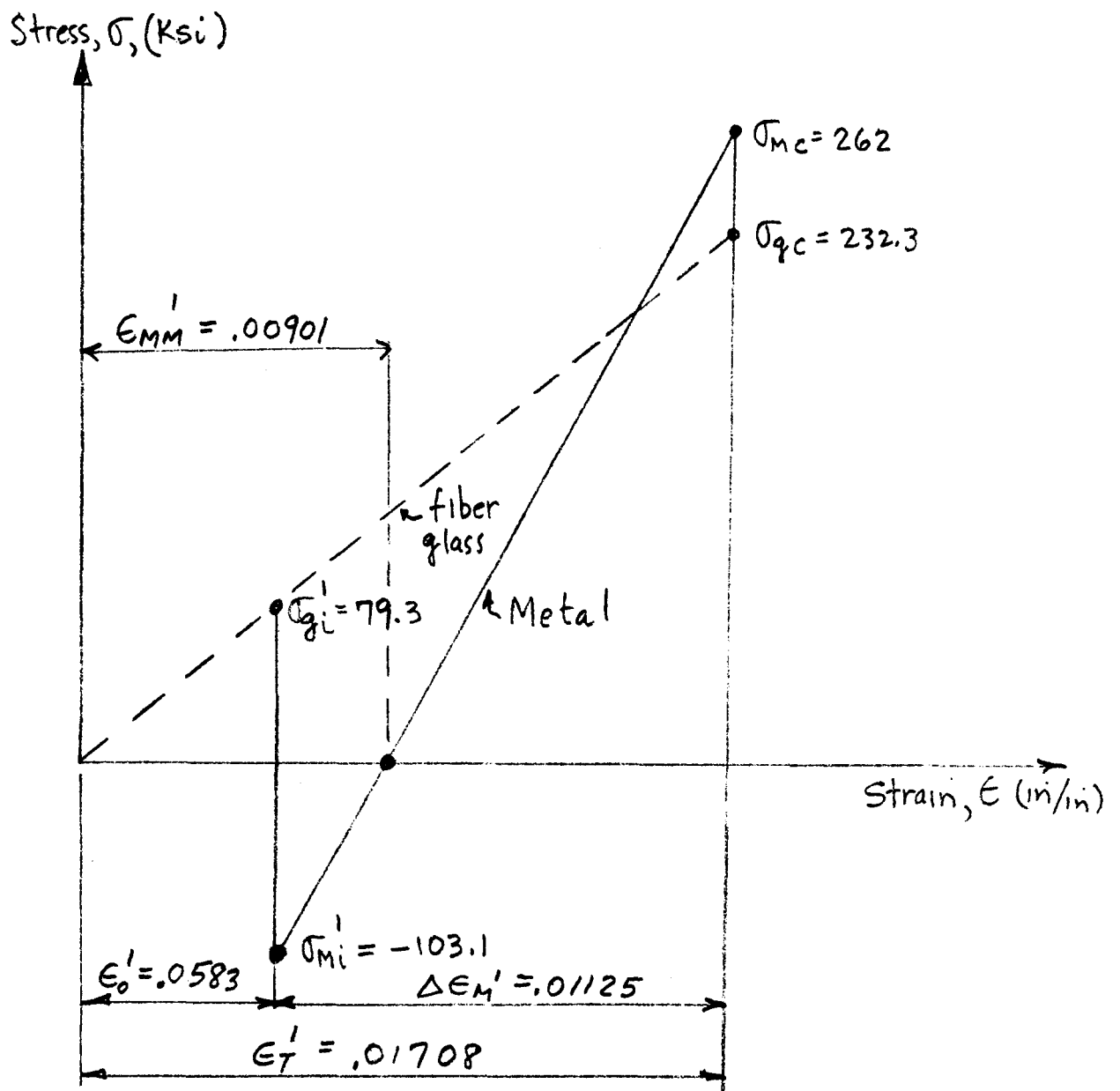
7.6.1 Fiberglass Sphere Wrap Test

Calculation of the glass ultimate strength achieved in the burst test of the fiberglass sphere described in Section 3.5.2.1 is detailed herein.

$$\text{Resin Density} = P_r - \text{Specific Gravity} \times \frac{62.4}{1728} = 1.16 \times \frac{62.4}{1728}$$

$$.0419 \text{ \#/in}^3$$

$$\text{S Glass Density} = P_g = 2.54 \times \frac{62.4}{1728} = .0917 \text{ \#/in}^3$$



STRESS-STRAIN DIAGRAM AT -320°F

FIGURE A-27

A-55

If β = resin fraction by weight, the density, ρ_c , of the glass-resin composite is,

$$\rho_c = \frac{1}{\frac{\beta}{.0449} + \frac{(1-\beta)}{.0917}} = \frac{1}{10.9 + 12.96 \beta} \quad (7.26)$$

Also, the volume ratio of glass, (VR)_g may be determined as,

$$(VR)_g = \frac{\frac{(1-\beta)}{.0917}}{\frac{\beta}{.0449} + \frac{(1-\beta)}{.0917}} = \frac{1-\beta}{1 + 1.19 \beta} \quad (7.27)$$

The structural efficiency of the fiberglass spherical vessel, PV/W, is expressed by,

$$\frac{PV}{W} = \frac{\{(PR/2) \div t_{g/2}\} \left\{ \frac{4}{3} \pi R^3 \right\}}{4\pi R^2 t_c \rho_c} = \frac{1}{3} \left(\frac{\sigma_g}{\rho_c} \right) \left(\frac{t_g}{t_c} \right) \quad (7.28)$$

where,

t_g = total glass structural thickness

t_c = Thickness of glass-resin composite

σ_g = glass stress

But,

$t_c = \frac{t_g}{(VR)_g}$ and using this in (7.28) yields the glass stress as,

$$\sigma_g = 3 \left(\frac{PV}{W} \right) \frac{\rho_c}{(VR)_g} \quad (7.29)$$

The burst test results (see Section 3.5.2.1) gave, $PV/W = .92 \times 10^6$ and $\beta = .219$ which when used in (7.26) and (7.27) yield,

$$\frac{\rho_c}{(VR)_g} = \frac{.073}{.062}$$

Substituting the appropriate values in (7.29) gives finally, the glass stress, σ_{gb} , achieved in the burst test as,

$$\sigma_{gb} = (3) (.92 \times 10^6) \frac{.073}{.062} = 324 \text{ ksi}$$

7.6.2 Liner Failure Mode Tests

GFR vessel liner "Go-No-Go" processing

and hydrostatic tests were performed to isolate the probable cause of liner failures. The test results are summarized in Table A-13.

TABLE A-13 - LINER FAILURE MODE TEST RESULTS SUMMARY

<u>S/N</u>	<u>Remarks</u>
9	No failure; cryostrains exceeded total liner strain required for GFR vessel. Proved material satisfactory if no thermal cure cycle effects present.
10	Demonstrated lack of elongation due to weld distortion effects, high first cryostretch and thermal aging effects.
11	Plastic strain at burst much more than required in GFR vessel. Proved that reduction in first cryostrains would result in sufficient elongation to failure.
13	Failure mode same as for tests with water. Proved hydrogen embrittlement not the problem.
33	This thicker vessel with much less weld distortion subsequently hydrostretched to 1.5% plastic strain without failure. Demonstrated material and construction satisfactory if weld distortion effects minimized.

These liner tests indicated that the failure mode was a combination of the effect of local weld distortion curvature producing high strains, magnified by reduction in available material elongation caused by the relatively high first cryogenic straining followed by subsequent thermal aging. The modified GFR vessel design and processing, discussed in Section 3.3.4, which reduced weld distortion effects by vessel "rounding" prior to cryostretching for strength and, in addition, lowered the first cryogenic strain level, was thus evolved.

As an aid in defining and verifying the modified GFR vessel processing, uniaxial tensile tests on S/N 500, 503 and 504 tensile specimens were performed. These test results are summarized in Table A-14 herein. The results of S/N 504 tensile test were selected for the modified GFR vessel processing.

TABLE A-14

SUMMARY OF TENSILE COUPON TESTS

	S/N 500	S/N 503	S/N 504
A_0 (Initial Area) - in^2	.0617	.0626	.0627
P_1 (Initial Stretch Load) - #	6170	7500	8480
σ_{N1} (Nominal Stress - 1st Stretch) - #/in^2	100,000	120,000	135,000
A_1 (Area After 1st Stretch) - in^2	.0589	.0590	.0585
ϵ_{p1} (Plastic Strain) - in/in	.047	.060	.072
σ_{T1} (True Stress - 1st Stretch) - #/in^2	105,000	127,000	145,000
Thermal Aging 2 hrs. @ 150°F & 4 hrs. @ 300°F			
P_2 (2nd Stretch Load) - #	9600	11,900	13,000
σ_{N2} (Nominal Stress) - #/in^2	163,000	202,000	222,000
A_2 (Area After 2nd Stretch) - in^2	.058	.058	.0576
ϵ_{p2} (Plastic Strain) - in/in	.017	.018	.017
σ_{T2} (True Stress) - #/in^2	165,000	205,000	226,000
Room Temperature Nominal Yield Strength - #/in^2	134,000	143,000	163,000
Room Temperature Nominal Ultimate Strength - #/in^2	192,000	202,000	199,000

7.6.3 Hydrostatic Tests of S/N 14, 15, 16 GFR Vessels

GFR spherical vessels S/N 14, 15, 16 were hydrostatically tested with demineralized water internal pressure slowly applied at room temperature to determine operating and burst pressure (PV/W) structural performance parameter values. The test description and test procedure as well as other data have been described in Section 3.5.4. Table A-15 herein gives fabrication processing details and summarizes the test data.

7.6.3.1 S/N 14 Vessel Test

A) Liner and Fiberglass Stresses at Burst Pressure

The vessel was designed so that the liner resisted 3/8 of the cryogenic stretch pressure. With 3370 psi stretch pressure, vessel radius 6.7", liner thickness of 21.9 mils (Table A-15) the cryogenic true stress in the metal liner (σ_{tm}) was,

$$\sigma_{tm} = (PR/2) (3/8) \times \frac{1}{t_m} = \frac{3370}{2} \times 6.7 \times \frac{3}{8} \times \frac{1}{21.9} = 194 \text{ ksi}$$

For this cryogenic true stress, we estimate a room temperature nominal metal liner ultimate strength of $\sigma_{mb} \approx 200$ ksi based on the tensile data given in Table A-14. At 4000 psi burst pressure with a glass total structural thickness of $t_g = 57$ mils we then compute the glass stress at burst, σ_{gb} , as,

$$\sigma_{gb} = (PR/2 - \sigma_{mb} t_m) / \left(\frac{t_g}{2} \right) = \frac{\frac{4000 \times 6.7}{2} - 200 (21.9)}{\frac{57}{2}}$$

$$\sigma_{gb} = 316 \text{ ksi}$$

B) Strain to Liner Rupture

Using the measured fiberglass prestress of $\sigma_{gi} = 71$ ksi (Table A-15) and the glass stress at burst pressure $\sigma_{gb} = 316$ ksi computed above, we find the strain to liner rupture $\Delta \epsilon$ as,

$$\Delta \epsilon = \frac{(316-71)}{E_g} = \frac{245}{12.4 \times 10^3} \approx 2\%$$

TABLE A-15
GFR SPHERICAL VESSEL DATA

P/N	S/N	Metal Wt. (#)	Lamin Wt. (#)	Total Wt. (#)	Volume (in ³)		Liner I.D. (in)	Thickness (Mils)		Pressure (#/in ²)		Pre- strain V-V ₀ = ϵ_i 3V ₀ (in/in)	Glass Pre- stress σ_{gi}^{**} (ksi)	Metal Liner Pre- stress σ_{wi}^{**} (ksi)	$\frac{\sigma_{wi}^{**}}{\sigma_y}$	$\frac{p_y \times 10^{-6}}{W}$	$\frac{p_y \times 10^{-6}}{W}$	Vessel Type
					Before Final Cryo- Stretch	After Final Cryo- Stretch		Metal t _m	Total Glass Struct t _g	Final Cryo- Stretch P _c	Oper. P _o							
D3731	14	3.50	1.85	4.12	1231	1249*	13.40	21.9	57.0	3370 [⊕]	2700*	.00573*	71.0*	-104*	.72*	.443	.656	Room Temp.
D3731	15	3.31	1.96	4.94	1250	1268	13.46	20.9	75.8	3825	3000	.00480	59.5	-108	.66	.462	.538	Hydro
D3731	16	3.42	1.85	4.83	1240	1261	13.50	21.6	72.6	3850	3000	.00565	70.0	-118	.72	.461	.547	static Test
D3731	17	3.32	1.90	4.97	1240.5	1259.8	13.40	20.6	72.4	3900	3000	.00518	64.2	-113	.69			NASA
D3731	19	3.36	1.96	4.99	1194.8	1208.1	13.20	21.5	74.4	3900	3000	.00371	46.1	-79.8	.49			Deliv.
D3731	21	3.49	1.96	5.01	1184.8	1199.7	13.18	22.4	74.6	4000	3000	.00419	52.0	-86.5	.53			Units
D3731	22	3.42	1.59	5.16	1241.6	1258.3	13.40	21.2	72.2	4000	3000	.00448	55.5	-94.5	.58			Heavy
D3731	23	3.39	1.93	5.23	1224.4	1241.7	13.33	21.2	73.0	4000	3000	.00471	58.4	-100.5	.61			Wt.
D3731	25	3.57	1.90	5.08	1230.5	1249.9	13.35	22.3	73.0	4000	3000	.00525	65.1	-106.5	.65			Boss
D3731	26	3.49	1.95	5.17	1208.6	1228.0	13.29	22.0	73.4	4000	3000	.00535	66.3	-110.5	.67			
D3730	1	3.31	0.81	4.79	1220.3	1239.3	13.32	20.8	73.2	3900	3000	.00520	64.5	-113.5	.68			NASA Deliv.
D3730	2	3.29	0.87	4.81	1234.4	1252.6	13.38	20.5	73.4	3900	3000	.00492	61.0	-109.3	.67			Units Light
D3730	3	3.26	1.02	5.24	1209.7	1228.5	13.30	20.5	74.4	4000	3000	.00519	64.3	-116.7	.71			Wt. Boss

Notes:

⊕ Fitting Leaked during cryostretch - further pressurization aborted (lower pressure than desired)

* (1) Reduced operating pressure due to lower yield point resulting from lower cryogenic stretch pressure (estimate 145 ksi room temperature yield point)

(2) Volume after 2700 psi pressurization was 1253.5 in³

(3) Prestrain prior to burst test was $\epsilon_i = \frac{(1253.5 - 1231)}{3 \times 1231} = .00573$

(4) Prestress values based on $\epsilon_i = .00573$

(5) 145 ksi σ_y used in $\sigma_{wi}^{**}/\sigma_y$ value

** $\sigma_{gi} = E_g \epsilon_i = 12.4 \times 10^6 \epsilon_i$

Based on 163 ksi σ_y (except as noted for S/N 14)

Weight used is membrane weight (total weight less boss weight) for comparison purposes with other data

7.6.3.2 S/N 15 and S/N 16 Vessel Tests

The "average" hoop strain to liner rupture for S/N 15 vessel was $\Delta\epsilon = 1/2 (.0120 + .0094) = .0107$ in/in (see Figures 23 and 24). This corresponds to an incremental fiberglass stress, $\Delta\sigma_g = E_g\Delta\epsilon = 12.4 \times 10^6 \times .0107 = 132.7$ ksi. With a measured fiberglass prestress of 59.5 ksi, detailed in Table A-15, we find the fiberglass stress at liner rupture as $\sigma_{gb} = 132.7 + 60.5 = 192.2$ ksi. Equilibrium considerations at 3500 psi burst pressure require for vessel radius of 6.73" and metal and fiberglass thicknesses of 20.9 and 75.8 mils, respectively (see Table A-15) that,

$$\frac{(3500) 6.73}{2} = (192.2) \frac{(75.8)}{2} + \sigma_{mb} (20.9) \text{ or } \sigma_{mb} = 216 \text{ ksi}$$

average membrane ultimate strength of the liner.

Similar calculations for S/N 16 GFR vessel at 3560 psi burst pressure give,

$$\sigma_{gb} = 198 \text{ ksi and } \sigma_{mb} = 223 \text{ ksi.}$$

7.7 Appendix 7 - Increased Ductility Liner High Performance Spherical GFR Vessel

The GFR vessel design point is tabulated below.

D = Vessel diameter = 13.5"

t_m = Liner wall thickness = 20 mils

p_o = Operating pressure = 3000 psi

σ_{mo} = Liner stress at operating pressure = .9
yield point = .9 x 200 = 180 ksi

σ_{go} = Fiberglass stress at operating pressure
= 200 ksi

σ_{mb} = Liner stress at burst pressure = 220 ksi

σ_{gb} = Fiberglass stress at burst pressure = 330 ksi

β = Fiberglass resin content = 20%

σ_{gi} = Fiberglass prestress at zero pressure = 80 ksi

Equilibrium at 3000 psi operating pressure requires,

$$\sigma_{mo} t_m + \sigma_{go} \frac{t_g}{2} = \frac{p_o R}{2} = \frac{3000}{2} (6.75) = (180)(20) + (200) \left(\frac{t_g}{2} \right)$$

The total fiberglass structural thickness t_g is

then,

$$t_g = 65.25 \text{ mils}$$

In a similar manner we find the burst pressure P_b as,

$$P_b = \frac{2}{R} \left\{ \sigma_{mb} t_m + \sigma_{gb} \frac{t_g}{2} \right\} = \frac{2}{6.75} \left\{ (220)(20) + (330) \left(\frac{65.25}{2} \right) \right\}$$

$$P_b = 4500 \text{ psi}$$

We next compute the composite fiberglass-resin density and thickness, ρ_c and t_c , respectively, using the formula detailed in Section 7.6.1 herein as,

$$\rho_c = \frac{1}{10.9 + 12.96\beta} = \frac{1}{10.9 + 12.96(.2)} = .0741 \text{ #/in}^3$$

$$t_c = \frac{t_g(1 + 1.19\beta)}{1 - \beta} = \frac{(65.25)(1 + 1.19 \times .2)}{1 - .2} = 101 \text{ Mils}$$

The structural performance values (PV/W) are found from,

$$PV/W = P \frac{4/3 \pi R^3}{4 \pi R^2 \{t_m \rho_m + t_c \rho_c\}} = \frac{(PR/3)}{t_m \rho_m + t_c \rho_c}$$

$$P_o V/W = \frac{(3000)(6.75/3) \times 10^3}{\{(20)(.285) + (101)(.0741)\}} = .513 \times 10^6 \text{ (in)} - \text{operating}$$

$$P_b V/W = .513 \times 10^6 \times \frac{4500}{3000} = .77 \times 10^6 \text{ (in)} - \text{burst}$$

The strain increment, $\Delta \epsilon$, required to attain the 330 ksi fiberglass ultimate strength at burst is,

$$\Delta \epsilon = \frac{\sigma_{qb} - \sigma_{qi}}{E_g} = \frac{(330-80)}{12.4 \times 10^3} \approx 2\%$$

which meets the design assumption of 2% minimum liner strain to rupture capability.

If the fiberglass resin content is reduced to 16% by vacuum bag curing techniques,

$$\rho_c = \frac{1}{10.9 + 12.96 (.16)} = .077 \text{ \#/in}^3$$

$$t_c = \frac{(65.25) (1 + 1.19 \times .16)}{(1 - .16)} = 92.3 \text{ mils}$$

The structural performance values are then,

$$\frac{P_o V}{W} = \frac{3000 \times \frac{6.75}{3}}{(20) (.285) + (92.3) (.077)} = .527 \times 10^6 \text{ (in) (operating)}$$

and

$$\frac{P_b V}{W} = .527 \times 10^6 \times \frac{4500}{3000} = .791 \times 10^6 \text{ (in) (burst)}$$

7.8 Appendix 8 - Low Stress Liner GFR Vessel Configuration

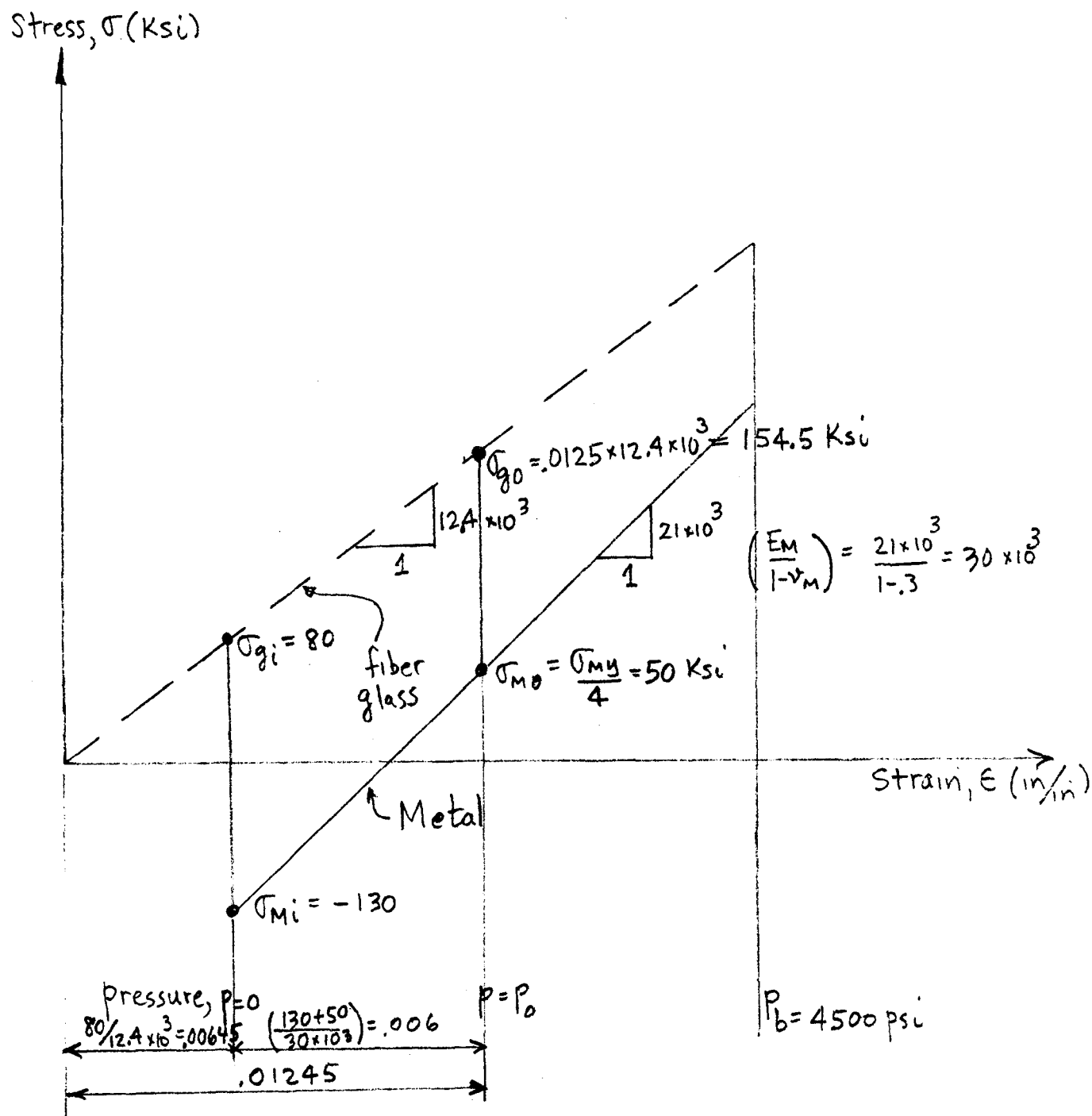
Calculations for the low stress liner configuration, whose design point values are given in Section 7.7, are presented in this appendix. Some of the computations are detailed on the metal liner and fiberglass stress-strain curve given in Figure A-28.

For sphere radius $R = 6.75$ " and metal and glass structural thicknesses t_m and $t_g = 20$ and 65.25 mils, respectively, we compute^m the operating pressure from equilibrium requirements as,

$$P_o = \frac{2}{R} \left[\sigma_{go} \left(\frac{t_g}{2} \right) + (\sigma_{mo}) (t_m) \right] = \frac{2}{6.75} \frac{(154.5)(65.25) + (50)(20)}{2} = 1790 \text{ psi.}$$

By comparison with the results given in Section 7.7 we obtain the structural efficiency at operating pressure,

$$\left(\frac{P_o V}{W} \right) = \left(\frac{1790}{3000} \right) \times (.527 \times 10^6) = .315 \times 10^6.$$



STRESS-STRAIN DIAGRAM
(Low Stress Liner)

FIGURE A-28

7.9 Appendix 9

DISTRIBUTION

REPORT
COPIES
R D

RECIPIENT

DESIGNEE

National Aeronautics & Space Administration
Lewis Research Center
21000 Brookpark Road
Cleveland, Ohio 44135

1 Attn: Contracting Officer, MS 500-313
5 Liquid Rocket Technology Branch, MS 500-209
1 Technical Report Control Office, MS 5-5
1 Technology Utilization Office, MS 3-16
2 AFSC Liaison Office, MS 4-1
2 Library
1 Office of Reliability & Quality
 Assurance, MS 500-111
1 D. L. Nored, Chief, LRTB, MS 500-209
3 J. R. Faddoul, Project Manager, MS 500-209
1 E. W. Conrad, MS 500-204
1 R. H. Kemp, MS 49-1

2 Chief, Liquid Experimental Engineering, RPX
Office of Advanced Research & Technology
NASA Headquarters
Washington, D. C. 20546

2 Chief, Liquid Propulsion Technology, RPL
Office of Advanced Research & Technology
NASA Headquarters
Washington, D. C. 20546

1 Director, Launch Vehicles & Propulsion, SV
Office of Space Science & Applications
NASA Headquarters
Washington, D. C. 20546

1 Chief, Environmental Factors & Aerodynamics
Code RV-1
Office of Advanced Research & Technology
Washington, D. C. 20546

1 Chief, Space Vehicles Structures
Office of Advanced Research & Technology
NASA Headquarters
Washington, D. C. 20546

DISTRIBUTION

REPORT COPIES		<u>RECIPIENT</u>	<u>DESIGNEE</u>
<u>R</u>	<u>D</u>		
1		Director, Advanced Manned Missions, MT Office of Manned Space Flight NASA Headquarters Washington, D. C. 20546	
6		NASA Scientific & Technical Information Facility P. O. Box 33 College Park, Maryland 20740	
1		Director, Technology Utilization Division Office of Technology Utilization NASA Headquarters Washington, D. C. 20546	
1	1	National Aeronautics & Space Administration Ames Research Center Moffett Field, California 94035 Attn: Library	C. A. Syvertson
1		National Aeronautics & Space Administration Flight Research Center P. O. Box 273 Edwards, California 93523 Attn: Library	
1		National Aeronautics & Space Administration Goddard Space Flight Center Greenbelt, Maryland 20771 Attn: Library	
1		National Aeronautics & Space Administration John F. Kennedy Space Center Cocoa Beach, Florida 32931 Attn: Library	
1		National Aeronautics & Space Administration Langley Research Center Langley Station Hampton, Virginia 23365 Attn: Library	

DISTRIBUTION

REPORT
COPIES
R D

RECIPIENT

DESIGNEE

1		National Aeronautics & Space Administration Manned Spacecraft Center Houston, Texas 77001 Attn: Library	J. G. Thiobodaux Chief, Propulsion Power Division
1	1	National Aeronautics & Space Administration George C. Marshall Space Flight Center Huntsville, Alabama 35812 Attn: Library	J. Blumrich
1	1	Jet Propulsion Laboratory 4800 Oak Grove Drive Pasadena, California 91103 Attn: Library	W. Jensen
1		Defense Documentation Center Cameron Station Building 5 5010 Duke Street Alexandria, Virginia 22314 Attn: TISIA	
1		Office of the Director of Defense Research & Engineering Washington, D. C. 20301 Attn: Office of Asst. Dir. (Chem. Technology)	
1		RTD (RTNP) Bolling Air Force Base Washington, D. C. 20332	
1		Arnold Engineering Development Center Air Force Systems Command Tullahoma, Tennessee 37389 Attn: Library	Dr. H. K. Doetsch
1		Advanced Research Projects Agency Washington, D. C. 20525 Attn: Library	D. E. Mock

DISTRIBUTION

REPORT COPIES			<u>RECIPIENT</u>	<u>DESIGNEE</u>
<u>R</u>	<u>D</u>			
1			Aeronautical Systems Division Air Force Systems Command Wright-Patterson Air Force Base, Dayton, Ohio Attn: Library	D. L. Schmidt Code ARSCNC-2
1			Air Force Missile Test Center Patrick Air Force Base, Florida Attn: Library	L. J. Ullian
1			Air Force Systems Command Andrews Air Force Base Washington, D. C. 20332 Attn: Library	Capt. S.W. Bowen SCLT
1			Air Force Rocket Propulsion Laboratory (RPR) Edwards, California 93523 Attn: Library	
1			Air Force FTC (FTAT-2) Edwards Air Force Base, California 93523 Attn: Library	Donald Ross
1			Air Force Office of Scientific Research Washington, D. C. 20332 Attn: Library	SREP, Dr. J.F.Masi
1			Space & Missile Systems Organization Air Force Unit Post Office Los Angeles, California 90045 Attn: Technical Data Center	
1			Office of Research Analyses (OAR) Holloman Air Force Base, New Mexico 88330 Attn: Library RRRD	
1			United States Air Force Washington, D. C. Attn: Library	Col. C. K. Stambaugh, Code AFRST

DISTRIBUTION

REPORT COPIES			<u>RECIPIENT</u>	<u>DESIGNEE</u>
<u>R</u>	<u>D</u>			
1			Commanding Officer U. S. Army Research Office (Durham) Box CM, Duke Station Durham, North Carolina 27706 Attn: Library	
1			U. S. Army Missile Command Redstone Scientific Information Center Redstone Arsenal, Alabama 35808 Attn: Document Section	Dr. W. Wharton
1			Bureau of Naval Weapons Department of the Navy Washington, D. C. Attn: Library	J. Kay, Code RTMS-41
1			Commander U. S. Naval Missile Center Point Mugu, California 93041 Attn: Technical Library	
1			Commander U. S. Naval Weapons Center China Lake, California 93557 Attn: Library	W. F. Thorm Code 4562
1			Commanding Officer Naval Research Branch Office 1030 East Green Street Pasadena, California 91101 Attn: Library	
1			Director (Code 6T80) U. S. Naval Research Laboratory Washington, D. C. 20390 Attn: Library	H. W. Carhart J. M. Kralli
1			Picatinny Arsenal Dover, New Jersey 07801 Library	I. Forsten

DISTRIBUTION

REPORT COPIES			<u>RECIPIENT</u>	<u>DESIGNEE</u>
<u>R</u>	<u>D</u>			
1			Air Force Aero Propulsion Laboratory Research & Technology Division Air Force Systems Command United States Air Force Wright-Patterson AFB, Ohio 45433 Attn: APRP (Library)	R. Quigley C. M. Donaldson
1			Space Division Aerojet-General Corporation 9200 East Flair Drive El Monte, California 91734 Attn: Library	S. Machlawski
1	1		Ordnance Division Aerojet-General Corporation 11711 South Woodruff Avenue Downey, California 90241 Attn: Library	W. L. Arter
1			Propulsion Division Aerojet-General Corporation P. O. Box 15847 Sacramento, California 95803 Attn: Technical Library 2484-2015A	R. Stiff
1			Aerospace Corporation P. O. Box 95085 Los Angeles, California 90045 Attn: Library-Documents	
1			Air Products and Chemicals Company Allentown, Pennsylvania 18105 Attn: P. J. DeRea	
1	1		Electronics Division Aerojet - General Corporation Azusa, California 91702	E. E. Morris
1			ARO, Incorporated Arnold Engineering Development Center Arnold Air Force Station, Tennessee 37389 Attn: Dr. S. H. Goethert Chief Scientist	

DISTRIBUTION

REPORT COPIES		<u>RECIPIENT</u>	<u>DESIGNEE</u>
<u>R</u>	<u>D</u>		
1		Atlantic Research Corporation Shirley Highway & Edsall Road Alexandria, Virginia 22314 Attn: Security Office for Library	
1		Battelle Memorial Institute 505 King Avenue Columbus, Ohio 43201 Attn: Defense Metals Information Center	
1		Bell Aerosystems Box 1 Buffalo, New York 14205 Attn: T. Rainhardt	
1		The Boeing Company Aerospace Division P. O. Box 3707 Seattle, Washington 98124 Attn: Ruth E. Peerenboom (1190)	
1		Brunswick Corporation Defense Products Division 1700 Messler Street Muskegon, Michigan 49441	
1		Western Division McDonnell Douglas Aircraft Company, Inc. 3000 Ocean Park Boulevard Santa Monica, California 90406 Attn: J. M. Toth	J. L. Waisman
1		Hercules Powder Company Chemical Propulsion Division 910 Market Street Wilmington, Delaware 19804	
1		Narmco Research & Development Company Whittaker Corporation 131 North Ludlow Street Dayton, Ohio 45402	

DISTRIBUTION

REPORT COPIES			<u>RECIPIENT</u>	<u>DESIGNEE</u>
<u>R</u>	<u>D</u>			
1			Plastics Technical Evaluation Center Picatinny Arsenal Dover, New Jersey 07801	
1			Rocketdyne 6633 Canoga Avenue Canoga Park, California 91304 Attn: Library, Department 596-306	
1			Rohr Corporation Department 145 Chula Vista, California 91312	
1			TRW Systems 1 Space Park Redondo Beach, California 90200 Attn: Tech. Library Doc. Acquisitions	
1			Sandia Corporation Sandia Base Albuquerque, New Mexico 87115 Attn: H. E. Montgomery	
1			Swedlow, Incorporated 6986 Bandini Boulevard Los Angeles, California 90022	
1	1		Thiokol Chemical Corporation Wasatch Division P. O. Box 524 Brigham City, Utah 84302 Attn: Library Section	D. Hess
1			United Aircraft Corporation United Technology Center P. O. Box 358 Sunnyvale, California 94088 Attn: Librarian	

DISTRIBUTION

REPORT COPIES			
<u>R</u>	<u>D</u>	<u>RECIPIENT</u>	<u>DESIGNEE</u>
1		Chemical Propulsion Information Agency Applied Physics Laboratory 8621 Georgia Avenue Silver Springs, Maryland 20910	
1		The Garrett Corporation 20545 Center Ridge Road Cleveland, Ohio 441161	
1		Grumman Aircraft Engineering Corporation Bethpage, Long Island, New York	
1		General Dynamics/Convair P. O. Box 1128 San Diego, California 92712 Attn: Library and Information Services (128-00)	
1		B. F. Goodrich Company Aerospace & Defense Products 500 South Main Street Akron, Ohio 44311	
1		Goodyear Aerospace Corporation 1210 Massilon Road Akron, Ohio 44306	
1		Hamilton Standard Division United Aircraft Corporation Windsor Locks, Connecticut 06096 Attn: Library	
1		Allegany Ballistics Laboratory Division of Hercules Powder Company Cumberland, Maryland 21502 Attn: Thomas Bates	
1		IIT Research Institute Technology Center Chicago, Illinois 60616 Attn: C. K. Hersh, Chemistry Division	

DISTRIBUTION

REPORT COPIES			<u>RECIPIENT</u>	<u>DESIGNEE</u>
<u>R</u>	<u>D</u>			
1	1		Martin-Marietta Corporation Denver Division P. O. Box 179 Denver, Colorado 80201 Attn: A. Feldman	F. Schwartzberg
1			North American Aviation, Inc. Space & Information Systems Division 12214 Lakewood Boulevard Downey, California 90242 Attn: Technical Information Center D/096-722 (A107)	
1			U. S. Rubber Company Mishawaka, Indiana 46544	
1			General Electric Company Apollo Support Department P. O. Box 2500 Daytona Beach, Florida 32015 Attn: C. Day	
1			Aerojet-General Corporation Park West Building - Suite 227 20545 Center Ridge Road Cleveland, Ohio 44116 Attn: W. Snapp	
1			Marine Engineering Laboratory NSRDC ANNADIV Annapolis, Maryland 21402 Attn: Karl H. Keller, Code 560	
1			Brunswick Corporation Defense Products Division P. O. Box 4594 43000 Industrial Avenue Lincoln, Nebraska 68504 Attn: J. Carter	

DISTRIBUTION

REPORT
COPIES

R D

RECIPIENT

DESIGNEE

1 Celanese Corporation
Box 1000
Summit, New Jersey 07901
Attn: J. D. Lassiter

1 Philco Ford Corporation
Aeronutronics Division
Ford Road
Newport Beach, California 92663
Attn: Technical Information Department

Dr. L.H. Linder